JAERI 1234

JAERI 1234

Critical Experiments and Analyses on 7×7 PuO_2-UO_2 Lattices in Light-Water Moderated UO_2 Core

June 1974

日 本 原 子 力 研 究 所
Japan Atomic Energy Research Institute

JAERI レポート

この報告書は，日本原子力研究所で行なわれた研究および技術の成果を研究成果編集委員会の審査を経て，不定期に刊行しているものです．

入手（資料交換による），複製などのお問わせは，日本原子力研究所技術情報部（〒319-11 茨城県那珂郡東海村）あて，お申しこみください．なお，このほかに財団法人原子力弘済会情報サービス事業部（茨城県那珂郡東海村日本原子力研究所内）で複写による実費頒布をおこなっております．

JAERI Report

Inquiries about the availability of reports and their reproduction should be addressed to the Division of Technical Information, Japan Atomic Energy Research Institute, Tokai-mura, Naka-gun, Ibaraki-ken, Japan.

編集兼発行　日本原子力研究所

印　　刷　三美印刷株式会社

Critical Experiments and Analyses on 7×7 PuO_2–UO_2 Lattices in Light-Water Moderated UO_2 Core*

Harumichi TSURUTA, Shojiro MATSUURA, Iwao KOBAYASHI, Masao HASHIMOTO, Takenori SUZAKI, Akio OHNO, Kiyonobu MURAKAMI, Ryozo YUMOTO**, Saburo KIKUCHI**, Takashi KAJIYAMA**, Hideyoshi SASAJIMA**, Koichi KITAMOTO*** and Michio HATA***

Tokai Research Establishment
Japan Atomic Energy Research Institute
Tokai-mura, Naka-gun, Ibaraki-ken

Received December 27, 1973

Abstract

A series of critical experiments and analyses on the 7×7 PuO_2–UO_2 lattices in a light-water moderated UO_2 core were carried out using the TCA critical facility. The purposes of the present study were: (1) to compare the criticality as well as the neutron flux and power distributions of the plutonium fueled core with those of the uranium fueled core, and (2) to evaluate the accuracy of the current calculational technique in applying to plutonium fueled cores.

Multi-regional cores used in this experiments consisted of the central 7×7 test lattice with 3.4 wt% PuO_2–UO_2 or 2.6 wt% UO_2 fuels, and the surrounding driver lattice with 2.6 wt% UO_2 fuels. Water-to-fuel volume ratio of the 7×7 lattice was parametrically changed as 1.76, 2.00, 2.38, and 2.95. Critical core configuration as well as activity and power distributions were measured for every core of them.

The unit cell calculations were performed using the multigroup transport code LASER. The neutron balance calculations for the critical cores were performed using the two-dimensional diffusion code PDQ-5. The calculated results agreed with measured values in ±0.3% for the effective multiplication factor, while for the neutron density and power distributions the maximum differences between the calculated and measured values were 16% and 9%, respectively.

---

* The work has been performed under the joint research by the Japan Atomic Energy Research Institute and the Power Reactor and Nuclear Fuel Development Corporation.

** Power Reactor and Nuclear Fuel Development Corporation.

*** Visiting researcher from Chubu Electric Power Co., Ltd.

軽水減速 UO_2 炉心内の 7×7 PuO_2–UO_2 格子に関する臨界実験と解析*

日本原子力研究所　東海研究所

鶴田晴通・松浦祥次郎・小林岩夫・橋本政男・須崎武則
大野秋男・村上清信・湯本鐐三**・菊池三郎**・梶山登司**
笹島秀吉***・北本紘一***・秦　道雄***

（受理　1973年12月27日）

要　旨

軽水減速 UO_2 燃料炉心に 7×7 の配列をした PuO_2–UO_2 燃料格子を装荷した体系に関して，一連の臨界実験とその解析が TCA を用いて行なわれた．この研究の目的は一部にプルトニウム燃料を装荷したウラン燃料炉心について，(1) 反応度，中性子束分布，および出力分布をウラン燃料のみの場合と比較すること，(2) ウラン燃料体系に適用されている計算方法をプルトニウム混合炉心に適用した場合の精度を評価すること，にあった．

実験に用いられた多領域炉心は，中央部に 3.4 wt% 富化 PuO_2–UO_2 燃料または細径の 2.6 wt% 濃縮 UO_2 燃料を装荷した 7×7 格子配列の試験領域と，それをとり囲む太径の 2.6 wt% 濃縮 UO_2 燃料のドライバ領域とから構成された．7×7 格子の水対燃料体積比は 1.76, 2.00, 2.38 および 2.95 の4種類が用いられその各々について臨界量，中性子密度分布，および出力分布が測定された．

単位格子についての計算は多群輸送理論コード LASER によって，臨界計算は2次元拡散コード PDQ-5 によって行なわれた．計算値は実験値に対して，実効増倍係数に関して ±0.3% 以内，中性子密度分布および出力分布に関してはそれぞれ最大 16% および 9% の誤差であった．

---

* この研究は日本原子力研究所と動力炉・核燃料開発事業団との共同研究のもとに行なわれた．

** 動力炉・核燃料開発事業団

*** 外来研究員（中部電力株式会社）

Contents

目　次

1. Introduction

During the last decade, interest in using plutonium in light-water reactors is increasing. This is due to the rapidly rising surplus of plutonium from the light-water reactors. Plutonium as a fuel material is more valuable in fast reactors than in the thermal reactors. However, storage of the plutonium for use in the fast reactors does not seem desirable, because a sufficient number of them are not expected to be available enough to use the surplus plutonium.

Substitution of plutonium into the uranium fueled light-water reactors will require reoptimization of uranium lattices for plutonium[1),2),3)]. The most significant factors in the lattice reoptimization for the water reactors are plutonium fuel composition, lattice pitch, and fuel rod size. When plutonium fuel assemblies are placed next to uranium fuel assemblies of the same fissile enrichment, the specific power will be higher in the plutonium fuel. This creates serious power peaking problems.

Significant experimental programs[4),5),6)] concerned with the physics of the plutonium recycling and fuel technology have been carried out at many laboratories throughout the world. It is recognized that knowledge in the fields of physics and technology of plutonium utilization in thermal reactors has reached now the point where the plutonium recycling can be started in existing power reactors. The physics characteristics of plutonium enriched reactors are, however, inherently more difficult to calculate than those for uranium enriched reactors. Problems which occur in predicting the behaviour of the uranium fueled reactors are also present in the plutonium system, because the fuel of interest is a mixture of the oxides of plutonium and uranium. The experimental information for the plutonium fueled reactors is sparse relative to that available for the uranium fueled system. Thus, it is required to conduct more works for the plutonium system.

A program of critical experiments concerned with plutonium utilization in light-water reactors is being conducted[7),8)] under the joint research by the Japan Atomic Energy Research Institute and the Power and Nuclear Fuel Development Corporation. The general objectives of the program are to investigate the characteristics of plutonium fueled lattices, and to evaluate and improve the calculational methods so that the reliable engineering design can be made for fuel loadings containing plutonium.

As a step of this program, multi-regional experiments using 3.4 wt% PuO_2-UO_2 and 2.6 wt% UO_2 fuels were conducted at various lattice pitches in the TCA critical facility. The atomic number density of the fissile materials of the PuO_2-UO_2 fuel was designed to be the same as that of the UO_2 fuel. The fourty-nine PuO_2-UO_2 or UO_2 rods were arranged into 7×7 square geometry and surrounded by UO_2 fuels.

The purposes of the present study were: (1) to compare the criticality as well as the neutron flux and power distributions in the plutonium fueled core with those in the uranium fueled core, and (2) to evaluate the accuracy of the current calculational technique in applying to plutonium fueled cores. The results of these analyses will be described in subsequent chapters and the numerical values of the foil activation and power distributions are available in the appendices.

2. Experimental facility

2.1 Tank-type Critical Assembly (TCA)

The critical assembly TCA has been used for reactor physics experiments on the light-water moderated lattices. It has a very flexible construction, and many kinds of cold critical experiments can be carried out for various systems from a simple regular lattice to a complex mock-up system of a power reactor.

The core is assembled at the central part of the cylindrical tank (183.2cmϕ×207.8cmh). The fuel rods are vertically inserted, and positioned by the upper and the lower grid plates. These fuel rods are arranged to form a square lattice. The water-to-fuel volume ratio of the lattice is determined by the lattice pitch of the grid plates. The grid plates are changeable, and the proper set of plates is selected for each experiment. Usually, the reactivity control on operation is performed by the adjustment of water level and any other control element is not used to avoid the undesirable neutron flux disturbance. The general view and the mechanical construction are shown in **Figs. 1**, **2** and **Photo. 1**.

2.2 Fuel rods

Three kinds of fuel rods were used in this work. They are described as the PuO_2-UO_2, the JP-II·UO_2, and the 26PA·UO_2 in this report, respectively. The specifications of these fuel rods are shown in **TABLE 1** and **Fig. 3**, and the general description of them are as follows.

(1) PuO_2-UO_2

Forty-nine mixed oxide (PuO_2-UO_2) fuel rods were used. The enrichment of PuO_2 and the density of pellet were designed so as the fissile atomic number density (^{235}U, ^{239}Pu, and ^{241}Pu) of the fuel to be equal to that of the JP-II·UO_2. Besides, the diameters of the fuel pellet and the Zircaloy-2 cladding were fabricated to be the same as those of the JP-II·UO_2. The reason why such design was chosen was to compare directly the nuclear properties of PuO_2-UO_2 fuel with that of UO_2 fuel under the same experimental condition. The fuel pellet was fabricated by the cold-press-dewax-heating technique and the density was 6.82g/cm^3 (62.2% of theoretical density). It was about two-third of the density of usual sintered pellet. The active length of this fuel rods was 70.6cm, in other words, it was about one-half of the other type of the fuels. This type of fuel was loaded at the central region of the core.

(2) JP-II·UO_2

This type of fuel was fabricated to simulate the nuclear properties of the fuel for the JPDR-II core[9]. The active size was 1.07cm in diameter and 144.15cm in length, and the fuel material was 2.6wt% enriched UO_2 pellet. The fuel pellets were clad in aluminum cladding. Forty-nine fuel rods of this type were used for comparing with the PuO_2-UO_2 fuel rods. These were also loaded at the central region of the core.

(3) 26PA·UO_2

The surrounding driver region of the core consisted of this type of fuel. The adjustment of the critical water level was performed by triming the size of the driver zone. The active size of this fuel rod was 1.25cm in diameter and 144.15cm in length. The fuel material was

2.6wt% enriched UO_2 pellet clad in aluminum cladding.

2.3 Core construction

The every critical core was so constructed that the plan view was a square or almost square to maintain the symmetry. Examples of core configuration were illustrated in **Photo. 2** and **Fig. 4**. The cores consisted of a central test region and a surrounding driver region except the reference core of single region which consisted entirely of the 26PA·UO_2 fuel. The central test region was formed in a square lattice of seven by seven rod array. Hereafter the test region is described as the 7×7 region in this report. The PuO_2-UO_2 or the JP-II·UO_2 fuel rods were loaded in the 7×7 region, and the 26PA·UO_2 fuel rods were added in the driver region. The number of driver fuels was adjusted to obtain the assigned critical water level for each measurement.

The water-to-fuel volume ratio of the driver region was fixed to be 1.83, while four kinds of volume ratio were used for the 7×7 region. When the volume ratio of the 7×7 region was 1.76, 2.00, or 2.38, a water gap existed between the 7×7 region and the driver region. Their widths of the gap were 0.058, 1.788 and 1.452cm, respectively. The definition of the water gap was the width between the outer boundary of the unit lattice cell of the 7×7 region adjacent to the water gap and that of the driver region.

Two kinds of test fuel, *i.e.* the PuO_2-UO_2 and the JP-II·UO_2 fuel, and four kinds of lattices of the 7×7 region made eight combinations of the experimental core. Another one was the single regional core made of the 26PA·UO_2 fuel. The name of each core and the dimension are shown in **TABLE 2**. The core configurations are shown in **Fig. 5**.

As mentioned before, the active length of the PuO_2-UO_2 was about a half of others, and in case of use, the bottom ends of the active parts were set at the same height. The experimental water level* was always kept lower than the upper end of the fuel. When the PuO_2-UO_2 were loaded, the water level was lower than 70.6cm, and when the JP-II·UO_2 were loaded, it was lower than 144.15cm. Thus, the mixed region of the fuel, the cladding, the upper end-plug and air existed above the active core, and the another mixed region of the lower end-plug, the water reflector, the lower grid plate and the fuel support plate existed under the active core. The horizontal reflector was thick enough. The vertical arrangement of the core are shown in **Fig. 6**.

* The height from the bottom end of the active fuel to the water surface.

TABLE 1 Fuel specifications.

Fuel type	PuO_2-UO_2	JP-II·UO_2	26PA·UO_2
Fuel pellet	Pre-sintered	Sintered	Sintered
Density, g/cm³	6.82±0.01 (62.2±0.1%T.D.)	10.4 ±0.1	10.4
Diameter, mm	10.70±0.06	10.70±0.04	12.5
Enrichment, wt%	$3.37\pm0.03\left(\frac{PuO_2}{PuO_2+UO_2}\right)$	2.588±0.006(^{235}U)	2.596 (^{235}U)
Fuel rod			
Cladding material	Zircaloy-2	Al	Al
Cladding I.D., mm	10.83±0.04	10.83±0.10	12.65
Cladding thick., mm	0.70±0.07	0.70±0.07	0.76
Fuel length, mm	70.55±1.0	1441.5±3.0	1441.5
Mass of Pu, g/rod	12.9		
Composition, wt%			
^{235}U, ^{238}U	Natural		
^{239}Pu	90.64±0.06		
^{240}Pu	8.46±0.03		
^{241}Pu	0.84±0.02		
^{242}Pu	0.05±0.01		

TABLE 2 Core specifications.

Core name	7×7 region			Water gap	Driver region			Note
	Fuel type	Lattice pitch, cm	Volume ratio	Width, cm	Fuel type	Lattice pitch, cm	Volume ratio	
1.76Pu	PuO_2-UO_2	1.660	1.76	0.058	26PA·UO_2	1.956	1.83	Multi-regional core
2.00Pu		1.725	2.00	1.787				
2.38Pu		1.820	2.38	1.454				
2.95Pu		1.956	2.95	none				
1.76U	JP-II·UO_2	1.660	1.76	0.058				
2.00U		1.725	2.00	1.787				
2.38U		1.820	2.38	1.454				
2.95U		1.956	2.95	none				
1.83TU	Same as driver region			none				Single regional core

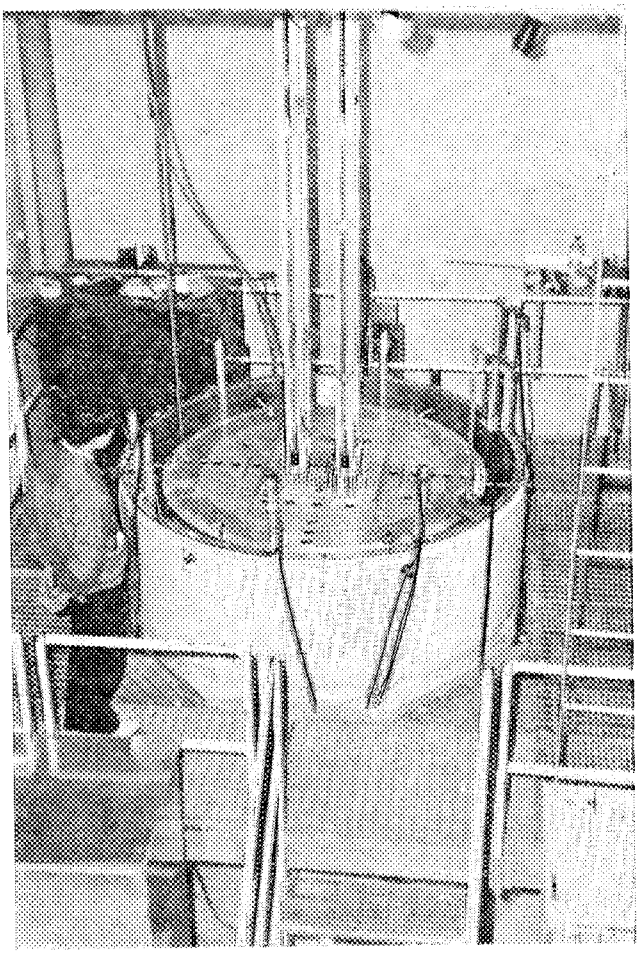

Photo. 1 General view of Tank-type Critical Assembly (TCA).

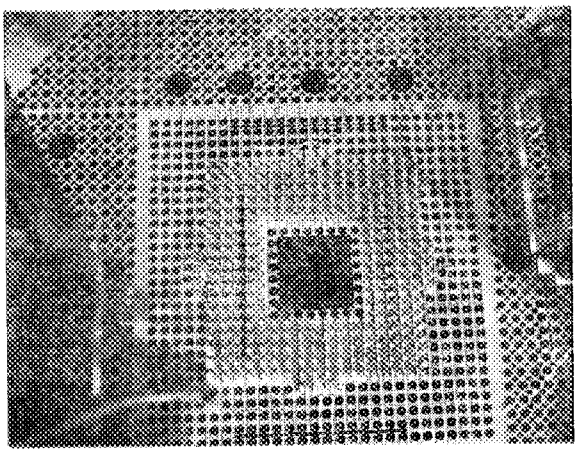

Photo. 2 Upper grid plate.
Fuels in the central 7×7 region are not loaded.

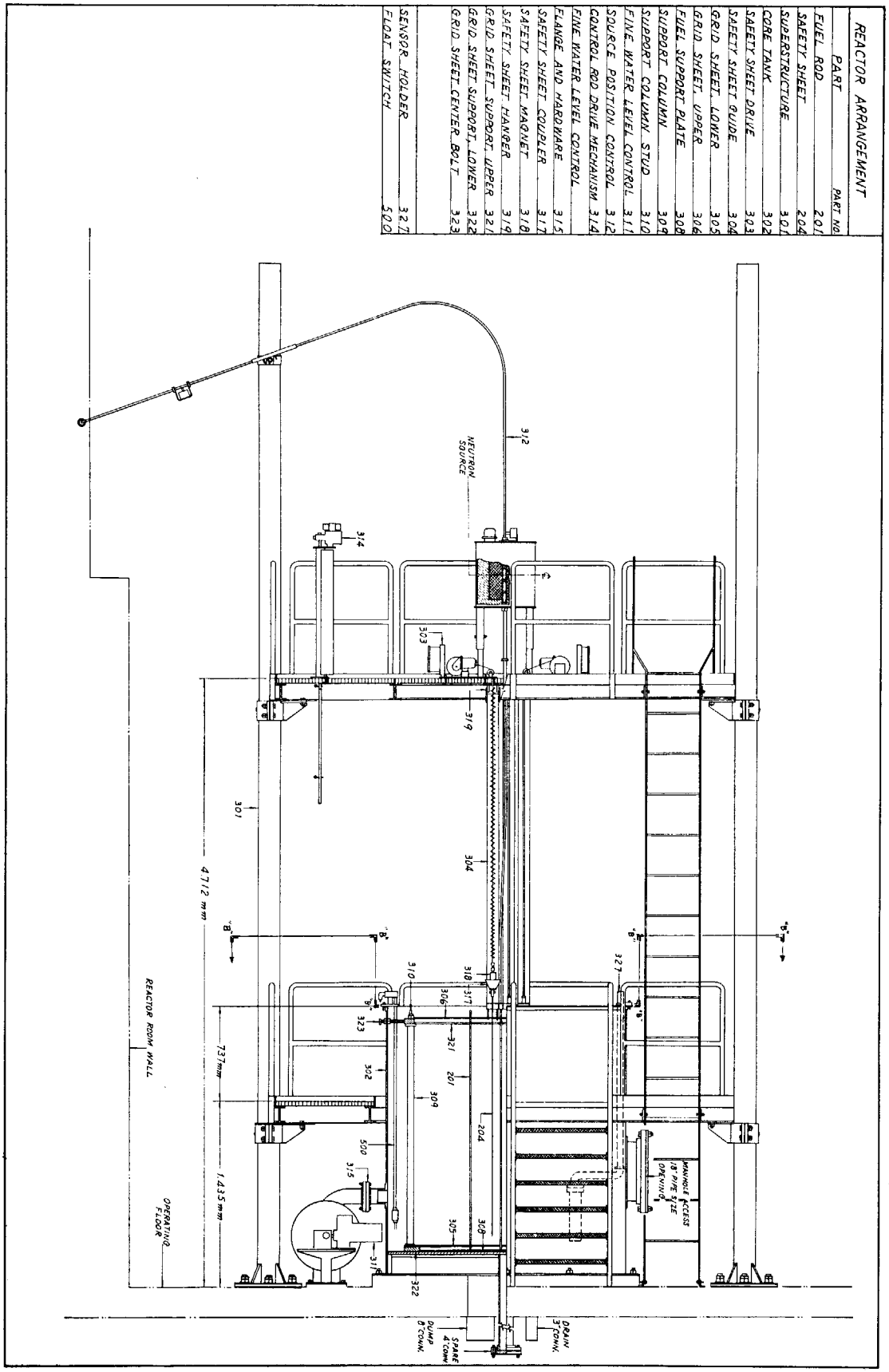

Fig. 1 Vertical cross-sectional view of TCA.

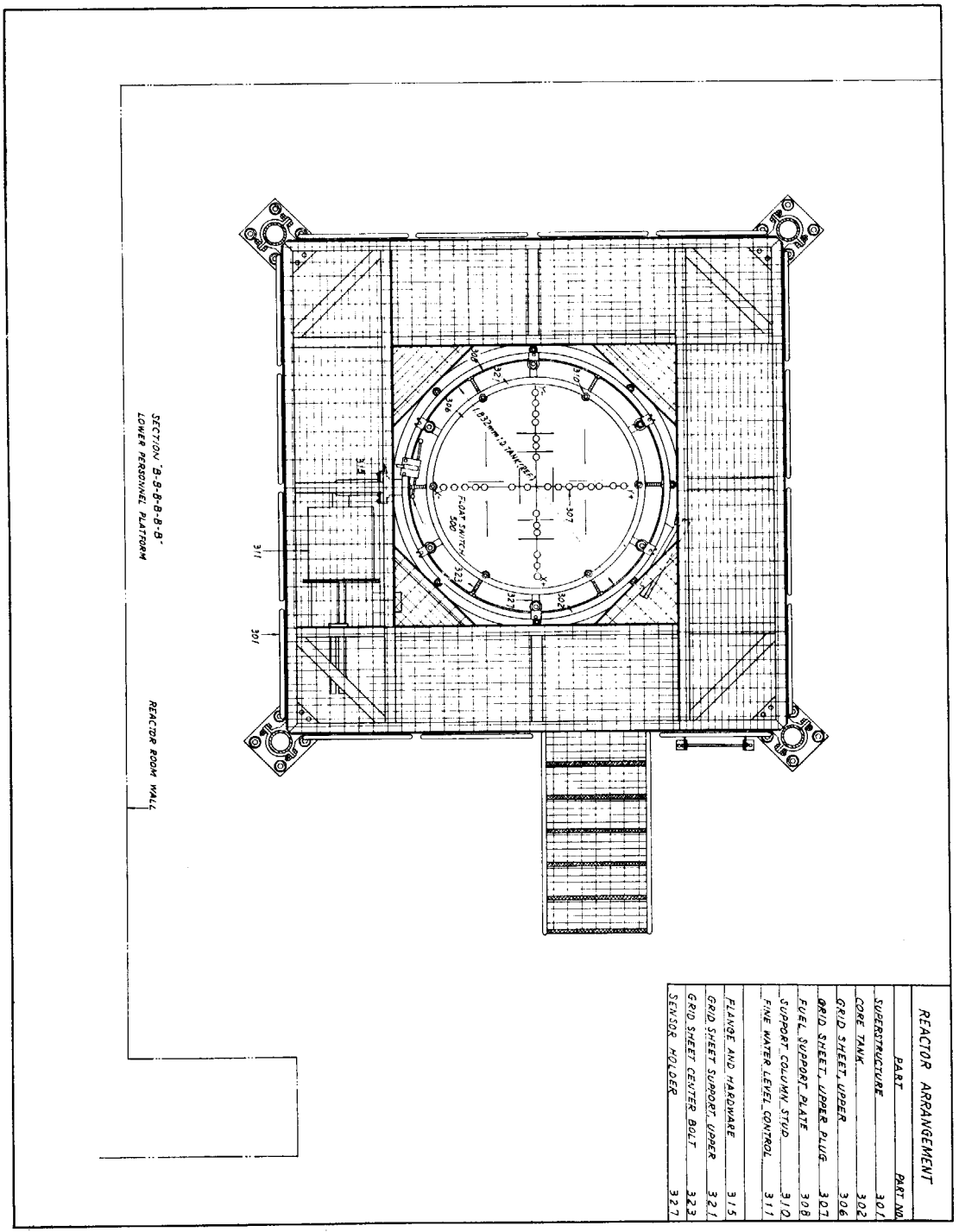

Fig. 2 Plan view of TCA.

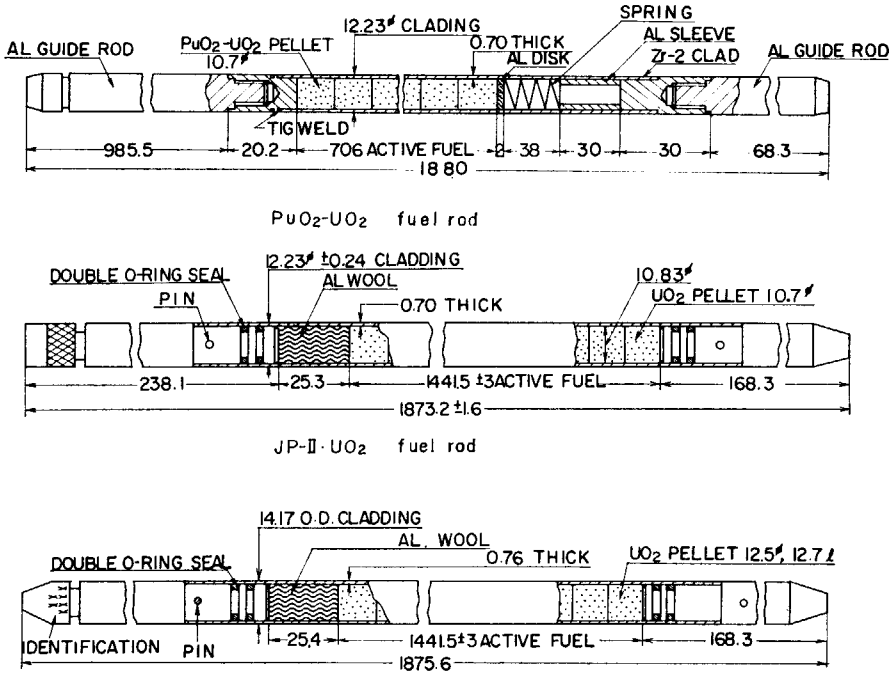

Fig. 3 Fuel rods.

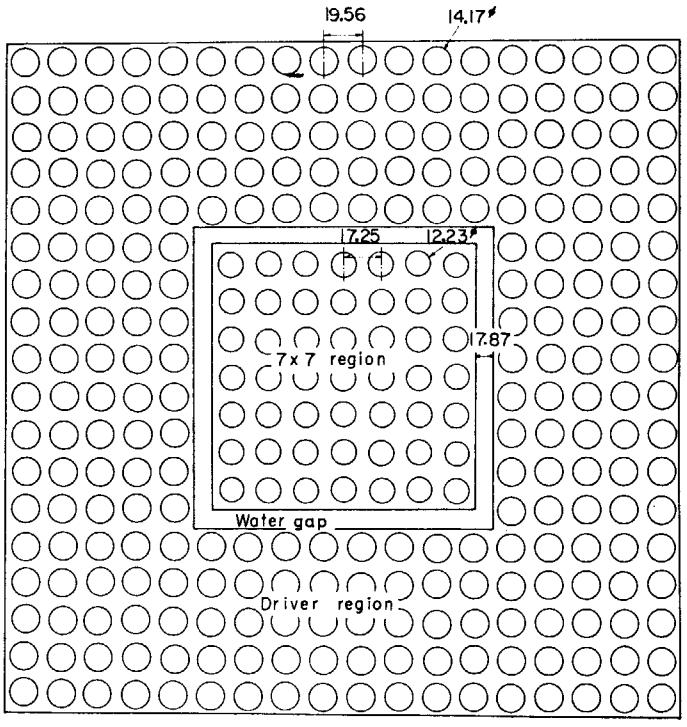

Fig. 4 Plan view of 2.00 Pu core.

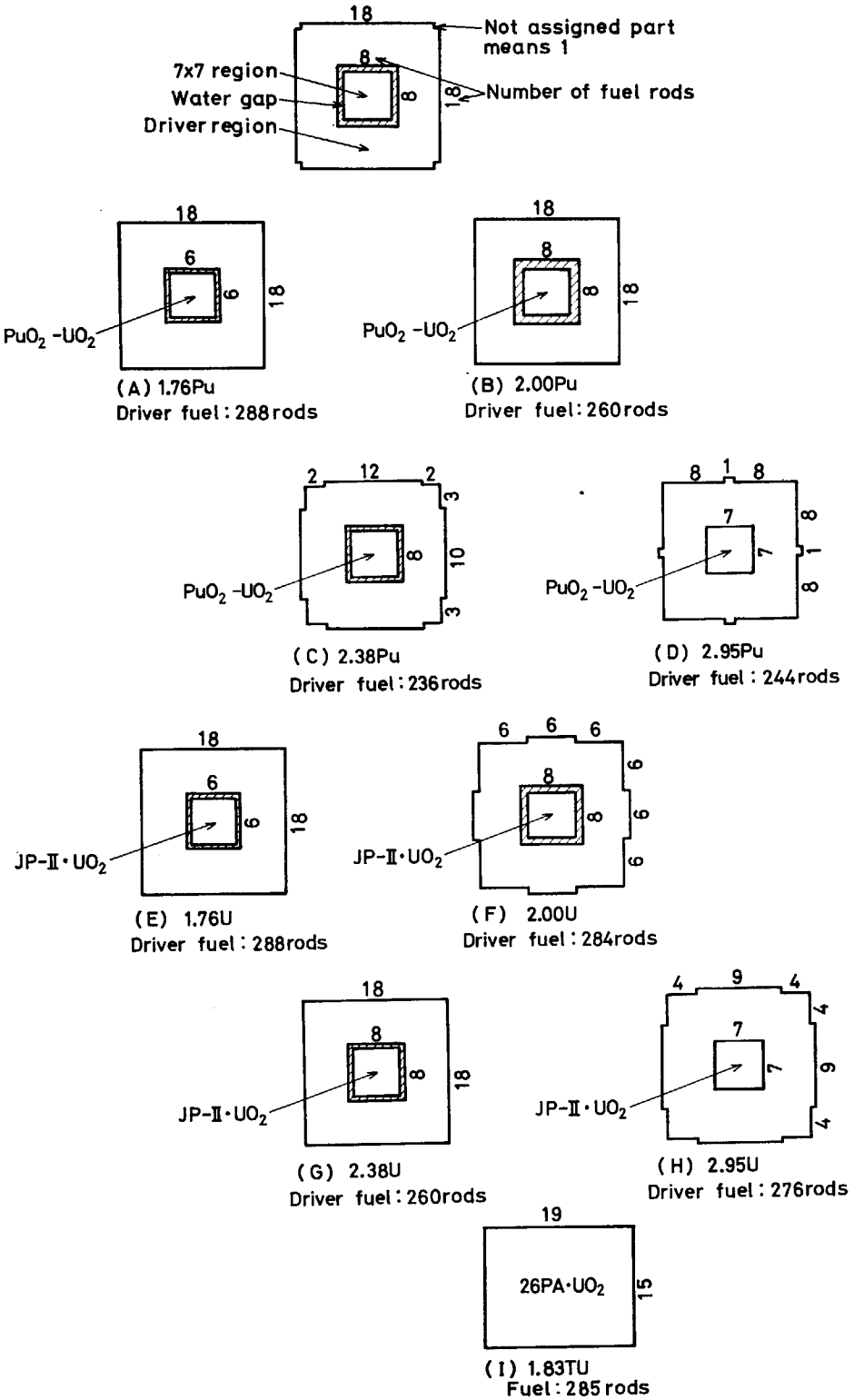

Fig. 5 Typical critical core configurations.

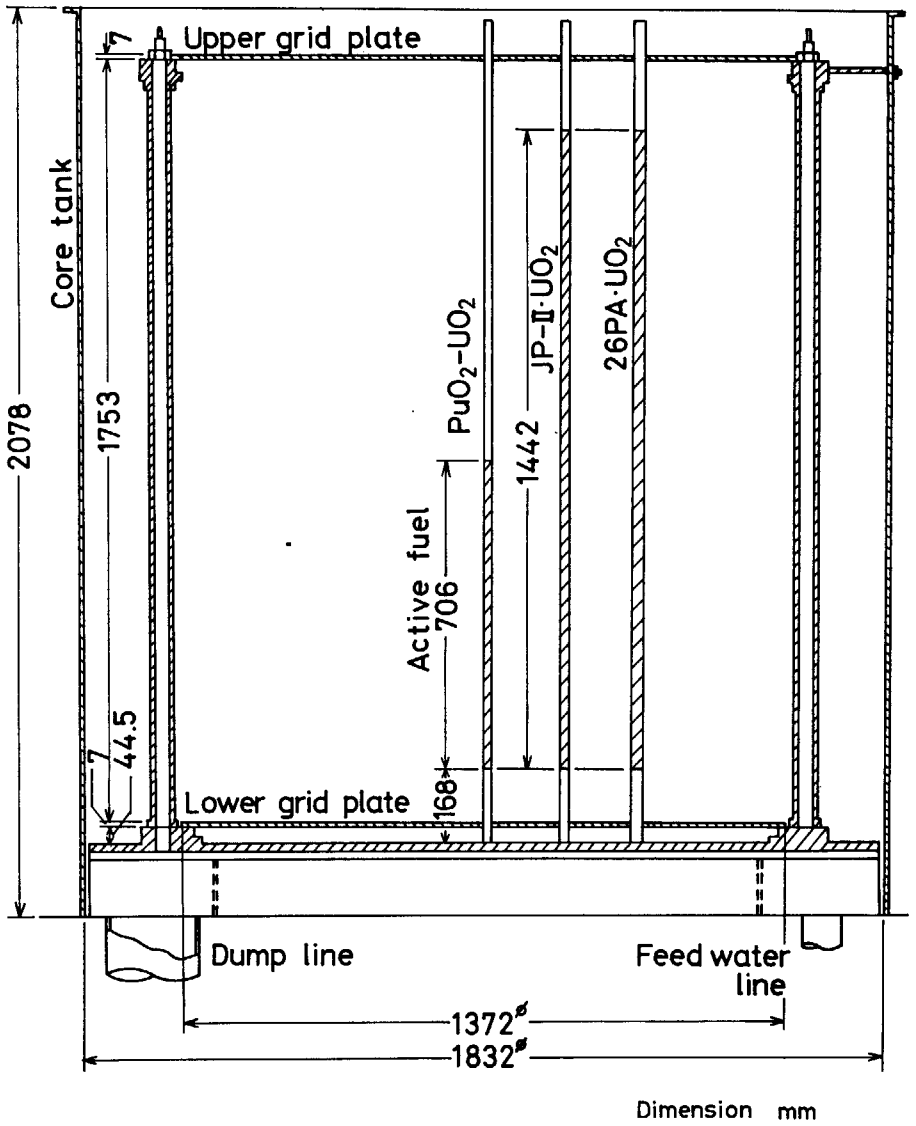

Fig. 6 Vertical arrangement of fuel rods.

3. Criticality

3. 1 Criticality measurements

3. 1. 1 Critical configurations

The critical core configurations were determined under a room temperature for eight types of the multi-regional cores and for one single regional core. The measured quantities were the number of the driver fuel rods and the water level which were required to maintain the core critical. Those measured quantities are shown in TABLE 3 with the calculated effective multiplication factors.

The critical water level was determined to an accuracy of about 0.01cm by means of the servo-manometer; the total absolute ambiguity of the critical water level was estimated to be about 0.05cm, because the ambiguity of about 0.04cm should have been taken into account on the correspondence between the bottom end of the active fuel and the reference reading of the servo-manometer. The equivalent reactivity worth corresponding to the level difference of 0.05 cm was about 5.0×10^{-5} $\Delta k/k$. The reactor water temperature shifted from 16.0°C to 21.0°C during the experimental period, while it was assumed to be 20°C in the calculation. The maximum temperature difference of 4°C was equivalent to the reactivity worth of about $3.2\times10^{-4}\Delta k/k$. Consequently, the measured effective multiplication factor to be compared with the calculated one was considered as 1.0000 ± 0.0004.

3. 1. 2 Material bucklings and critical masses

The critical cores determined in this measurements were multi-regional except the 1.83TU core. The power fraction of the 7×7 region was about 25% or less of the whole core. Then the contribution to the criticality from the 7×7 region was relatively small.

The measured multiplication factors of those multi-regional cores can be used to evaluate the calculational method for estimating the effects on criticality by the partial substitution of the PuO_2-UO_2 fuels for the UO_2 ones. However, from the point of view of obtaining the multiplying characteristics of those lattices, and verifying the calculational method for those lattices, the results on multi-regional cores were not explicit.

In order to obtain the more explicit information about the multiplying characteristics of the lattices of the 7×7 region, the material bucklings B_m^2 and the critical masses M_c of the lattices were derived from the measured geometrical bucklings, and the calculated values were compared with the derived results.

(1) Estimation of material buckling

It is well known that the material buckling B_m^2 of a multiplying medium is equal to the geometrical buckling B_g^2 of the single regional bare critical core. Even when the single regional core is surrounded by a thick reflector, the theory is applicable for the most of practical cases by adopting an appropriate reflector saving.

When a core consists of two different multiplying media, such as the central 7×7 region and the surrounding driver region, the shape of the eigen function is not simple. In general, the definition of the geometrical buckling and the relation between the material and geometrical

bucklings are obscure for such a multi-regional core. But when the physical properties are not so different from that of the driver region, the existence of the central 7×7 region is considered to be a partial disturbance to the single regional core entirely composed of the driver region. For that case, the treatment based on perturbation theory is applicable to define the buckling B^2 of the whole core[10].

If the 7×7 and driver lattices have the material bucklings B_1^2 and B_2^2, respectively, it can be shown that the material buckling of the whole reactor is given by

$$B^2=B_1^2\cdot W(R_1)+B_2^2\cdot W(R_2). \tag{3.1}$$

The factors $W(R_1)$ and $W(R_2)$ are the statistical weights of the 7×7 and driver regions, and are defined as

$$W(R)=\frac{\int_R \phi^2\cdot dV}{\int_{core} \phi^2\cdot dV}, \tag{3.2}$$

where R assigns a region and ϕ is a solution of $\nabla^2\phi+B^2\cdot\phi=0$. The coefficient B^2 can be considered as the synthesized material buckling for the multi-regional core.

On the contrary, if B^2 and B_2^2 are known, the other material buckling B_1^2 of the 7×7 lattice can be obtained by

$$B_1^2=\frac{B^2-B_2^2}{W(R_1)}+B_2^2. \tag{3.3}$$

The material bucklings of the 7×7 lattices of the Pu and the U systems were obtained by Eq. (3.3). The buckling B^2 was determined as the geometrical buckling for each critical size of the outer shape of the core. The reflector savings were assumed to be equal to those of the reference core 1.83TU. They were 14.44±0.03 and 12.5±0.2cm in horizontal and vertical directions according to the results of the variable loading method[11]. The value of B_2^2 was $9.317\times10^{-3}cm^{-2}$, which was obtained for the 1.83TU core. The cosine function was used as the eigen function.

The measured critical cores were not necessarily complete rectangular parallelepiped, while the $W(R_1)$ were calculated for the nearest size of rectangular parallelepiped. The correction for the B^2 due to the difference of the shape was carried out considering of the reactivity worths of the water level and the fuel rods loaded at periphery of the core.

In case of the cores of which water-to-fuel volume ratios in the 7×7 region were 2.00 and 2.38, a water gap existed between the 7×7 and the driver regions. The water gap had some negative reactivity worth. In other words, the B^2 of those cores were slightly decreased due to the negative reactivity effect by the water gap. The correcting amount δB^2 were estimated under the assumption that the reactivity effect due to the water gap was proportional to its area, when the variation of the area were small in a core.

The estimated results of the material bucklings are shown in TABLE 4 and **Fig. 7** with the calculated values. The calculated values were obtained as the solution of the following equation with the constants in TABLE 8.

$$1=\frac{\nu\Sigma_{f1}}{\Sigma_{a1}+\Sigma_{r1}+D_1\cdot B^2}+\frac{\nu\Sigma_{f2}}{\Sigma_{a2}+\Sigma_{r2}+D_2\cdot B^2}\cdot\frac{\Sigma_{r1}}{\Sigma_{a1}+\Sigma_{r1}+D_1\cdot B^2}$$
$$+\frac{\nu\Sigma_{f3}}{\Sigma_{a3}+D_3\cdot B^2}\cdot\frac{\Sigma_{r1}}{\Sigma_{a1}+\Sigma_{r1}+D_1\cdot B^2}\cdot\frac{\Sigma_{r2}}{\Sigma_{a2}+\Sigma_{r2}+D_2\cdot B^2}. \tag{3.4}$$

The validity of the above mentioned method was checked by additional experiment. In the experiment, the size of the central test lattice of which water-to-fuel volume ratio was 2.95, was changed from one cell to 7×7 cells, and it was recognized that the term $(B^2-B_2^2)/W(R_1)$ was constant within experimental errors for the test lattices of larger than 4×4 cells. The results of

this additional experiment are shown in **Fig. 8**.

The results of the material bucklings shown in **Fig. 7** indicate the following differences between the UO_2 and PuO_2-UO_2 lattices in the range of this experiments when their fissile atomic number densities are similar.

a) The reactivity effect of PuO_2-UO_2 lattice is apparently larger than that of UO_2 lattice in the range of water-to-fuel volume ratio from 1.76 to 2.95.

b) The difference of the reactivity effect increases as the volume ratio. When a single regional core has the geometrical buckling about $10^{-2}cm^{-2}$, the difference in effective multiplication factors is estimated to be 3.5 and 6.3% for the lattices of which volume ratios are 1.76 and 2.95, respectively.

c) The volume ratios corresponding to the maximum material bucklings are different. The PuO_2-UO_2 lattice has the maximum material buckling at the larger volume ratio. This means that the PuO_2-UO_2 lattice under consideration has a larger reactivity coefficient against the ratio of moderator to fuel atomic number densities than the usual uranium fueled light-water lattices.

(2) Estimation of critical mass

The critical mass of a single regional core can be estimated setting $B_m^2=B_g^2$ and determining the core size corresponding to B_g^2. By using the estimated results on the material bucklings, the critical masses of the cores which consist of the PuO_2-UO_2 lattices used in this experiment were estimated by

$$M_c(\mathrm{Pu})=N\cdot W, \tag{3.5}$$

$$N=\left(\frac{\frac{\pi}{B_x}-2\cdot\delta x}{L}\right)^2=\left(\frac{\frac{\pi}{B_x}-14.44}{L}\right)^2, \tag{3.6}$$

$$B_x^2=\frac{B_m^2-B_z^2}{2}=\frac{(B_m^2-1.379\times10^{-3})}{2}(cm^{-2}), \tag{3.7}$$

where

$M_c(\mathrm{Pu})$: required critical mass of Pu,
W: weight of Pu in a fuel rod,
N: number of fuel rods in the core,
δx: horizontal reflector saving,
L: lattice pitch,
B_z^2: vertical buckling.

The cores were assumed to be single regional, rectangular parallelepiped, and fully reflected. The results are shown in **TABLE 5** and **Fig. 9**. The values based on the experimental results at BNWL[4] are also shown in **Fig. 9**.

The fuel rods of the BNWL experiments consisted of 2wt% mixed oxide sintered pellets and Zircaloy-2 cladding. The Pu composition was almost the same as the present experiments. The slight difference between the BNWL values and the present values should be admitted because the BNWL cores were cylindrical and consisted of the triangular lattices. Still, the both results are close in both points of quantity and inclination with H/Pu atomic number density ratio. It seems to show that the estimation made in this experiment is appropriate.

3. 2 Criticality calculations

3. 2. 1 Two-dimensional diffusion calculation with three group constants

The criticality calculation was carried out according to the procedure as shown in **Fig. 10**. Few group constants in the 7×7 and driver regions were obtained by the LASER code[12] which was developed for the burn-up calculation and was equivalent to MUFT-THERMOS[13] codes. The constants in the water gap and reflector regions were obtained by the UGMG41[14] (equivalent to MUFT) and the THERMOS codes. The number of few groups was two for fast groups and one for a thermal group. Cut-off energies of the groups were 5.53keV and 1.855eV. The number of the fine thermal energy groups was thirty-five, and the width of a energy band was made narrow in the neighborhood of the resonances of ^{239}Pu and ^{241}Pu. Calculational conditions on using the codes described above are summalized in TABLE 6. The atomic number densities of materials in each region of the fuel unit cell are shown in TABLE 7. Few group constants of each lattice and water regions are listed in TABLE 8. The volume of the void region between the fuel pellet and the cladding was smeared into the cladding region and the apparent atomic number density of the cladding was decreased.

The effective multiplication factor k_{eff} as well as the neutron flux and power distributions of each core were obtained by using the two-dimensional diffusion calculation code PDQ·5[15]. The vertical neutron leakage was estimated by the vertical buckling which was determined with the measured critical water height of each core and the measured vertical reflector saving of 12.0cm as shown in Section **5. 1. 3**. An example of the arrangement of spatial meshes in the diffusion calculation is shown in **Fig. 11**. The thickness of the reflector region is more than 20 cm in all cases. The calculated k_{eff} are shown in TABLE 3 and **Fig. 12**. The measured k_{eff} correspond to the calculated values are 1.0000 ± 0.0004.

From the comparison between the calculated and the measured k_{eff}, the following remarks were obtained:

(a) Except 2.38Pu and 2.95Pu cores the calculated values are underestimated.
(b) The errors of the calculated values are within $\pm 0.3\%$.
(c) The calculated values for the Pu system are 0.1~0.4% higher and closer to the measured values than for the U system.
(d) The dependence of the calculated values on the water-to-fuel volume ratio are recognized for the Pu system. Otherhand, the values of the U system are almost constant in all water-to-fuel volume ratio.
(e) The calculated value for the 1.83TU core which consists of uniform UO_2 lattice is 0.1% lower than the measured value, and closer to the experiment than for the multi-regional cores.

3. 2. 2 Dependence of accuracy on the calculational conditions and the core geometries

Dependence of the calculated k_{eff} were examined on the conditions in the diffusion calculation and on the geometry of the critical core.

(1) Condition in diffusion calculation

(a) Spatial mesh

To examine the error in k_{eff} due to the spatial mesh width, two-dimensional diffusion calculations were performed for the several combinations of the spatial meshes in 2.00Pu core as shown in **Fig. 13** with calculated results. Case 1 was standard and had the finest allocation, and Case 5 had the most coarse spacings. The k_{eff} of Case 5 was greatest, but the difference of k_{eff}

from the standard case (Case 1) was only 0.1% and negligible.

(b) Error of the measured vertical reflector saving

The measured reflector saving had the error of ±0.1 cm. The influence of this error on the calculated k_{eff} was examined by using two-group constants of the PuO_2-UO_2, JP-II·UO_2, and 26PA·UO_2 fuel cells. The variation of k_{eff} by the change of the reflector saving is expressed by

$$\frac{\Delta k_{eff}}{\Delta \delta_z} = \frac{k_{eff}(\delta_z+\Delta\delta_z)-k_{eff}(\delta_z)}{\Delta\delta_z}, \tag{3.8}$$

$$k_{eff}=\frac{\nu\Sigma_{f1}}{\Sigma_{r1}+\Sigma_{a1}+D_1B^2}+\frac{\nu\Sigma_{f2}}{\Sigma_{a2}+D_2B^2}\cdot\frac{\Sigma_{r1}}{\Sigma_{r1}+\Sigma_{a1}+D_1B^2}, \tag{3.9}$$

$$B^2=2\cdot\left(\frac{\pi}{X}\right)^2+\left(\frac{\pi}{Z}\right)^2, \tag{3.10}$$

$$Z=H+\delta_z, \tag{3.11}$$

where

δ_z: vertical reflector saving

H: critical water height

X: horizontal core width with reflector saving.

The change of 0.1 cm of δ_z resulted 0.0001 of k_{eff} for all cores as shown in TABLE 9.

(2) Dependence on core geometry

The most remarkable geometrical characteristic of the cores in this experimental series was the presence of the water gap. The water-to-fuel volume ratio also specified the geometrical characteristics. The relations between the geometrical characteristics and the calculated k_{eff} were examined.

(a) Water gap

The cores having water-to-fuel volume ratio of 1.76 and 2.95 had little or no water gap. To examine the water gap effect in those cores, the water gaps of which width was about 2.0 cm were made at the boundary between the 7×7 and driver regions as shown in **Fig. 14**, and their critical water heights were measured. The results of the two-dimensional diffusion calculation are shown in TABLE 10 and **Fig. 15**. From the comparison between the calculated and the measured k_{eff}, the following remarks were obtained.

(i) The calculated k_{eff} for the Pu system are influenced more than for the U system by the water gap.

(ii) The calculated k_{eff} of the 1.76Pu and 1.76U cores with water gap become smaller by about 0.1~0.2% than that of the cores without water gap. However, the calculated k_{eff} of the 2.95Pu and 2.95U cores are scarecely affected by the water gap.

(b) Water-to-fuel volume ratio

The calculated k_{eff} for the cores with water gap could be thought to show the dependence on the water-to-fuel volume ratio, because the cores had approximately the same cross-sectional area of water gap as shown in **Fig. 15**. As the effect of water-to-fuel volume ratio, the followings were obtained.

(i) The calculated k_{eff} of the U and Pu systems become greater with the increasing volume ratio.

(ii) The Pu system has more dependence on the volume ratio than the U system.

(iii) The dependence (i) is consistent with that of material buckling as shown in **Fig. 7**. But the ratio of the calculated to the measured material bucklings shows the greater dependence on water-to-fuel volume ratio for the U system than for the Pu system. This fact is inconsistent with (ii) and can be thought due to the water gap and the reflector. The characteristics on the uniform lattices should be necessary to be studied.

3.3 Summary on criticality

The ratio of neutron absorption and emission in the PuO_2-UO_2 lattice of the multi-regional core used in this experimental series was about 20% of the whole core. In these cores the reactivity effects of the PuO_2-UO_2 fuel rods surrounded by the low enriched UO_2 fuel rods were measured and compared with that of the JP-II·UO_2 fuel rods which had the almost same atomic number density of fissile materials as the PuO_2-UO_2 fuel rods. Water-to-fuel volume ratio in the 7×7 region ranged from 1.76 to 2.95. An accuracy of the calculational method was also examined for the multi-regional cores composed of above mentioned fuel rods. The conclusions reached as a result of this study are as follows:

(1) The PuO_2-UO_2 fuel rod has greater reactivity effect, or material buckling, than the JP-II·UO_2 fuel rod. This difference of the reactivity effect becomes greater with increasing water-to-fuel volume ratio. This is due to the fact that material buckling of the PuO_2-UO_2 lattice has maximum point at the greater water-to-fuel volume ratio than the JP-II·UO_2 lattice.

(2) The above fact suggests that by adjusting the enrichment of plutonium in a mixed oxide fuel rod, the reactivity effect of both fuel lattices could be made as same at any water-to-fuel volume ratio. However, particular attention should be called to the fact that the reactivity coefficients, such as void or temperature coefficients, may be different.

(3) Calculated k_{eff} are within the error of ±0.3% of the measured ones. From these results, the LASER code which was developed for burn-up calculation of uranium dioxide fueled cores, can be used for mixed oxide fueled cores in good accuracy.

TABLE 3 Measured critical core configurations and calculated effective multiplication factors k_{eff}.

Core name	Run number and core identification*	Water gap width, cm	No. of driver fuels	Critical water level, cm	Core temp., °C	Calculated k_{eff}
1.76 Pu	3804, A	0.058	288	68.72	18.9	0.9993
2.00 Pu	3837, B	1.787	260	68.15	20.6	0.9988
2.38 Pu	3744, C	1.454	236	69.28	16.2	1.0006
2.95 Pu	3829, D	none	244	69.26	20.4	1.0026
1.76 U	3821, E	0.058	288	75.88	21.0	0.9974
2.00 U	3840, F	1.787	284	68.80	20.8	0.9977
2.38 U	3710, G	1.454	260	80.85	16.0	0.9981
2.95 U	3833, H	none	276	66.53	20.0	0.9985
1.83 TU	3872, I	none	285	137.22	21.0	0.9988

* Reffer to Fig. 5 on alphabetical letters.

TABLE 4 Material bucklings of lattices.

Fuel	Water-to-fuel volume ratio	Experimental B_m^2, $\times 10^{-3}$cm^{-2}	Theoretical B_m^2, $\times 10^{-3}$cm^{-2}
JP-II·UO_2	1.76	9.22	8.88
	2.00	9.64	9.28
	2.38	10.08	9.59
	2.95	9.60	9.63
PuO_2-UO_2	1.76	10.41	9.43
	2.00	10.95	10.14
	2.38	11.76 11.55	10.89
	2.95	11.86 11.94	11.58
26PA·UO_2	1.83	9.32	9.22

TABLE 5 Estimated critical masses of PuO_2-UO_2 fuel.

Volume ratio (lattice pitch, cm)	Atomic number density ratio H/Pu	Experimental critical mass, kg	Theoretical critical mass, kg
1.76 (1.660)	230.0	4.90	5.77
2.00 (1.725)	261.4	4.17	4.74
2.38 (1.820)	311.1	3.37	3.78
2.95 (1.956)	385.6	2.82	2.95

TABLE 6 Calculational conditions for few group constants.

Energy boundary of few groups		10 MeV—5.53 keV, fast group 5.53 keV—1.855 eV, epi-thermal group 1.855 eV—0 eV, thermal group
Temperature		20°C
Fast and epi-thermal groups	Number of groups	50
	Spatial dependence	Bl approximation
	Slowing down model	Greuling-Goerzel approximation for H, Consistent age approximation for other nuclides
	Resonance escape probability	L-factor : Strawbridge's procedure for ^{238}U, : 1.0 for other nuclides
Thermal group	Number of groups	35
	Scattering model	Nelkin with transport correction
	Cell boundary condition	Isotropic scattering

TABLE 7 Atomic number densities.

Fuel Unit : $\times 10^{24} cm^{-3}$

Nuclide \ Fuel type	26PA·UO_2	PuO_2-UO_2	JP-II·UO_2
^{235}U	6.086×10^{-4}	1.062×10^{-4}	6.086×10^{-4}
^{238}U	2.255×10^{-2}	1.460×10^{-2}	2.262×10^{-2}
^{239}Pu		4.632×10^{-4}	
^{240}Pu		4.305×10^{-5}	
^{241}Pu		4.257×10^{-6}	
^{242}Pu		2.523×10^{-7}	
O	4.725×10^{-2}	3.044×10^{-2}	4.646×10^{-2}

Cladding

Nuclide	Zircaloy-2	Aluminum
Zr	4.217×10^{-2}	
Fe	9.917×10^{-5}	
Cr	7.418×10^{-5}	
Ni	4.013×10^{-5}	
Al		6.034×10^{-2}

Moderator

Nuclide	Water
H	6.676×10^{-2}
O	3.338×10^{-2}

TABLE 8 Few group constants.

Region		26PA·UO_2 lattice	PuO_2–UO_2 lattice				JP-II·UO_2 lattice				H_2O
Water-to-fuel volume ratio		1.83	1.76	2.00	2.38	2.95	1.76	2.00	2.38	2.95	
Fast (10 MeV～5.53 keV)	D_1	1.432	1.608	1.592	1.601	1.578	1.433	1.440	1.458	1.466	1.508
	Σ_{a1}	0.003454	0.002744	0.002598	0.002418	0.002191	0.003502	0.003308	0.003060	0.002755	0.0002317
	Σ_{r1}	0.04719	0.04467	0.04655	0.04941	0.05224	0.04622	0.04818	0.05079	0.05365	0.07281
	$\nu\Sigma_{f1}$	0.004307	0.003495	0.003272	0.002979	0.002614	0.004374	0.004114	0.003767	0.003327	0.0
	Σ_{f1}	0.001543	0.001211	0.001133	0.001031	0.000904	0.001568	0.001473	0.001347	0.001188	0.0
Epi-thermal (5.53 keV～1.855 eV)	D_2	0.7004	0.7574	0.7420	0.7231	0.7022	0.7090	0.6985	0.6856	0.6710	0.6071
	Σ_{a2}	0.02163	0.02131	0.01999	0.01828	0.1612	0.02268	0.02129	0.01945	0.01714	0.0006211
	Σ_{r2}	0.08878	0.08626	0.09197	0.1000	0.1088	0.08580	0.09176	0.09963	0.1087	0.1681
	$\nu\Sigma_{f2}$	0.01058	0.01393	0.01298	0.01178	0.01028	0.01076	0.01001	0.009051	0.007884	0.0
	Σ_{f2}	0.004355	0.004960	0.004621	0.004192	0.003658	0.004432	0.004123	0.003728	0.003247	0.0
Thermal (1.855 eV～0.0 eV)	D_3	0.2899	0.3066	0.2908	0.2719	0.2515	0.2997	0.2847	0.2668	0.2473	0.1564
	Σ_{a3}	0.08735	0.1374	0.1292	0.1181	0.1044	0.08974	0.08602	0.08070	0.07362	0.01906
	$\nu\Sigma_{f3}$	0.1388	0.2241	0.2101	0.1906	0.1659	0.1437	0.1359	0.1249	0.1103	0.0
	Σ_{f3}	0.05683	0.07871	0.07379	0.06699	0.05832	0.05885	0.05566	0.05114	0.04519	0.0

TABLE 9 Effect of increasing vertical reflector saving δ_z on calculated effective multiplication factor k_{eff}.

Fuel type	Water-to-fuel volume ratio	Core height, cm	Δk_{eff} due to $\Delta\delta_z=0.1$ cm
PuO_2–UO_2	1.76	68.72	1.2×10^{-4}
	2.00	68.15	1.2
	2.38	69.28	1.0
	2.95	69.26	1.0
JP-II·UO_2	1.76	75.88	0.9
	2.00	68.80	1.2
	2.38	80.85	0.7
	2.95	66.53	1.1
26PA·UO_2	1.83	137.22	1.0

TABLE 10 Water gap effect on effective multiplication factor k_{eff}.

Core name	Experiment				Calculation	
	Water gap width, cm	Number of driver fuels	Critical water level, cm	Temperature, °C	k_{eff}	Δk_{eff}
1.76 Pu	0.058 2.014	288 268	68.72 67.84	18.9 12.3	0.9993 0.9971	0.0022
1.76 U	0.058 2.014	288 284	75.88 72.13	21.0 12.9	0.9974 0.9961	0.0013
2.95 Pu	0.0 1.956	244 236	69.26 69.14	20.4 12.8	1.0026 1.0031	−0.0005
2.95 U	0.0 1.956	276 292	66.53 69.55	20.0 11.0	0.9985 0.9988	−0.0003

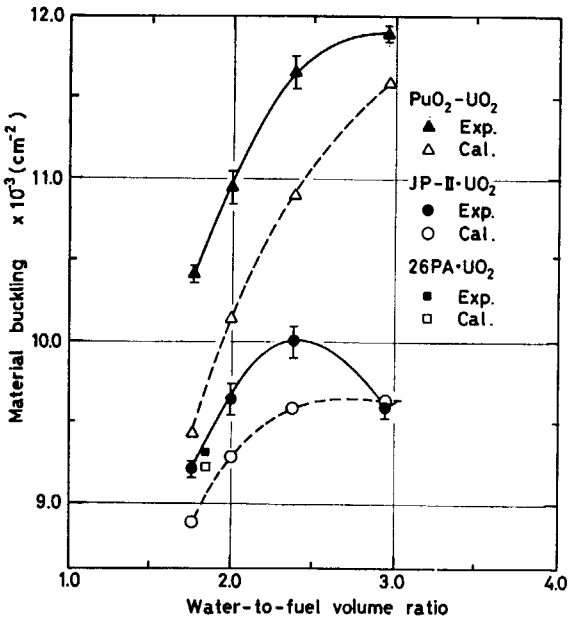

Fig. 7 Material bucklings of PuO_2-UO_2, JP-II·UO_2, and 26PA·UO_2 fuel lattices.

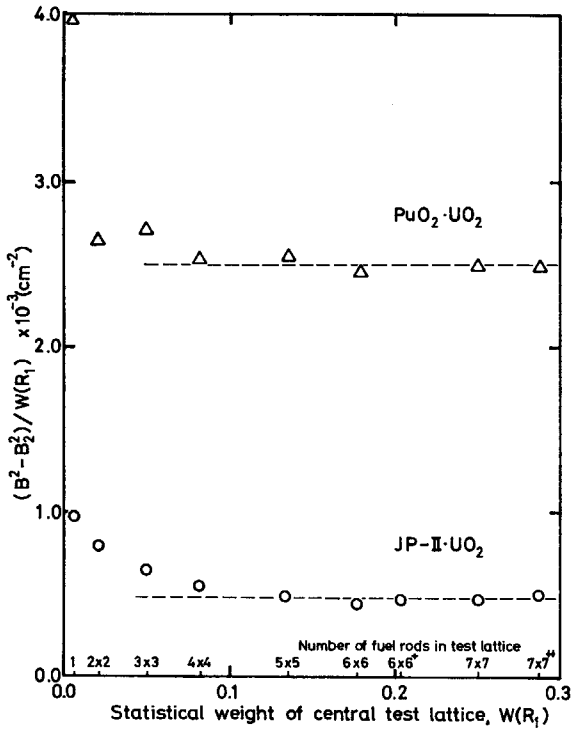

Fig. 8 Material bucklings measured in several sizes of test lattice.

Material buckling B_m^2 is obtained by

$$B_m^2=\frac{B^2-B_2^2}{W(R_1)}+B_2^2.$$

The number of the fuel rods loaded on outer boundary of the driver region was 19×19 arrays for odd combination of the fuels in the test region and 20×20 arrays for even combination. The test lattices of 6×6$^+$ and 7×7^{++} have 18×18 and 17×17 arrays of the fuels, respectively, on the outer boundary of the driver region.

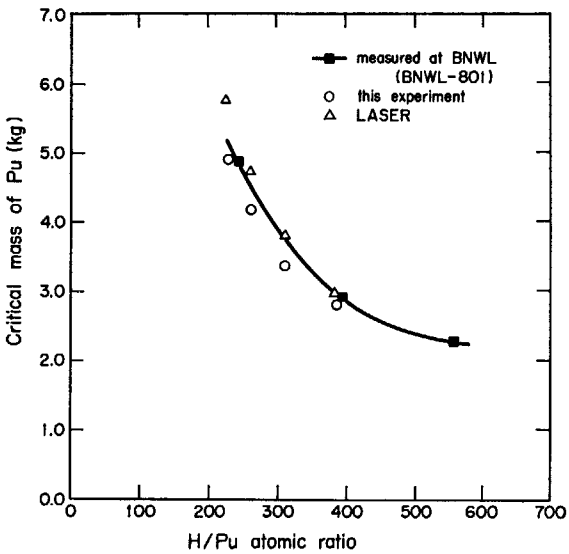

Fig. 9 Critical masses of mixed oxide fuels.

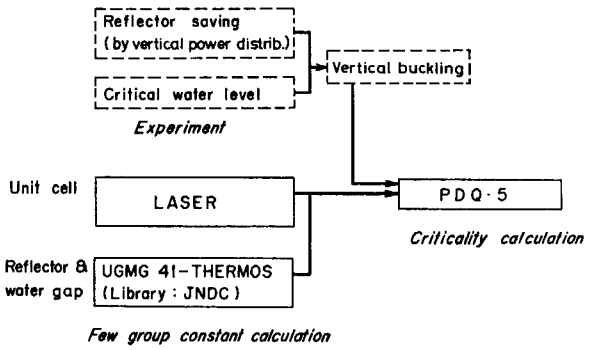

Fig. 10 Calculational scheme.

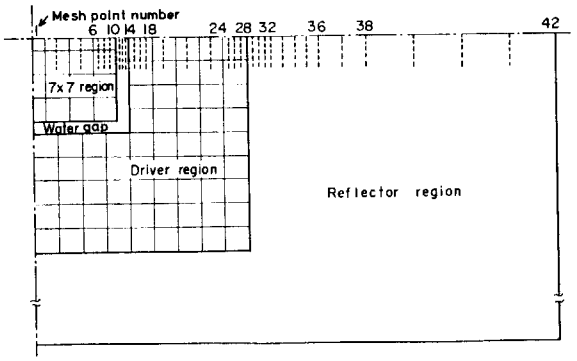

Fig. 11 Allocation of spatial meshes in 2.00 Pu core for two-dimensional diffusion calculation.

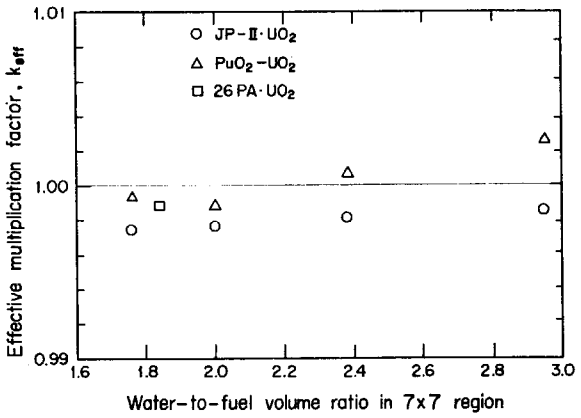

Fig. 12 Calculated effective multiplication factors. Calculated values correspond to measured values of 1.0000 ± 0.0004.

Case no.	No. of meshes	Calculated Keff
1	42x42	0.9986
2	38x38	0.9989
3	31x31	0.9995
4	24x24	0.9986
5	22x22	0.9997

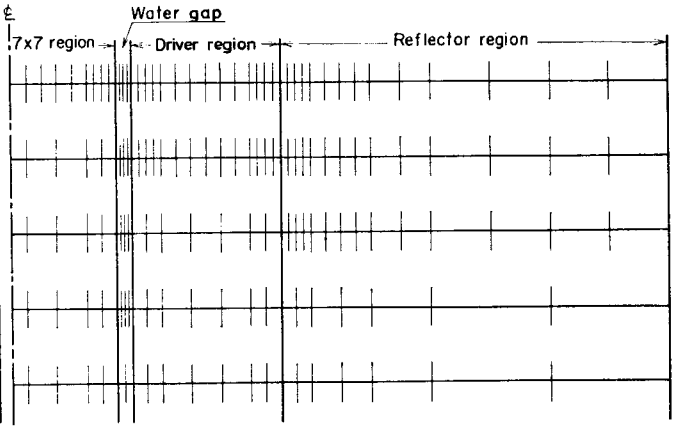

Fig. 13 Mesh effect on calculated effective multiplication factor for 2.00 Pu core.

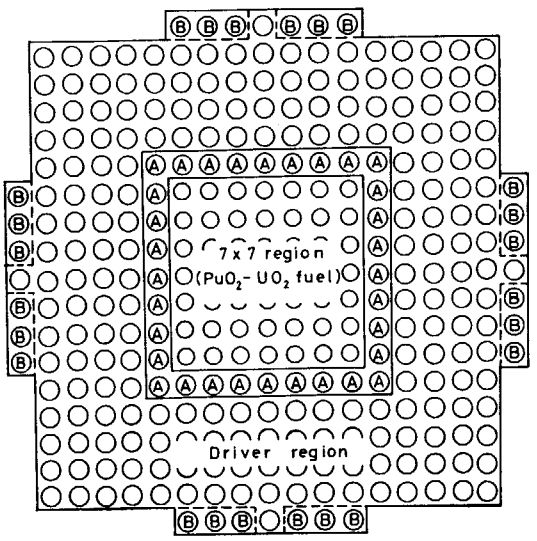

Without water gap: 26PA-UO_2 fuel rod at position A
With water gap: 26PA-UO_2 fuel rod at position B

Fig. 14 Configuration of 2.95 Pu core for analysis of water gap effect.

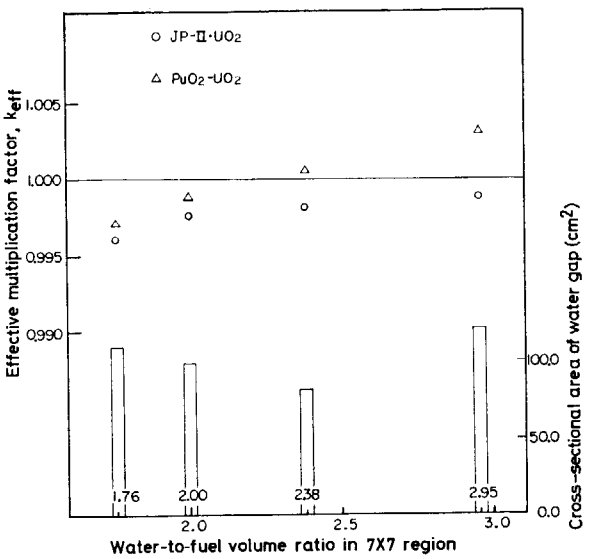

Fig. 15 Calculated multiplication factors of cores with water gap. Calculated values correspond to measured values of 1.0000 ± 0.0004.

4. Neutron flux distributions

4. 1 Measurements on neutron flux distributions

4. 1. 1 Method of activation traverses

The horizontal neutron flux distributions were obtained by activation traverses. The detectors used were small pellets of pure gold (hereafter described as Au pellet) with or without cadmium cover, and of aluminum-dysprosium alloy (hereafter described as Dy-Al pellet). The information on the epi-cadmium and the sub-cadmium neutron flux distributions and the spectral change in these cores were deduced from the activation travereses by the gold detector.

The detector pellets were planted in sample holders made of polymethylmetacrylate as shown in **Fig. 16**. The holder was set in cell moderator between fuel rods, so as to traverse the every core region, *i.e.* the 7×7, the water gap, the driver, and the reflector regions. The detector pellets were irradiated by about 400 W·min. After about 30 min of cooling time, the detector pellets were taken out of the core, then they were removed from the sample holder into counting holders which were small cups made of polymethylmetacrylate. The each counting holder was put in a well-type NaI(T*l*) scintillation counter, and the γ-ray activity was counted. The final activity results were obtained after making several corrections, which were regarding the background, the resolving time of the counting system, the time decay factor of activity, and the relative activation sensitivity of detector pellet. The sensitivity was assumed to be proportional to the weight of the detector pellet.

(1) Activation traversing by Dy-Al pellets

The Dy-Al pellet containing 10.5 wt% dysprosium was shaped into thin-short cylinder with 0.1 cm in diameter and 0.2 cm in length. The Dy-Al pellets were planted in three sample holders which were used to traverse the core at an irradiation since the lattice pitches in the 7×7 and in the driver regions were different. The three holders were fixed horizontally at the same height around the vertical mid position of the effective fuel zone. A typical example of detector positioning in the 2.00 U core is shown in **Fig. 17**. The detail dimensions of detector setting are shown in **Fig. 18** for each core. The γ-ray from ^{165}Dy (half-life: 139 min) were counted with the discrimination level of 30 keV.

(2) Activation traversing by Au pellets

The Au detector pellet of which purity was 99.993 wt% was also shaped into a small cylinder with 0.1 cm in diameter and 0.2 cm in length. The bare pellets were positioned for each a quarter interval of a lattice pitch in the west-side of the core, while the Cd-covered pellets were set in the opposite side for each a half lattice pitch. The typical example is shown in **Fig. 19** for the 2.00 U core. The cadmium covers were of 0.35 cm in outer-diameter, 0.28 cm in height and 0.05 cm in thickness. The equivalent cut-off energy by this cadmium cover was evaluated to be about 0.5 eV by the method in the Ref. 16. The discrimination level of γ-ray energy was fixed at 0.3 MeV so as to include the photo peak of 0.412 MeV from ^{198}Au. The cadmium ratios of the Au pellets in the lattices were derived by the following,

$$R_{cd}=N_{bare}/N_{cd} \tag{4.1}$$

where

N_{bare} : γ-ray activity of bare detector,

N_{cd} : γ-ray activity of Cd-covered detector.

The statistical errors on counting and on weighing were considered to be dominant among the sources of the error, therefore the relative error on the activity ratio of each detector pellet was estimated by the followings,

$$\sigma=\sqrt{\sigma_1^2+\sigma_2^2}, \tag{4.2}$$

$$\sigma_1=\sqrt{N}/N, \tag{4.3}$$

$$\sigma_2=\frac{1}{\overline{W}}\cdot\sqrt{\frac{\sum_{i=1}^{n}(W_i-\overline{W})^2}{n(n-1)}}, \tag{4.4}$$

where

σ_1 : relative standard error on counting,

σ_2 : relative standard error on weighing,

N : γ-ray counts,

n : repeating number of weighing for a pellet,

$\overline{W}$: average weight of the pellet weighed n times,

W_i : weight of the i-th weighing for the pellet.

The counting rate was 3,500~20,000 counts/30 sec for the bare Au and the Dy-Al pellets, and 1,600~3,500 counts/min for the Cd-covered pellets. The average weight of each pellet was obtained by weighing the pellet three times. The Au pellets which were around 30 mg were weighed by a balance having an accuracy of $\pm$0.02 mg. A finer balance having an accuracy of $\pm$0.003 mg was used for weighing the Dy-Al pellets, because their weights were around 4 mg.

4.1.2 Features of activation traverses

The measured results of the activation traverses by the Dy-Al and Cd-covered Au are shown in **Figs. 20** through **37**. with the corresponding calculated results. The measured results on the cadmium ratios are shown in **Figs. 38** through **46**. The experimental errors were estimated on the counting statistics and on the weighing accuracy by Eq. (4.2). The relative errors of the measured quantities were estimated to be less than 1.5% for the activity distributions by the Au and Dy-Al pellets and less than 3% for the cadmium ratios. The amounts of the errors are involved within the circles indicating the measured values in the figures.

Other sources of the experimental errors could be suggested. They were the neutron flux depression around and inside the detector pellet, and the neutron flux distortion due to the polymethylmetacrylate sample holder. The former effect was considered to be very small and neglected, because the measurement was to aim at the relative flux distribution. The latter effect was evaluated by carring out the supplemental experiment measuring the activity distributions of Dy-Al wires in a polymethylmetacrylate holder and in water through a lattice and a water gap regions. The water gap was made in the 26PA·UO_2 fueled core and its width was 3.9 cm. The cross-sectional dimension of the holder was 0.5×3.3 cm and considerably large compared with that of the holder used in the neutron density distribution measurement described in Section **4.1.1**. In this supplemental experiment, the depression rate of the activity by the holder was only 3.6% at the center of the water gap. Thus, the neutron flux distortion in the neutron density distribution was considered to be much less than above mentioned experimental errors and no correction was applied to the results, since the width of water gap was less than 1.8 cm and the cross sectional dimension of the holder was 0.3×1.5 cm.

The followings were observed from the measured reults.

(1) Activity distributions by Dy-Al

The activity distributions obtained by the Dy-Al pellets are understood as showing the distribution of thermal neutron density in the cores because of the 1/v cross-section characteristic of Dy. It is interesting in observing the measured results to compare the distribution in the Pu system with that in the U system, to watch the change of distribution with the water-to-fuel volume ratio, and to distinguish the difference between the UO_2 and the PuO_2-UO_2 7×7 lattices. The peak activity in the reflector of every core were selected as a reference level and the ratios of the averaged activity in the central 3×3 lattice to that of the peak activity in the reflector were examined. The ratios are plotted against water-to-fuel volume ratio in the 7×7 region in **Fig. 47.** The followings were observed on the activity ratios.

(i) The ratio increases as the increase of the water-to-fuel volume ratio for both cases of the U and the Pu systems.

(ii) The ratio in the U system is apparently larger than that in the Pu system under the same water-to-fuel volume ratio.

(iii) When a PuO_2-UO_2 lattice has the same atomic number of fissile materials as a UO_2 lattice, the water-to-fuel volume ratio in the PuO_2-UO_2 lattice should be much larger than that in the UO_2 lattice to get the same ratios as the U and the Pu systems. As an example, a PuO_2-UO_2 lattice of which water-to-fuel volume ratio is 2.95 has almost the same ratio as that of the UO_2 lattice of which water-to-fuel volume ratio is 2.00.

(2) Activity distributions by Au

The results on the sub-cadmium activity distributions indicated the similar features as those by the Dy-Al pellets. The epi-cadmium activity distributions had monotonous convex planes for all cores as shown in **Figs. 29** through **37**. The core with water gap around the 7×7 region seems to have a slightly flater distribution in the 7×7 region. This property is same in both of the Pu and the U systems.

(3) Distributions of cadmium ratio

The distributions of cadmium ratio minus 1.0 ($R_{cd}-1.0$) were almost flat in the central 3×3 lattice of the 7×7 region for all cores as shown in **Figs. 38** through **46**. The relation between $R_{cd}-1.0$ of the 7×7 region at the center and the water-to-fuel volume ratio is shown in **Fig. 48**. It shows that $R_{cd}-1.0$ increases monotonously and almost linearly with the water-to-fuel volume ratio. This inclination was similar for the both lattices of the U and the Pu systems. The quantities of $R_{cd}-1.0$ in the UO_2 lattice, however, were about 1.6 times larger than those in the PuO_2-UO_2 lattice.

The value of $R_{cd}-1.0$ in the uniform UO_2 lattice (1.83TU core) agreed well with that in the U system.

The driver and the 2.95Pu lattices had the almost same cadmium ratio and the activity distribution was continuous throughout these two regions like as in an uniform lattice.

4.2 Analysis on neutron flux distributions

4.2.1 Correlations of measurements and calculations

(1) Activity distributions by thermal neutrons

The measured activity distributions obtained by the Dy-Al are understood to express the relative thermal neutron density distributions. When the one-to-one correspondence between distributions of the measured activity and the calculated neutron flux is tried, firstly the calculated thermal neutron flux should be converted to the thermal neutron density, secondly the positional difference between the setting point of the detector and the mesh point in the calculation should

be taken into account, and thirdly the activity and the neutron density should be normalized to make the direct comparison possible.

The neutron flux $\phi(v)$ is connected with the neutron density $N(v)$ and the neutron velocity v under the relation of

$$\phi(v)=N(v)\cdot v. \tag{4.5}$$

Therefore, the thermal neutron density was obtained by dividing the thermal flux resulted from the diffusion calculation by the thermal neutron velocity obtained from the fuel cell calculation. The thermal neutron velocity depends on the position in the fuel cell. The average velocity $\bar{v}$ of the thermal group on the fuel cell boundary was used for converting the neutron flux to the neutron density, because the detector pellets were set on the fuel cell boundary. The fuel cell calculation were performed for the cylindrical geometry, while the shape of the actual fuel cells were square. But the differences on the average velocity due to the geometrical difference were neglected.

Second factor to be noticed was that the neutron density obtained by the above procedure indicated the average value in the fuel cell, while the measured neutron density corresponded to that on the fuel cell boundary. Therefore, the calculated neutron flux ϕ should have been corrected by the ratio d of the neutron flux ϕ_b on the fuel cell boundary to the neutron flux ϕ_{av} averaged in the fuel cell. Namely, the calculated neutron density on the cell boundary was deduced by

$$N=\frac{\phi\cdot d}{\bar{v}}. \tag{4.6}$$

The numerical values of d and $\bar{v}$ are listed in TABLE 11.

The average values of the measured and calculated neutron densities across the 7×7 region were normalized to unity as follows. The calculated relative neutron density was obtained by

$$N_i^{nor}=\frac{\phi_i}{\bar{v}_i}\cdot d_i \Big/ \frac{\sum_{i=1}^{n}\frac{\phi_i}{\bar{v}_i}\cdot d_i\cdot l_i}{\sum_{i=1}^{n} l_i}, \tag{4.7}$$

where

N_i^{nor} : normalized thermal neutron density at mesh point i,
ϕ_i : thermal neutron flux at mesh point i,
$\bar{v}_i$: Neutron velocity at the cell boundary of a region which includes mesh point i,
d_i : ratio of the neutron flux at mesh point i on the fuel cell boundary to the neutron flux averaged in the fuel cell,
l_i : mesh width,
n : total number of mesh points along correlating direction in the 7×7 region.

On the otherhand, the normalization was made for the measured relative neutron densities by,

$$A_j^{nor}=A_j \Big/ \frac{\sum_{j=1}^{m} A_j\cdot L_j}{\sum_{j=1}^{m} L_j}. \tag{4.8}$$

where

A_j^{nor} : normalized relative thermal neutron density at position j,
A_j : measured activity at position j,
L_j : interval represented by measured point j,
m : total number of measured points along correlating direction in the 7×7 region.

(2) Epi-thermal neutron flux distributions

Calculated distributions of epi-thermal neutron flux were compared with the Cd-covered Au activity distributions. The calculated epi-thermal flux was that of the second group in the few group diffusion calculation and had the energy range of 1.855eV to 5.5keV. The experimental epi-thermal flux was obtained from the activity of the Cd-covered Au which were irradiated by above 0.5eV neutron. The measured epi-thermal flux could be considered as almost as that of 4.9eV, because ^{198}Au has a giant resonance absorption at that energy.

4. 2. 2 Remarks on correlations

(1) Thermal neutron density distributions

The comparisons between the measured and calculated neutron densities are shown in **Figs. 20** through **28**.

The both distributions of the measured and the calculated neutron densities were normalized in the 7×7 region and correlated each other. Mean deviations of the theoretical results from the experimental ones in each region are listed in **Table 12**. The deviations in the driver region were less than 3% except the 2.95U core and its dependence on the water-to-fuel volume ratio were not recognized. In the reflector region, the deviations became smaller as the water-to-fuel volume ratio increased. The deviations in the multi-regional cores were, however, considerably great and were in the range from −3% to −16%. No distinct tendencies of the deviations were observed between two kinds of the fuels loaded in the 7×7 region.

On the uniform lattice core (1.83TU), the deviations in the reflector region was 2% and less than in the multi-region cores.

The deviations over the core were not affected by the presence of the water gap having the width less than 1.8cm, because the deviations in the driver regions of the core with the water gap were not so changed compared with that of the core without the water gap.

On the uranium fueled cores, the deviations in the reflector regions of the multi-regional cores were greater than that of the uniform lattice core. This means that the few group constants and other parameters $\bar{v}_i$ and d have some ambiguities in the water gap and the regions near the boundary.

(2) Eqi-thermal neutron flux distributions

The calculated neutron flux distributions were in good agreement with the experimental values. The normalizations of the measured and calculated distributions were made with the averaged flux levels in the 7×7 region, respectively. Comparisons between the experimental and theoretical values are shown in **Figs. 29** through **37**. In the water gap and the reflector regions, however, the calculation underestimated the distribution slightly. This cause was due to the difference of cut-off energies for the epi-thermal neutron between the experiment and calculation. They were about 0.5eV and 1.855eV, respectively, and the measured values were affected by the peaking of thermal neutron in water.

(3) Cadmium ratios

The relation between the cadmium ratios in the central 3×3 lattice and the cross-section ratio of the epi-thermal slowing down to the thermal absorption, Σ_{r2}/Σ_{a3}, were examined. In an infinite uniform medium, the ratio Σ_{r2}/Σ_{a3} is related to the ratio of the epi-thermal to the thermal neutron fluxes by the simple diffusion theory as

$$\frac{\Sigma_{r2}}{\Sigma_{a3}}=\frac{\phi_3}{\phi_2}. \tag{4.9}$$

Thus, the cadmium ratio has the following relation to the cross-section ratio as

$$\text{cadmium ratio} - 1.0 \propto \frac{\Sigma_{r2}}{\Sigma_{a3}}. \tag{4.10}$$

This relation is plotted with the experimental values in **Fig. 49**. A linear relationship exists between cadmium ratio−1.0 and the cross-section ratio over the U and the Pu systems.

It was noticed that the cadmium ratios and the cross-section ratios were nearly the same between the driver lattice and the 7×7 lattice of the 2.95Pu core, and the neutron density distributed smoothly through those lattices. Therefore, as an indication to get a neutron flux matching between those different regions, a cadmium ratio or a cross-section ratio Σ_{r2}/Σ_{a3} are suggested to be useful.

4.3 Summary on neutron flux distributions

The followings were summarized as the results of the study on the neutron density and flux distributions.

(1) The neutron density level in the 7×7 region relative to that in the driver region increases with the increase of the water-to-fuel volume ratio in the 7×7 region. The neutron densities distributed smoothly between the driver and the 7×7 regions of the 2.95Pu or the 1.76U core, and their lattices had a good neutron density matching. In those cases, the cadmium ratios were almost constant through the both regions.

(2) There were no distinct differences between accuracies of the calculated values for the multi-regional cores of the U and the Pu systems.

(3) However, the calculational accuracies for the multi-regional cores were worse than the uniform lattice core. This causes were considered due to the ambiguities in the few group constants and other parameters of the water gap and the regions near a boundary.

TABLE 11 Correction factors for neutron density distribution.

Region	Water-to-fuel volume ratio	Neutron speed at cell boundary, 2200 m/sec unit	Depression factor d
PuO_2-UO_2 lattice	1.76	1.650	1.113
	2.00	1.590	1.112
	2.38	1.521	1.109
	2.95	1.449	1.104
JP-II·UO_2 lattice	1.76	1.526	1.073
	2.00	1.484	1.074
	2.38	1.434	1.074
	2.95	1.382	1.072
26PA·UO_2 lattice	1.83	1.493	1.090
H_2O	—	1.149	1.000

TABLE 12 Difference between experimental and calculational thermal neutron density distributions.

Region / Core name	Difference; (Cal.−Exp.)/Exp., %			
	7×7 lattice	Water gap	Driver	Reflector
1.76Pu	0.0	—	−2.7	−12.7
2.00Pu	0.0	−3.7	1.2	−7.7
2.38Pu	0.0	−3.8	−0.6	−8.8
2.95Pu	0.0	—	−3.2	−8.7
1.76U	0.0	—	−0.9	−15.9
2.00U	0.0	−5.7	−3.4	−8.2
2.38U	0.0	2.9	3.2	−7.4
2.95U	0.0	—	11.9	−3.3
1.83TU	—		0.0	2.2

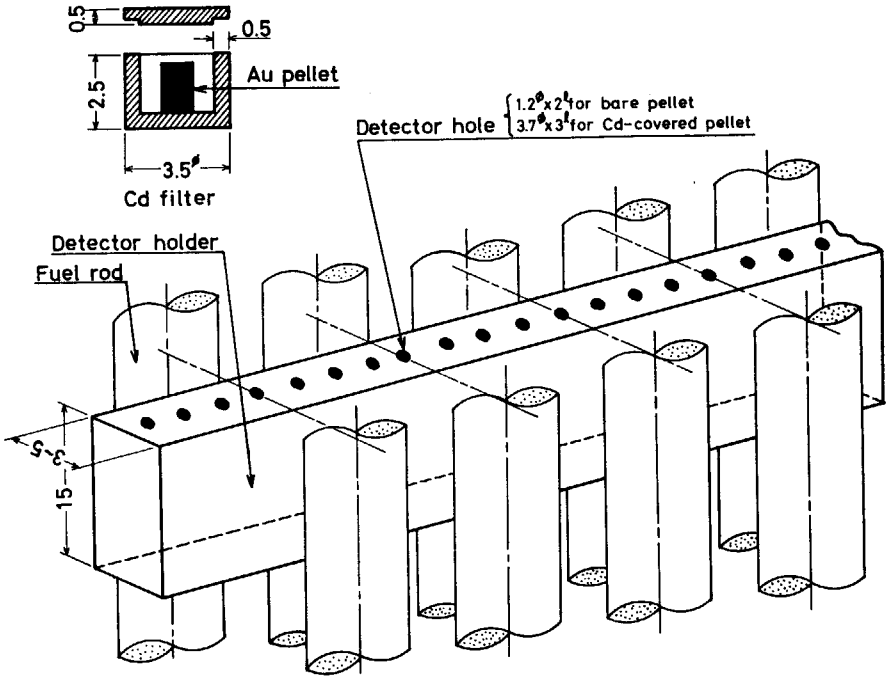

Fig. 16 Detector holder and cadmium cover for measurement of activity distributions.

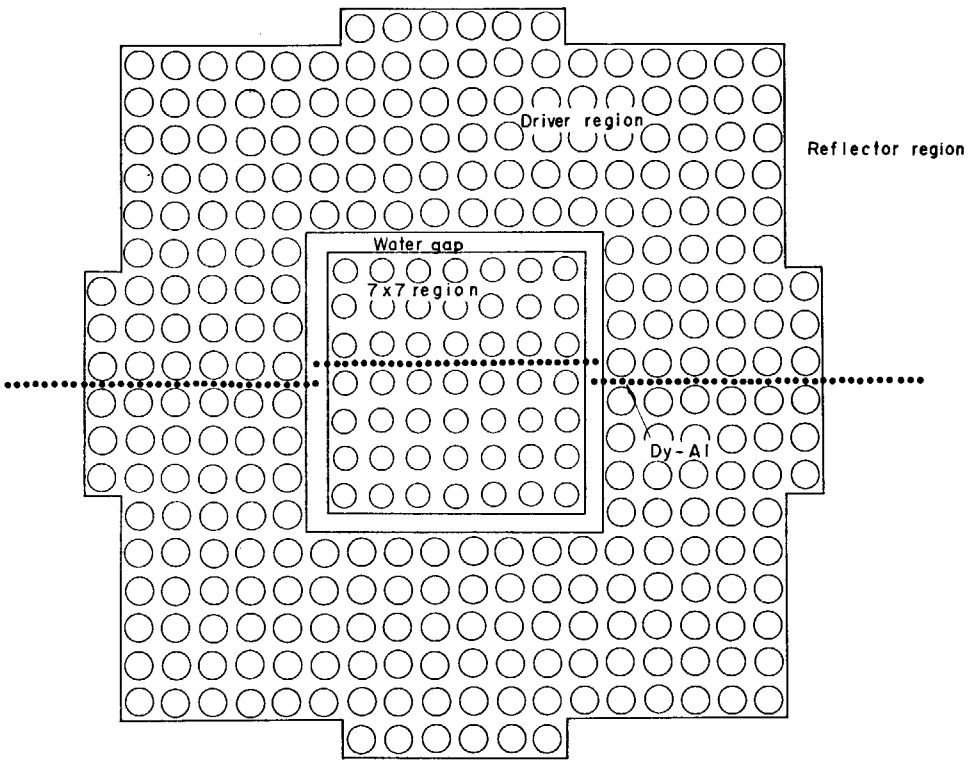

Fig. 17 Measured points of Dy activity in 2.00U core.

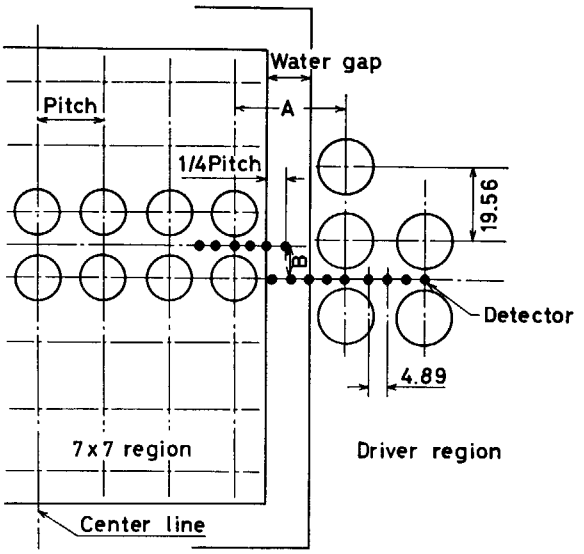

Volume ratio in 7x7 region	Width A mm	Width B mm	Water gap mm	7x7 region Pitch mm	7x7 region 1/4 Pitch mm
1.76	18.66	8.30	0.58	16.60	4.15
2.00	36.27	8.63	17.87	17.25	4.31
2.38	33.42	9.10	14.54	18.20	4.55
2.90	19.56	9.78	0	19.56	4.89

Fig. 18 Detail dimension of Dy-Al pellet setting.

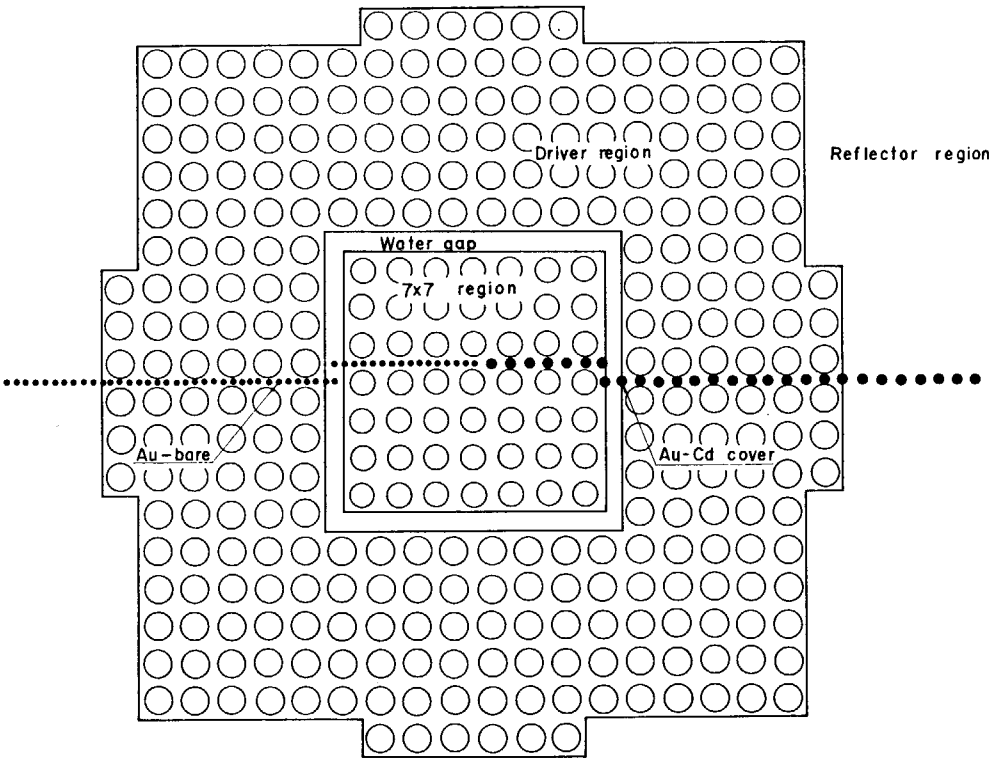

Fig. 19 Measured points of bare and Cd-covered Au activity in 2.00U core.

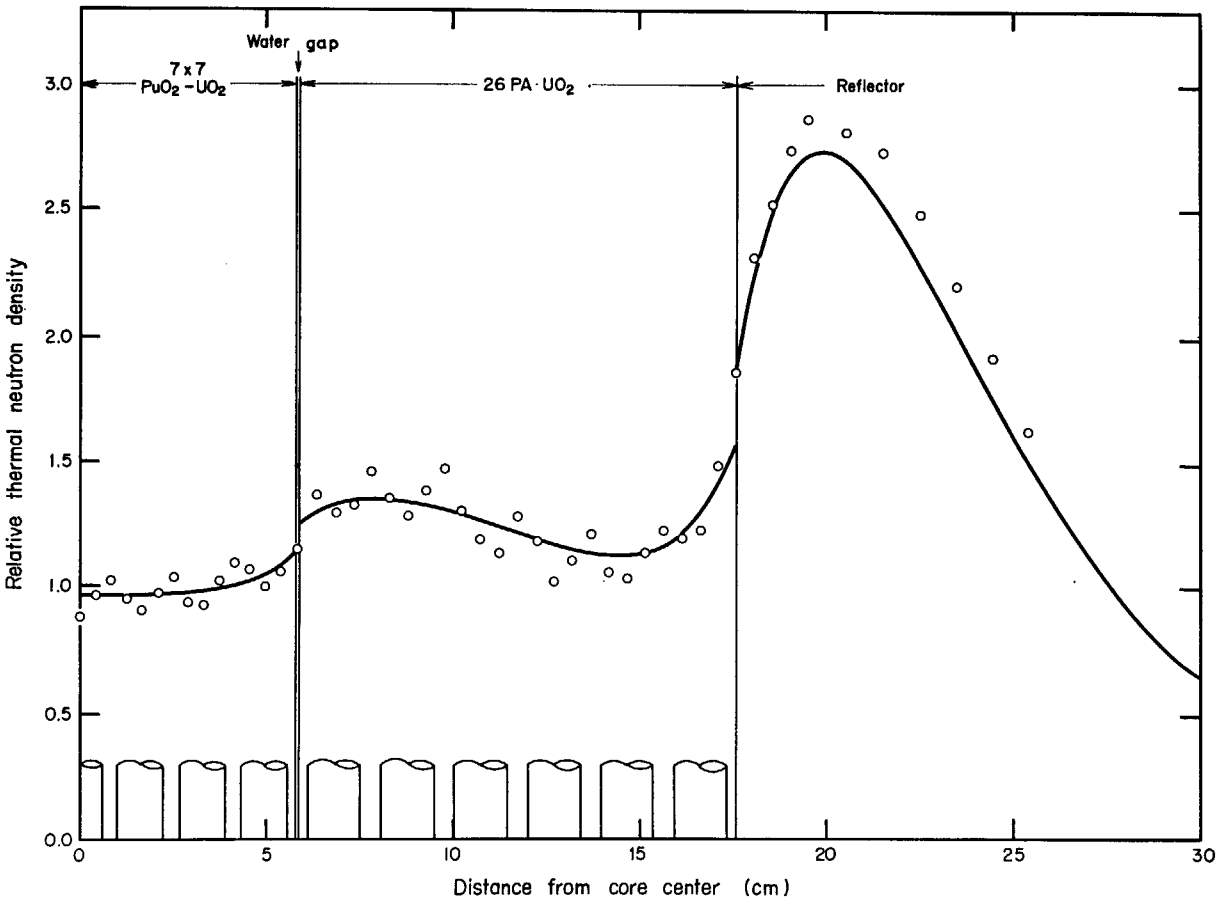

○: Measured with Dy, —: Calculated.

Fig. 20 Thermal neutron density distribution in 1.76Pu (RUN 3799) core.

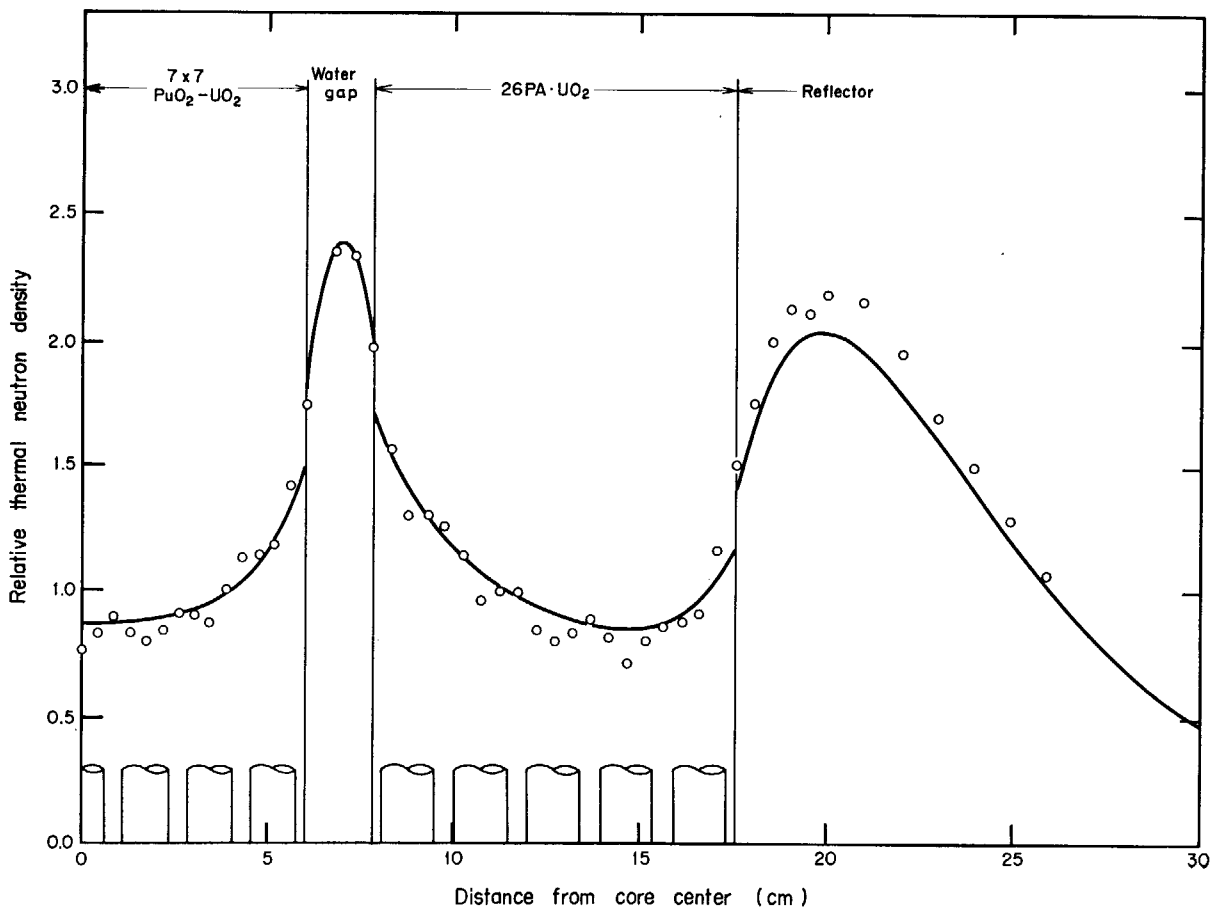

○: Measured with Dy, —: Calculated.

Fig. 21 Thermal neutron density distribution in 2.00Pu (RUN 3837) core.

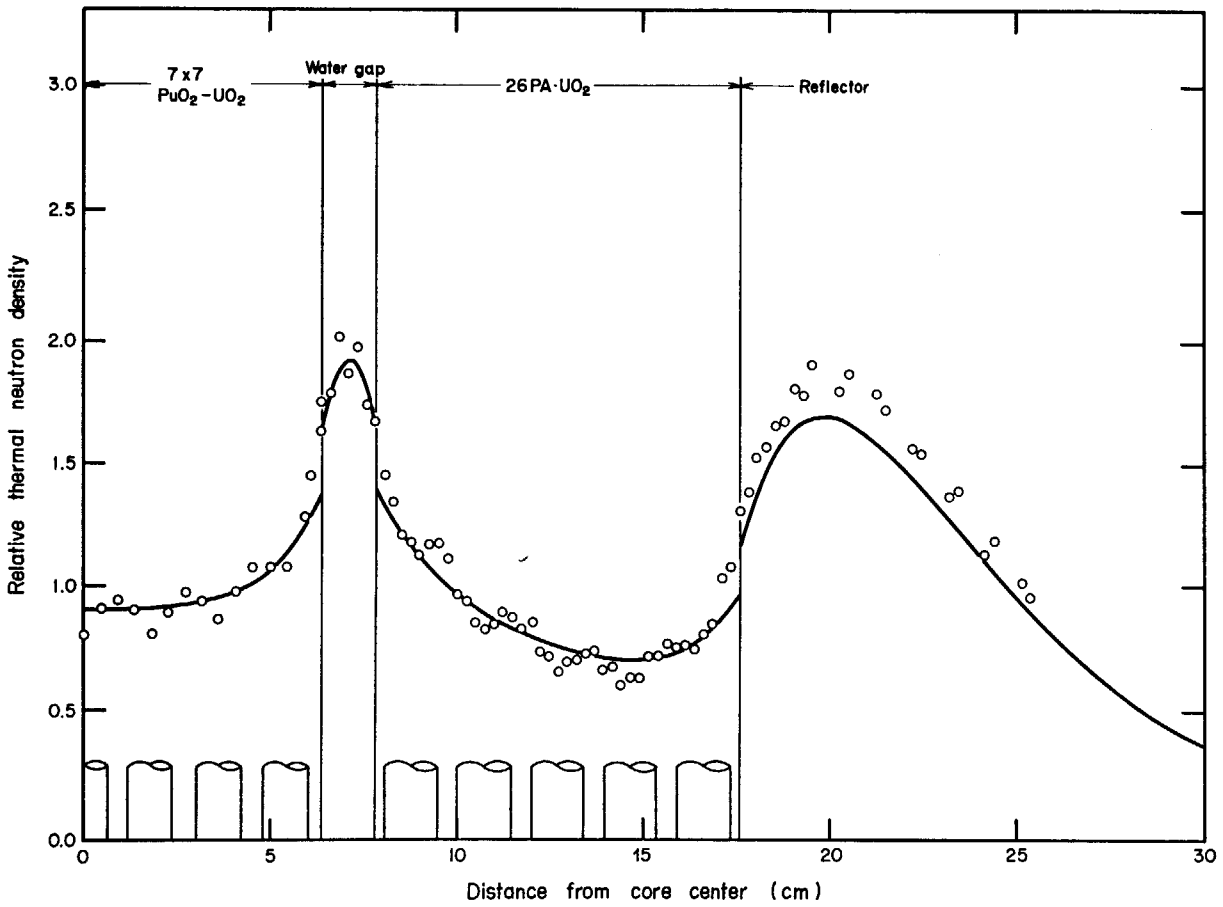

○: Measured with Dy, —: Calculated.
Fig. 22 Thermal neutron density distribution in 2.38Pu (RUN 3746) core.

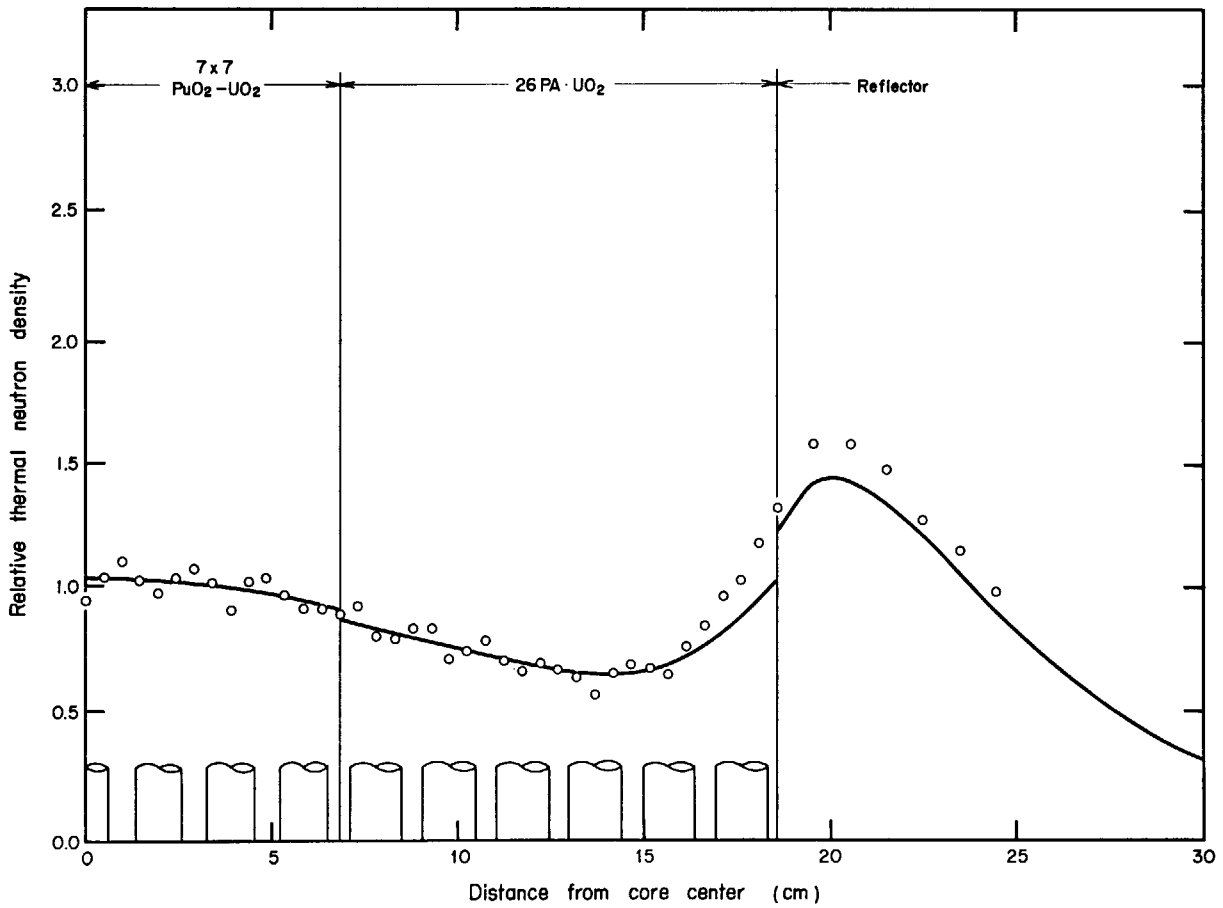

○: Measured with Dy, —: Calculated.
Fig. 23 Thermal neutron density distribution in 2.95Pu (RUN 3830) core.

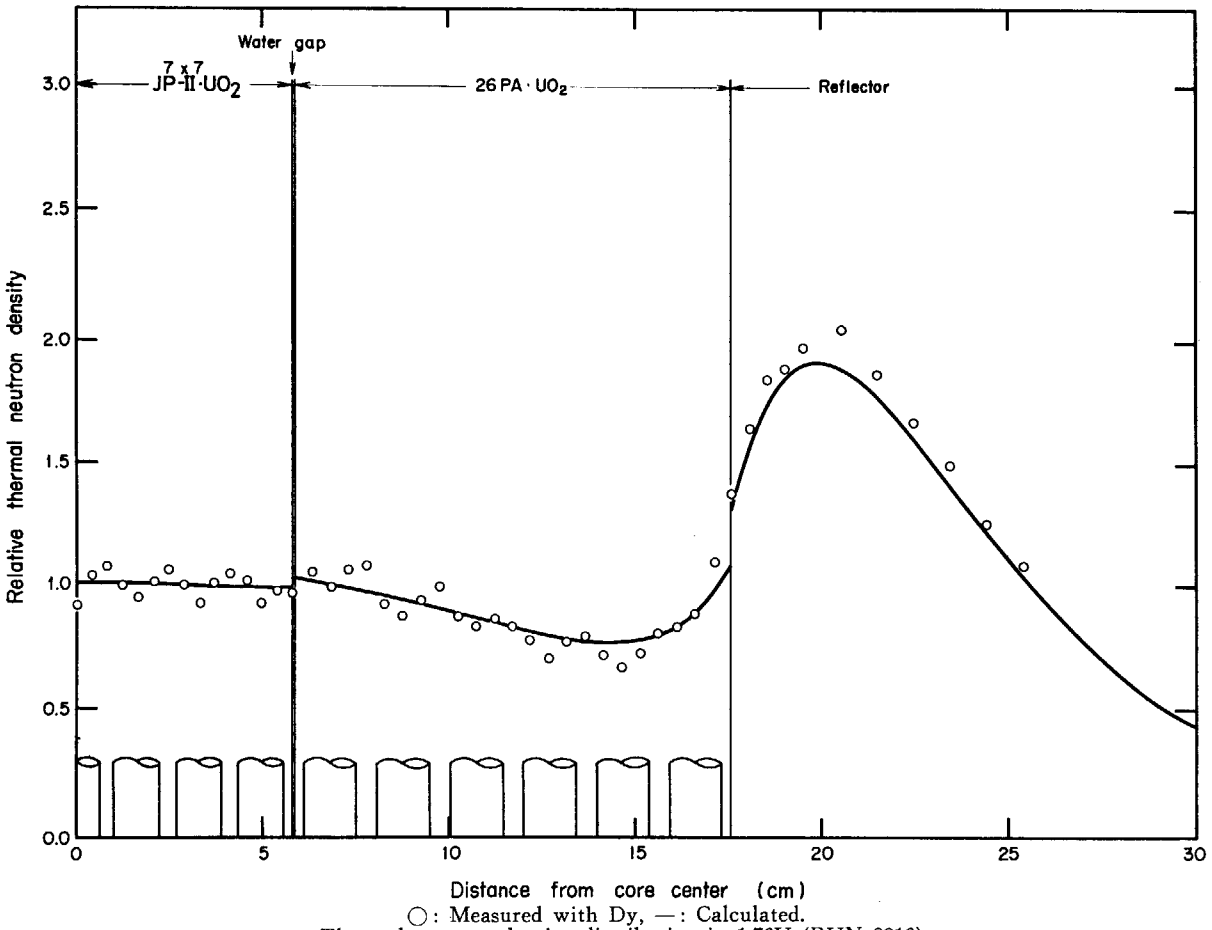

○: Measured with Dy, —: Calculated.
Fig. 24 Thermal neutron density distribution in 1.76U (RUN 3816) core.

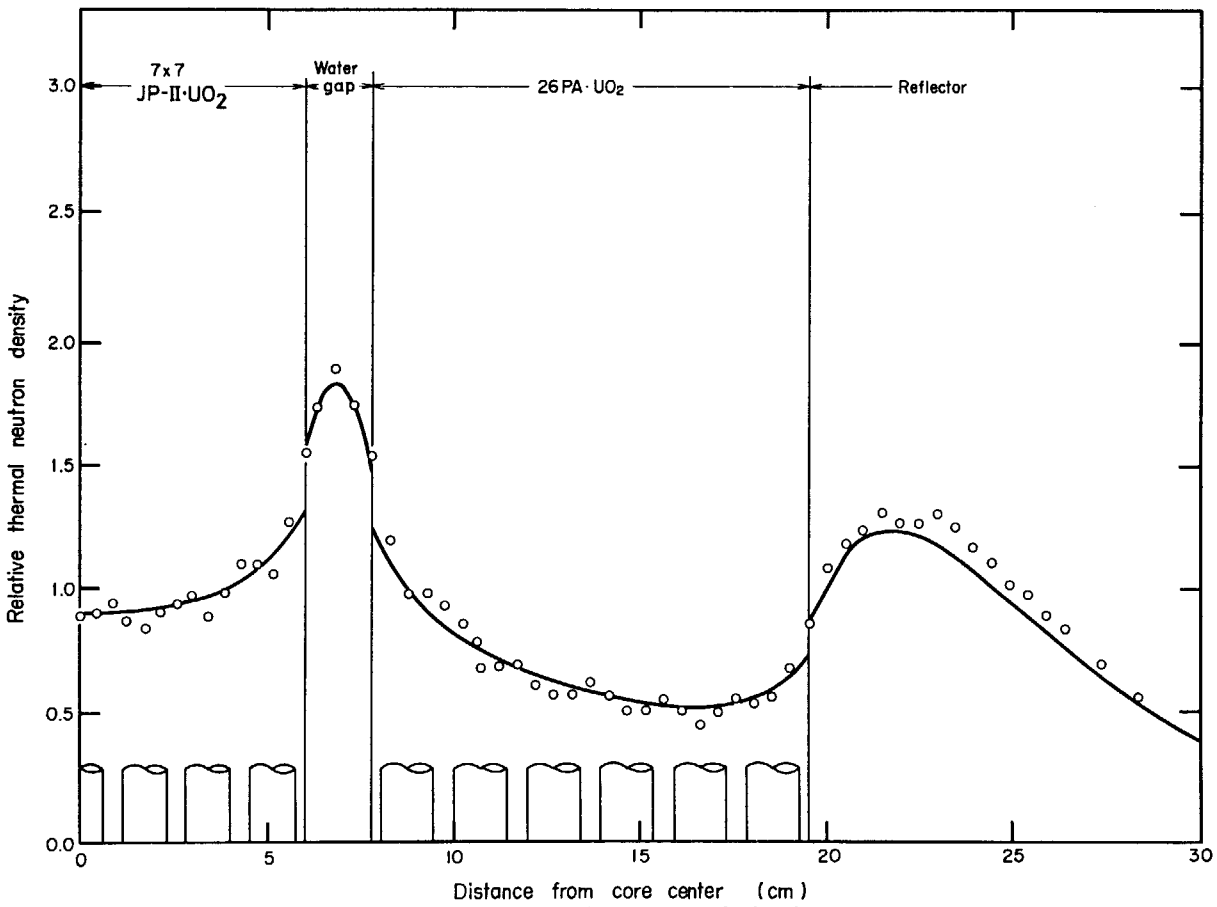

○: Measured with Dy, —: Calculated.
Fig. 25 Thermal neutron density distribution in 2.00U (RUN 3883) core.

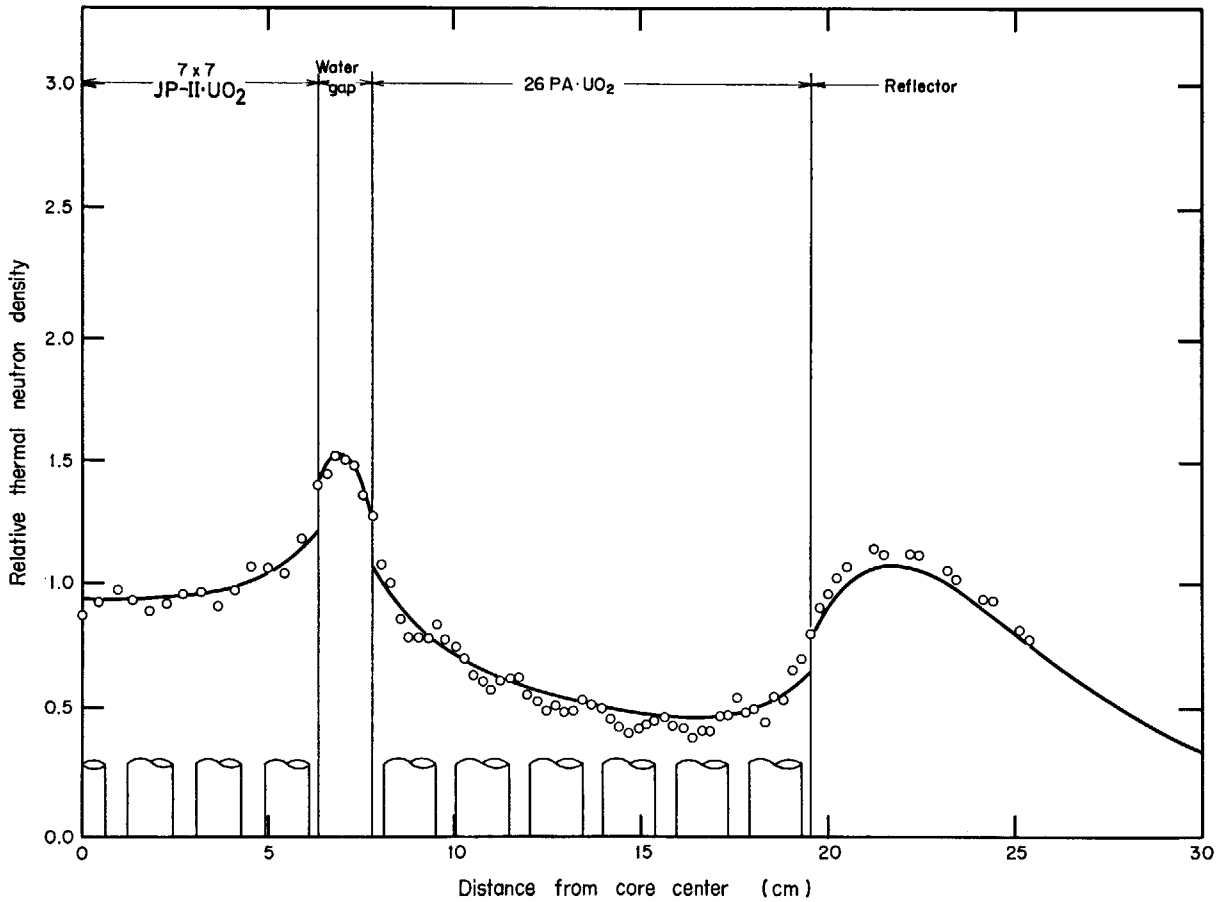

○: Measured with Dy, —: Calculated.
Fig. 26 Thermal neutron density distribution in 2.38U (RUN 3845) core.

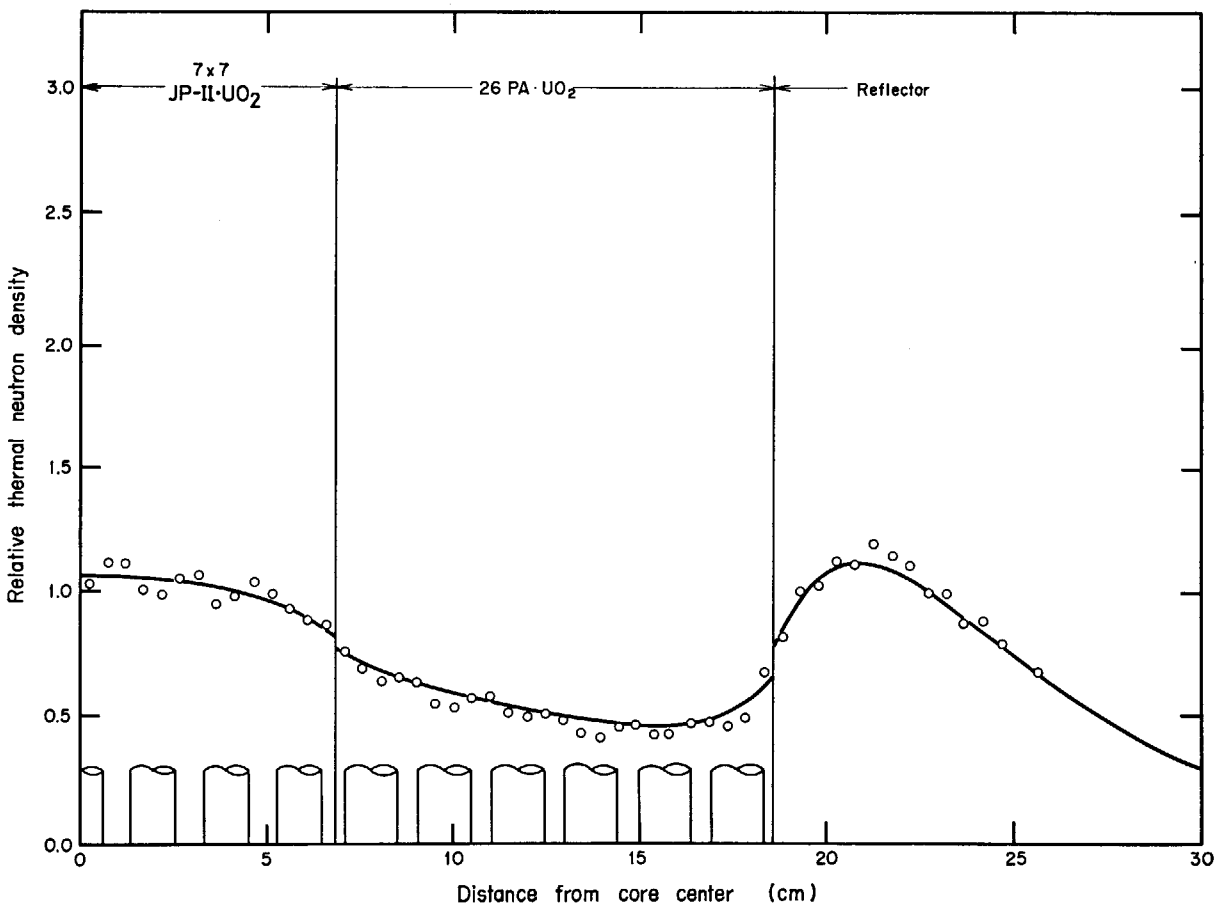

○: Measured with Dy, —: Calculated.
Fig. 27 Thermal neutron density distribution in 2.95U (RUN 3835) core.

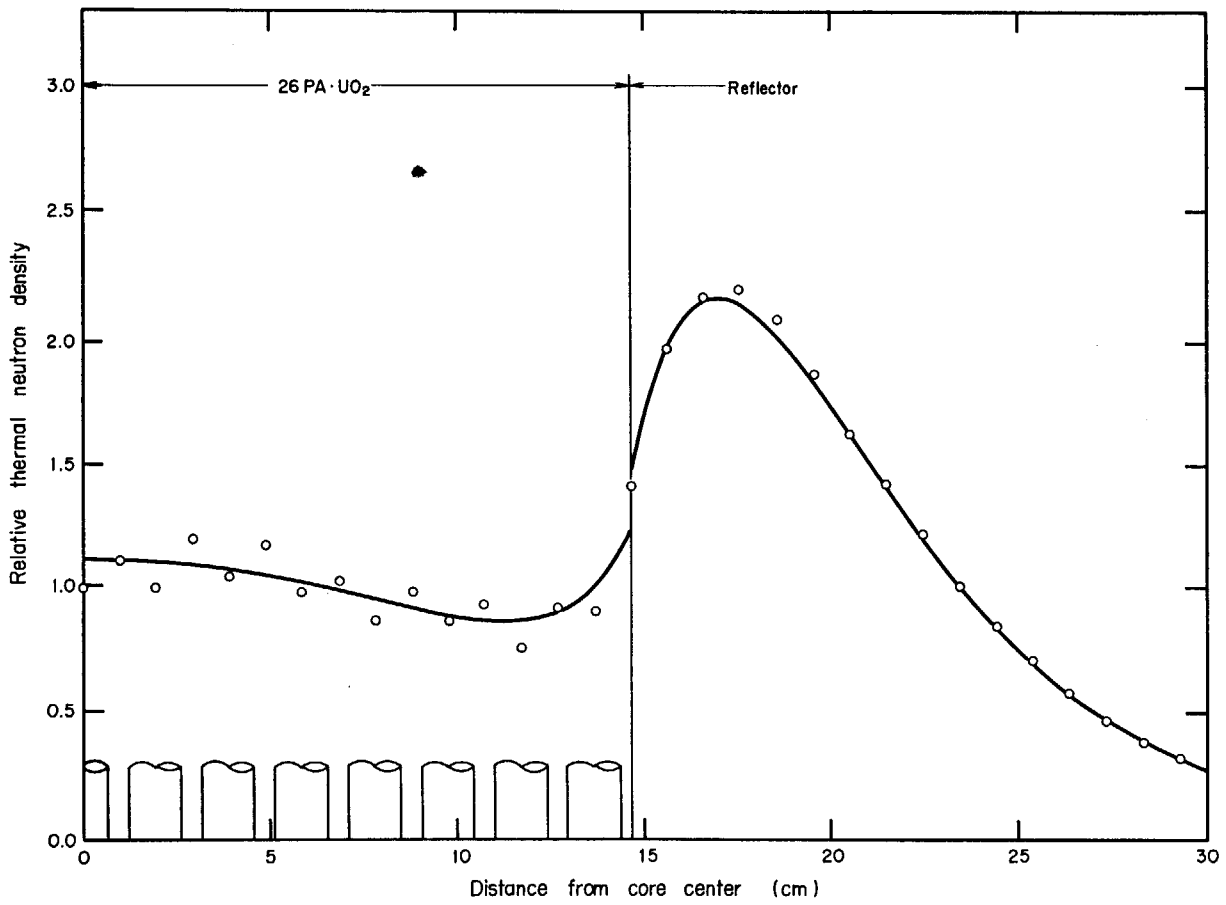

○: Measured with Dy, —: Calculated.

Fig. 28 Thermal neutron density distribution in 1.83TU (RUN 3872) core.

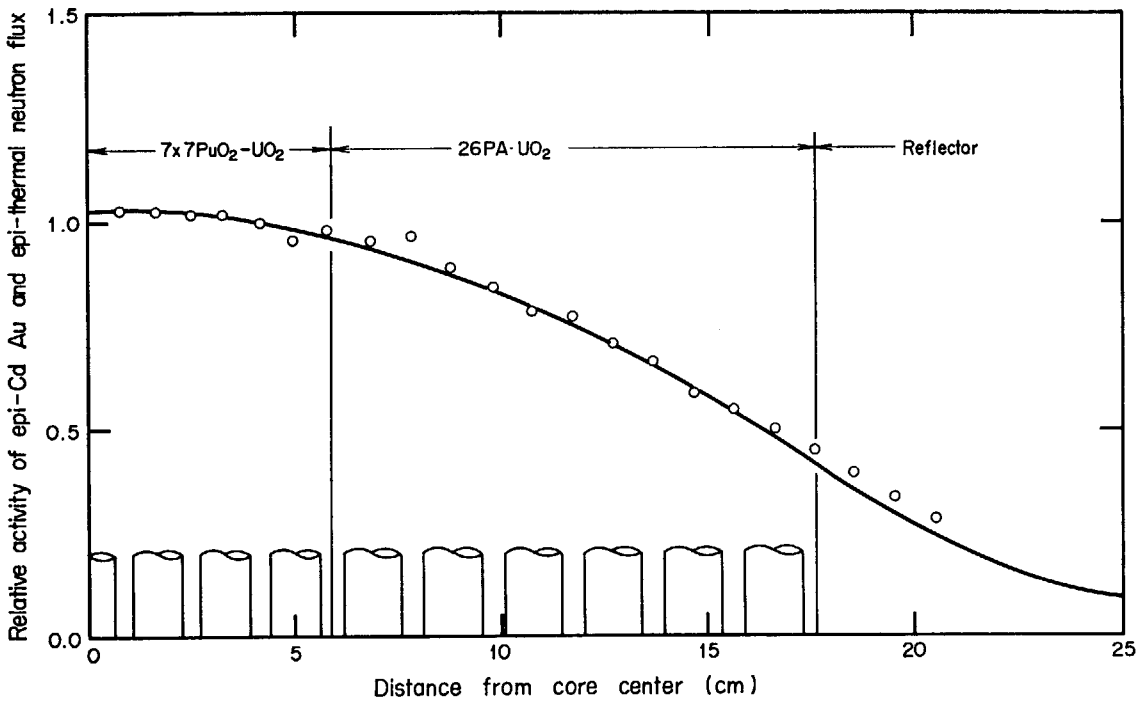

○: Measured, —: Calculated.

Fig. 29 Epi-thermal neutron flux distribution in 1.76Pu (RUN 3813) core.

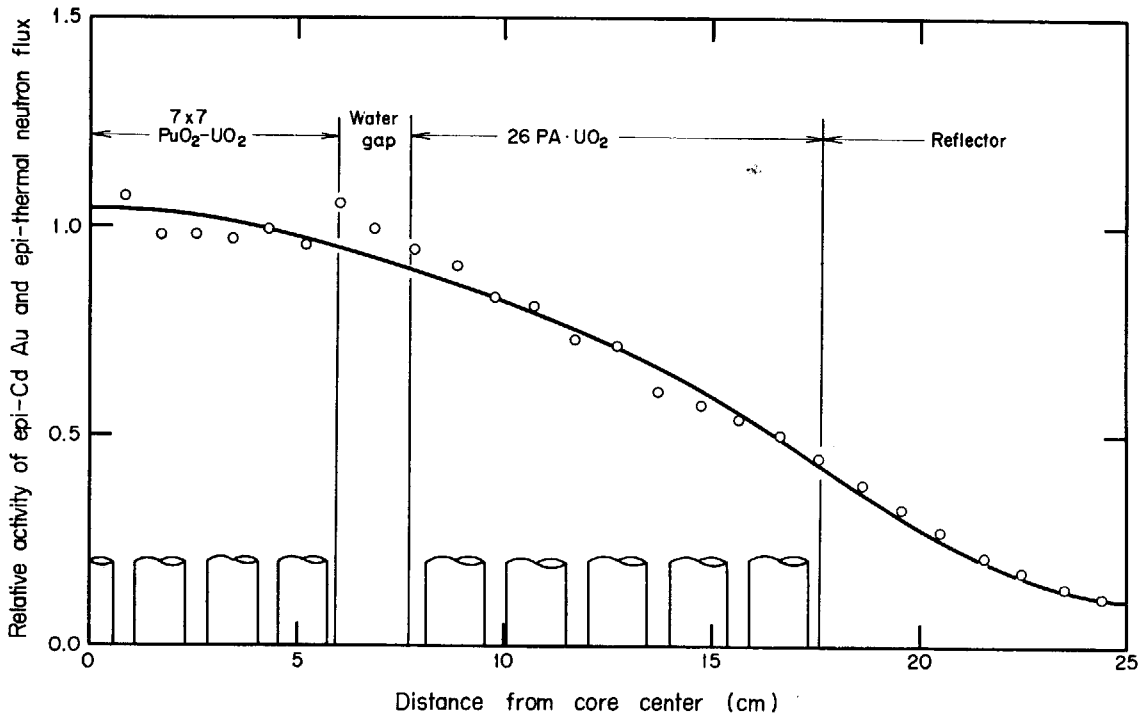

○: Measured, —: Calculated.

Fig. 30 Epi-thermal neutron flux distribution in 2.00Pu (RUN 3838) core.

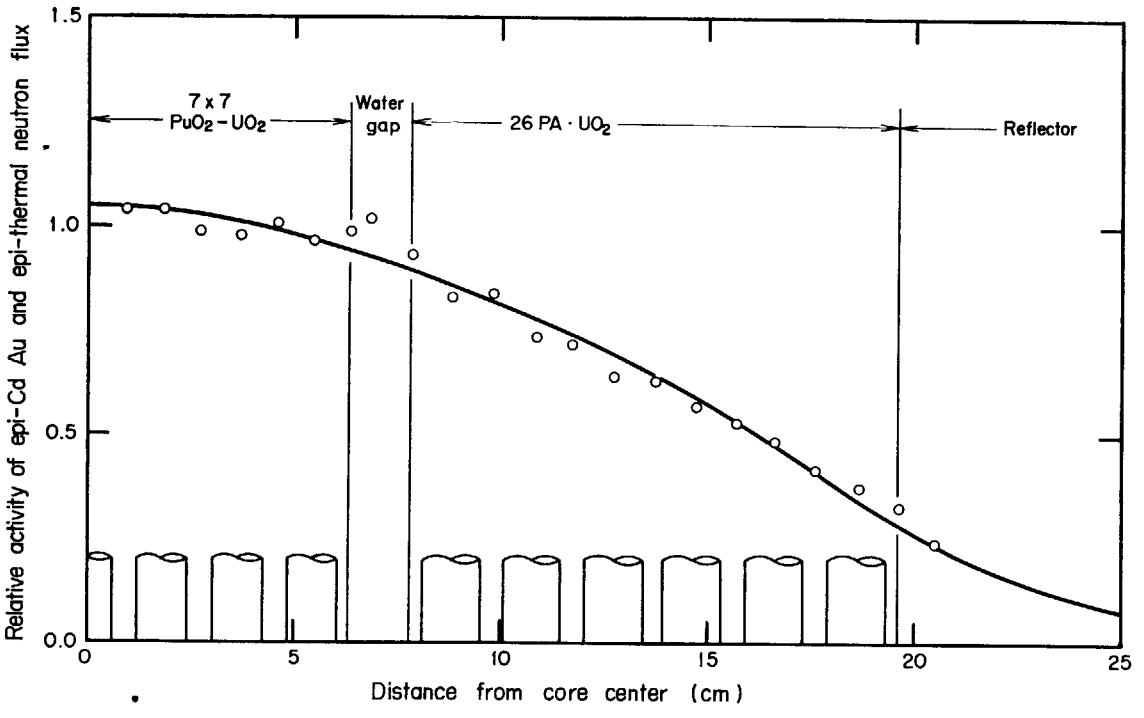

○: Measured, —: Calculated.

Fig. 31 Epi-thermal neutron flux distribution in 2.38Pu (RUN 3877) core.

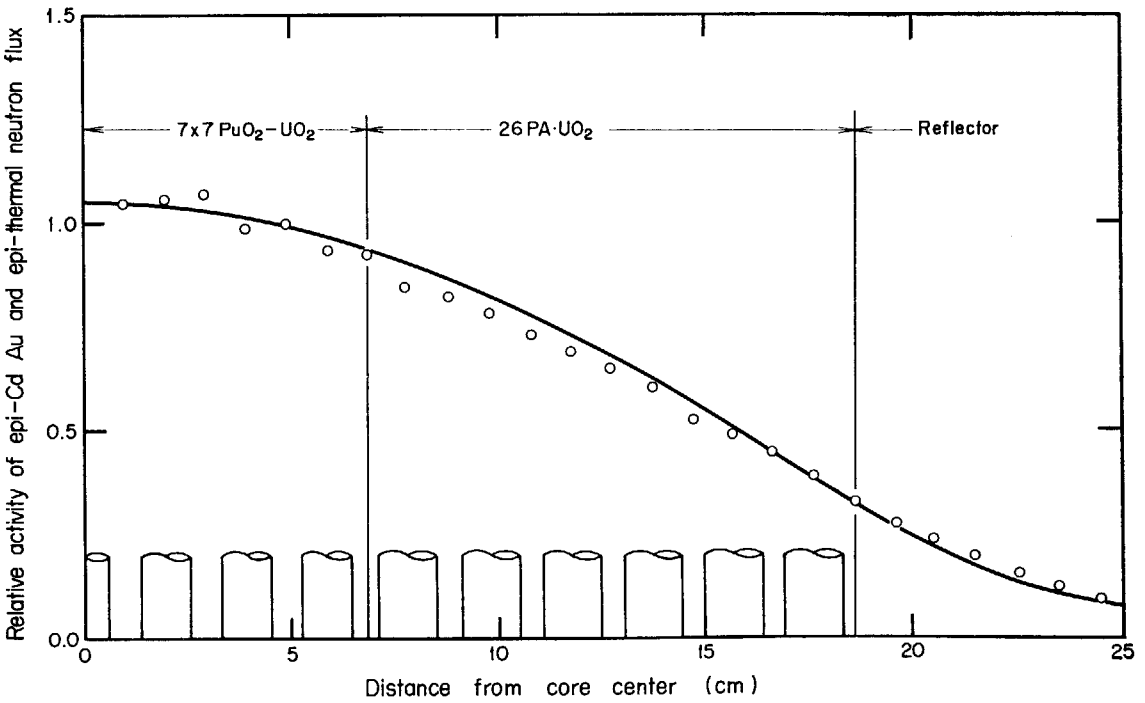

○: Measured, —: Calculated.

Fig. 32 Epi-thermal neutron flux distribution in 2.95Pu (RUN 3831) core.

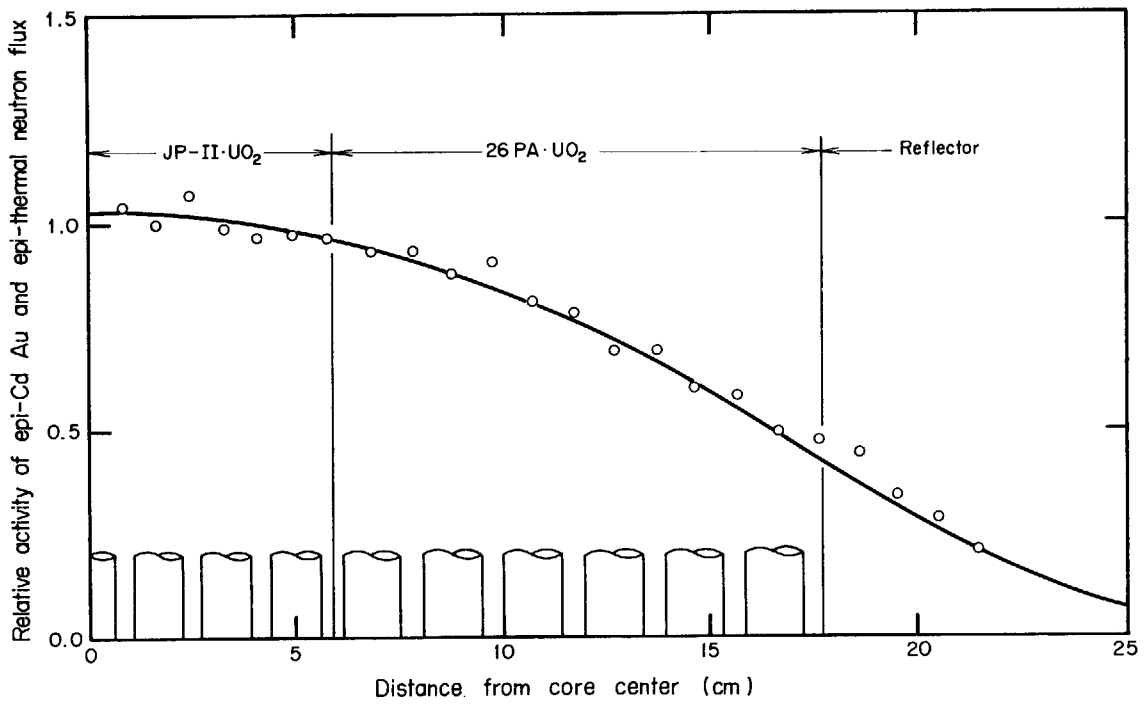

○: Measured, —: Calculated.

Fig. 33 Epi-thermal neutron flux distribution in 1.76U (RUN 3822) core.

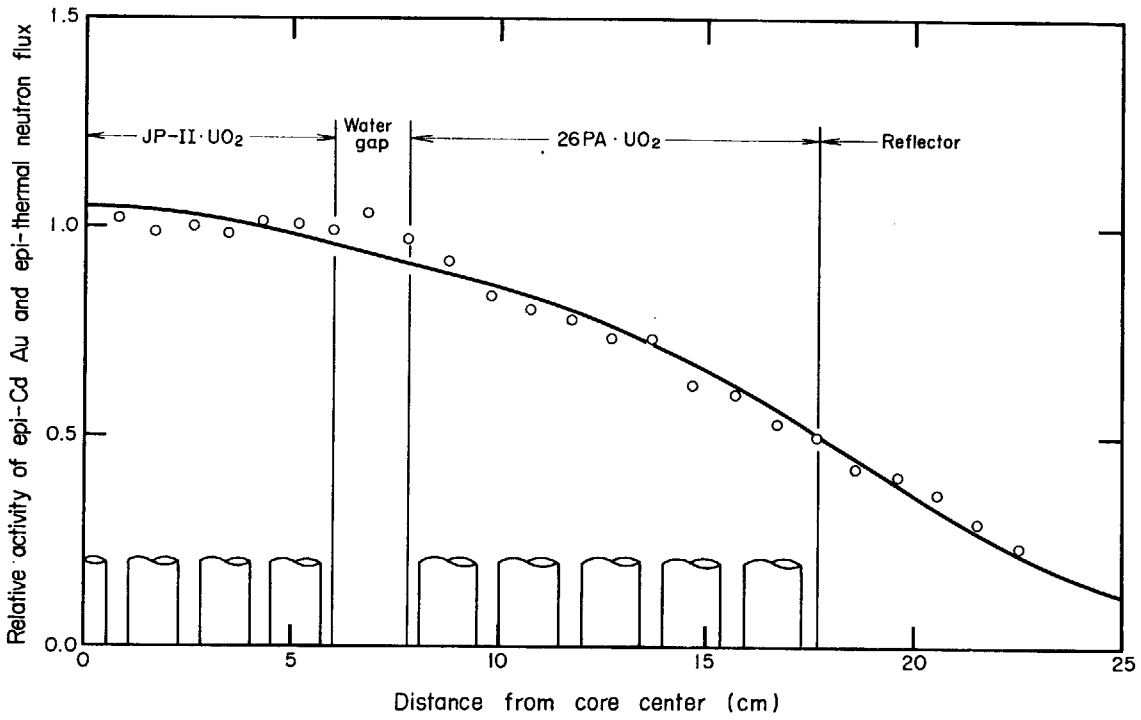

○: Measured, —: Calculated.

Fig. 34 Epi-thermal neutron flux distribution in 2.00U (RUN 3884) core.

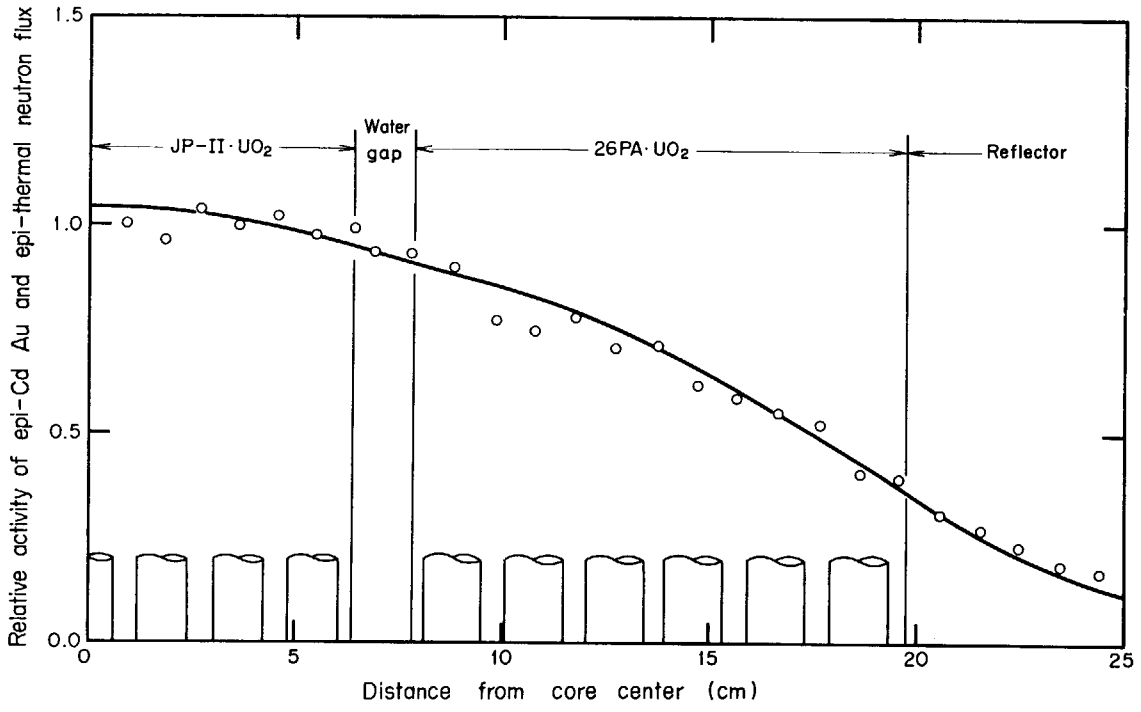

○: Measured, —: Calculated.

Fig. 35 Epi-thermal neutron flux distribution in 2.38U (RUN 3846) core.

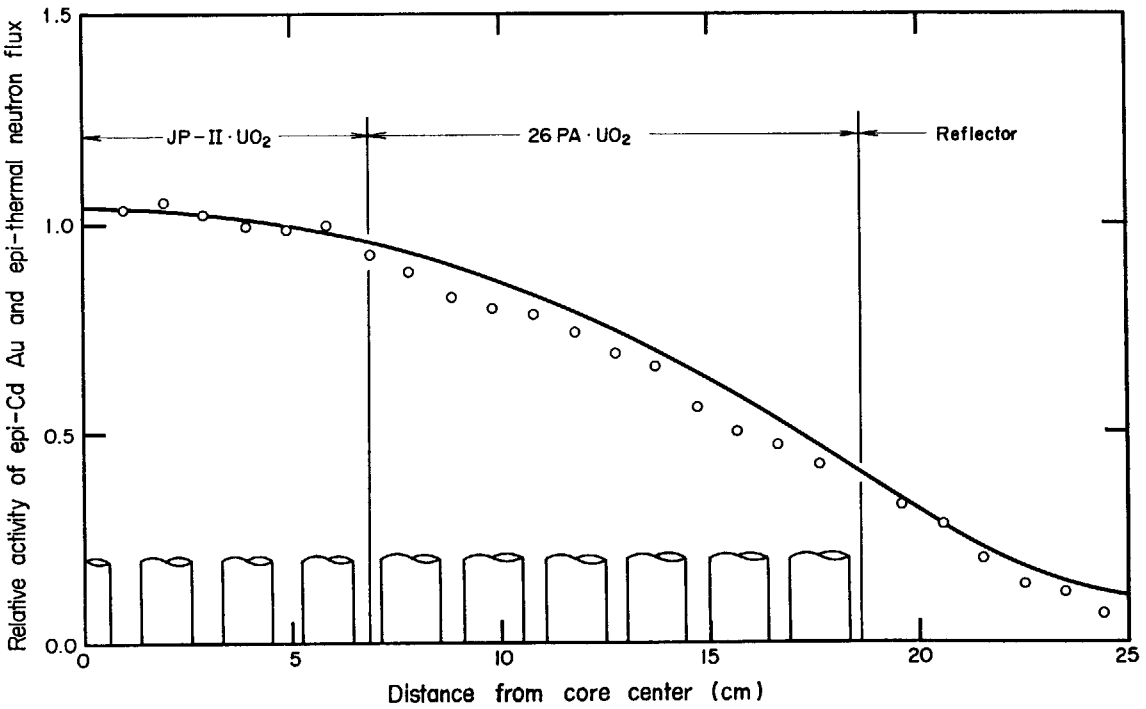

○: Measured, —: Calculated.

Fig. 36 Epi-thermal neutron flux distribution in 2.95U (RUN 3834) core.

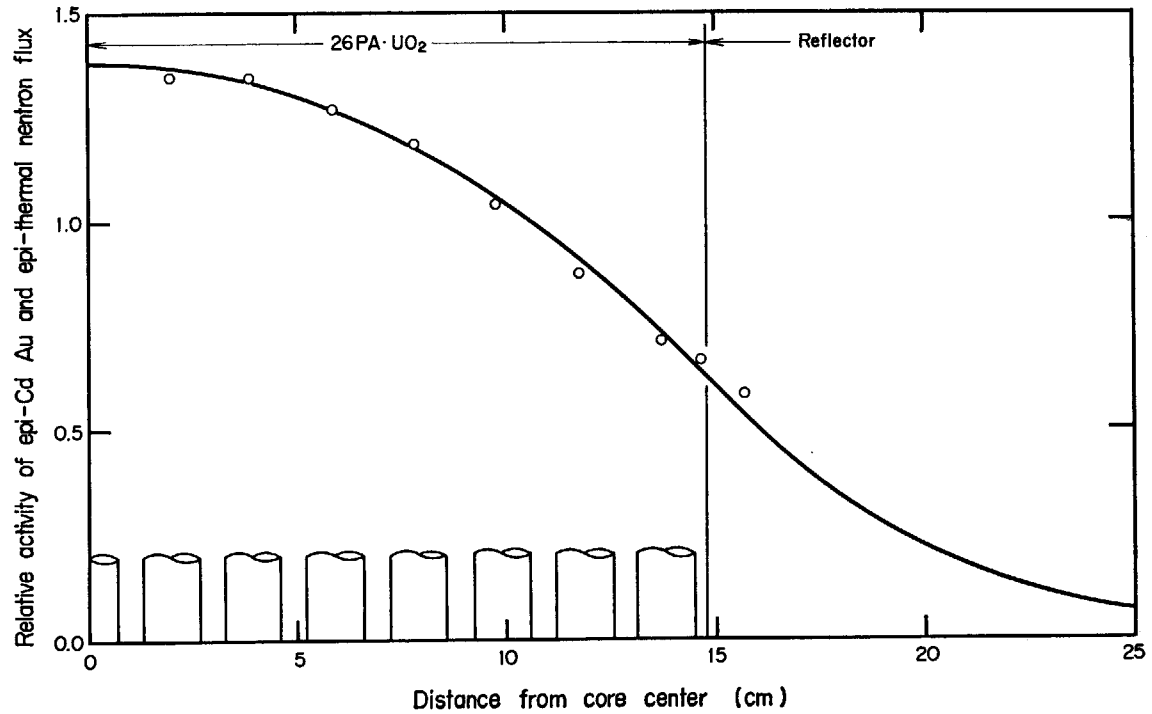

○: Measured, —: Calculated.

Fig. 37 Epi-thermal neutron flux distribution in 1.83TU (RUN 3872) core.

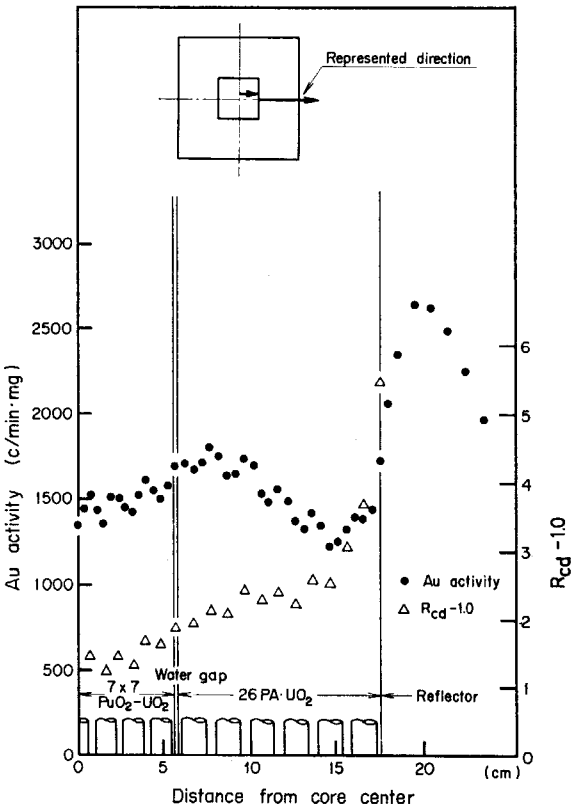

Fig. 38 Distributions of bare Au activity and cadmium ratio−1.0 in 1.76Pu core.

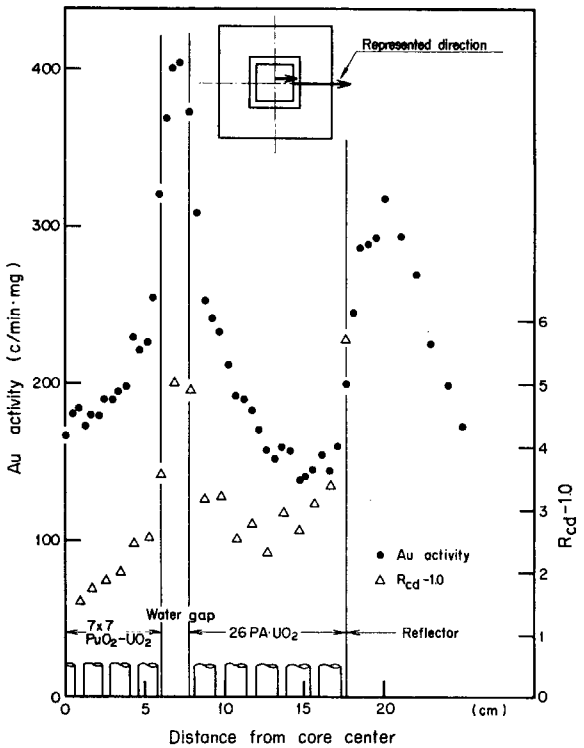

Fig. 39 Distributions of bare Au activity and cadmium ratio−1.0 in 2.00Pu core.

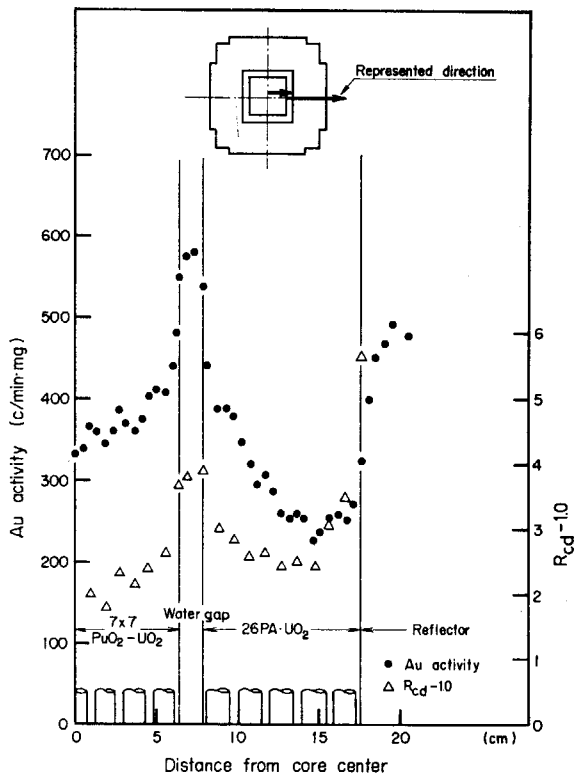

Fig. 40 Distributions of bare Au activity and cadmium ratio−1.0 in 2.38Pu core.

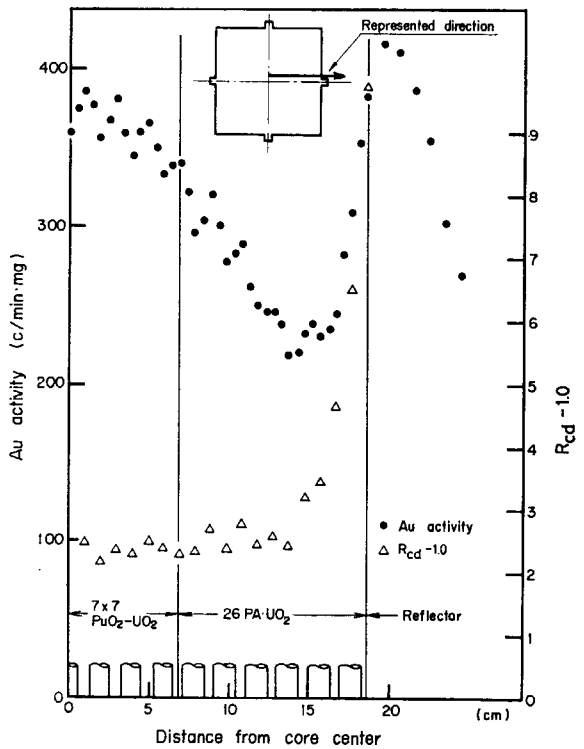

Fig. 41 Distributions of bare Au activity and cadmium ratio−1.0 in 2.95Pu core.

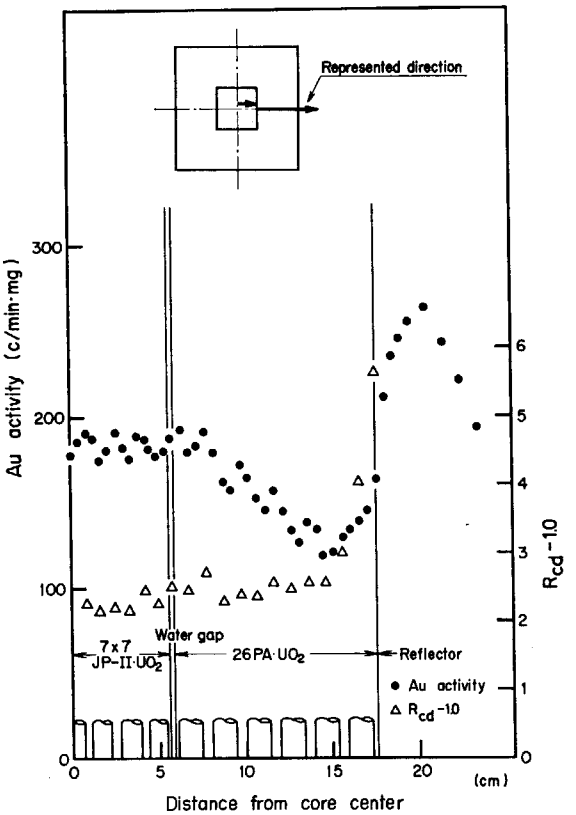

Fig. 42 Distributions of bare Au activity and cadmium ratio−1.0 in 1.76U core.

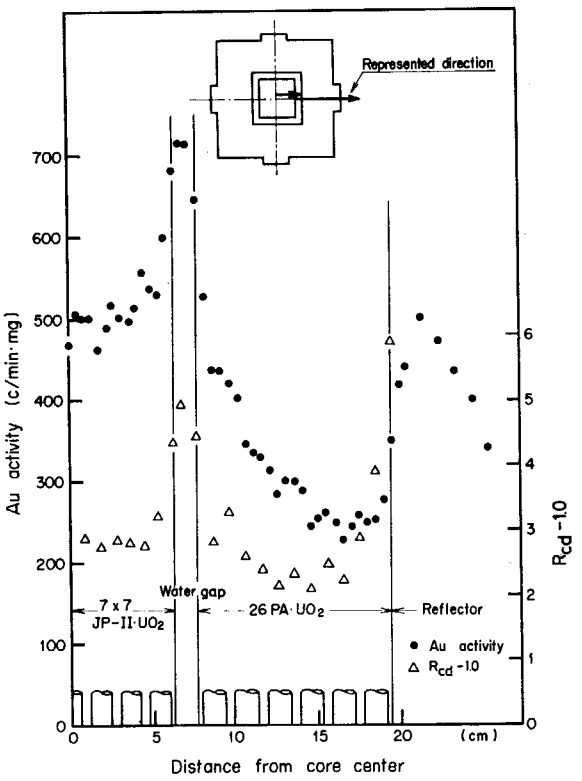

Fig. 43 Distributions of bare Au activity and cadmium ratio−1.0 in 2.00U core.

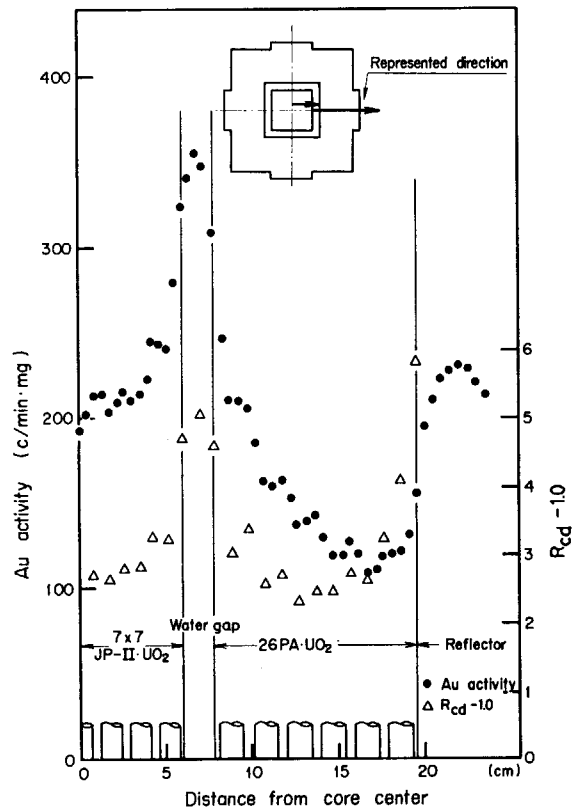

Fig. 44 Distributions of bare Au activity and cadmium ratio−1.0 in 2.38U core.

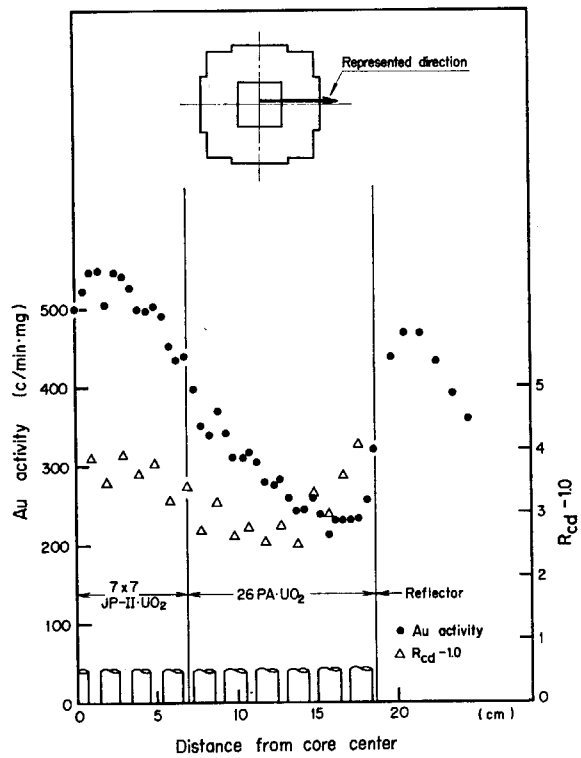

Fig. 45 Distributions of bare Au activity and cadmium ratio−1.0 in 2.95U core.

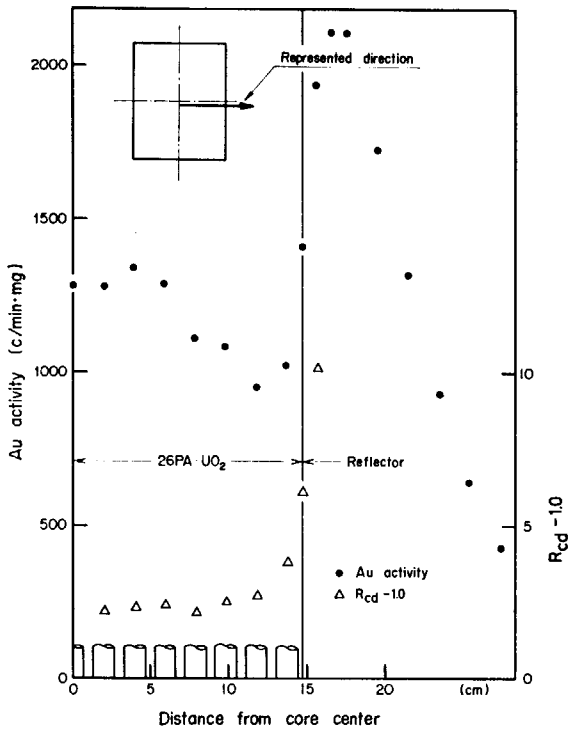

Fig. 46 Distributions of bare Au activity and cadmium ratio−1.0 in 1.83TU core.

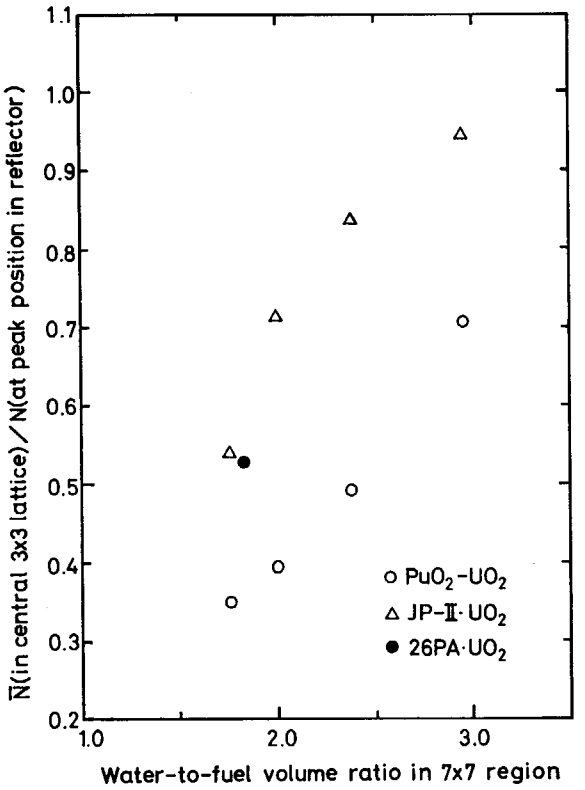

Fig. 47 Ratios of Dy activity averaged in central 3×3 lattice of 7×7 region to that at peak position in reflector.

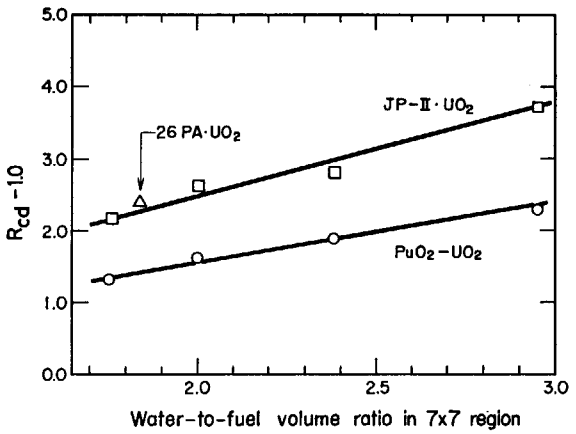

Fig. 48 Cadmium ratio−1.0 in central 3×3 lattice of 7×7 region.

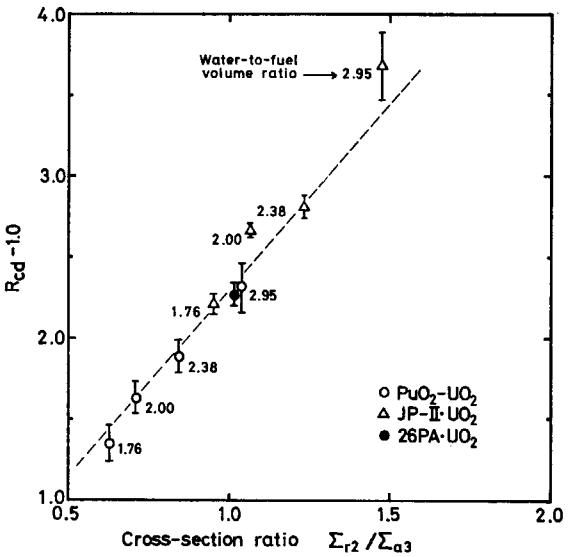

Fig. 49 Relation between cadmium ratio−1.0 and ratio of cross-sections of epi-thermal slowing down and thermal absorption in central 3×3 lattice of 7×7 region. A dotted straight line passes through the origin.

5. Power distributions

5. 1 Measurements on power distributions

5. 1. 1 Gamma scanning of fuel rods

The horizontal and vertical power distributions were obtained by scanning the γ-rays emmited from the fission products in the irradiated fuel rod. The core was operated at the power level of 30 W for about 5 min. After shutdown the fuel rods for the power distribution measurement were withdrawn from the core, and the fission product γ-rays above 0.6 MeV from each fuel rod were counted in the cooling time of 30 min to 3 hr. An example of the fuel rod position used for the gamma scanning is shown in **Fig. 50**, and the block diagram of the counting system is shown in **Fig. 51**.

The detector for the γ-ray counting was a solid type of a 3 in. dia. $\times$ 3 in. thick NaI(T*l*) scintillation counter and was shielded with lead blocks as shown in **Fig. 51**. Between the fuel rod and the detector, a slit was settled and its width was adjusted in 2 cm for the horizontal and 1 cm for the vertical distribution measurements. The countings was made for 20 sec and repeated twice to watch the reproducibility. The corrections for the resolving time of the counting system, background from the fuel rod and the room, and the decay of the fission product γ-ray were applied to the recorded count rates.

The value of the decay correction was obtained by a supplemental experiment described in Ref. 17. The samples of the fuel rods used in the experiment were 2.7 wt% and 3.2 wt% enriched UO_2 fuels and nine kinds of mixed oxide fuels of which plutonium enrichments were 2.5, 2.1, and 1.4 wt% in PuO_2-UO_2 and diameters of the fuel pellets were 12.5, 10.7, and 9.3 mm. Plutonium composition of the samples was almost the same as the PuO_2-UO_2 fuel. The difference of the decay characteristics could not be recognized between two UO_2 fuels. The difference between nine plutonium samples could not be also recognized. Between the decay characteristics of the UO_2 and mixed oxide fuels, some differences could be recognized as shown in **Fig. 52**, but they were in the range of the experimental errors. So, the decay correction factors of the mixed oxide fuel was also applied to the 2.6 wt% enriched JP-II$\cdot UO_2$ and 26PA$\cdot UO_2$ fuels.

5. 1. 2 Horizontal power distributions

In this series of the experiments, three kinds of fuel rod were used, which are classified into two kinds of fuel material or two kinds of fuel pellet diameter. Applying the gamma scanning method to the measurement of the horizontal power distribution in those multi-regional cores, following corrections should be applied to the measured count rate.

(1) Correction for the difference between the fission product γ-ray activity per fission of plutonium and uranium.

(2) Correction for the γ-ray shielding factor of fuel pellet and for the geometrical efficiency of the γ-ray counting due to the difference in pellet diameters. That is the case of the PuO_2-UO_2 or JP-II$\cdot UO_2$ fuel rod relative to the 26PA$\cdot UO_2$ fuel rod.

The details of these correction factors are described in Section **5. 2**.

The corrected values as the power distribution are shown in **Figs. 53a** through **61b** with the

calculated values. The values at the symmetric and eqivalent positions in the lattice are plotted in the same figure. The averaged numerical values are listed in Appendix 3. The average power in the 7×7 region was normalized to unity.

The random errors in the measured power were due to the statistical error of the γ-ray counts, to bowing of the fuel rod and to the inhomogeneities of the fuel pellet. The systematic errors in the correction factors are described in Section **5. 2. 2**. The statistical standard errors in the γ-ray counts were maximum 2% and almost less than 1%. In the figures, the error is within the represented symbol. The mean values in Appendix A3 have the errors in almost less than 2% which is smaller than the errors of the correction factors. This standard error of the mean value became generally greater at the position where a gradient of the power distribution was great.

From the experimental results, following remarks were obtained.

(1) In case of the same water-to-fuel volume ratio in the 7×7 PuO_2-UO_2 and JP-II·UO_2 regions, the power of the PuO_2-UO_2 fuel rod relative to the power in the driver region is higher than that of the JP-II·UO_2 fuel rod.

(2) The maximum power of the PuO_2-UO_2 fuel rod relative to the average power in the 7×7 region is higher than that of the JP-II·UO_2 fuel rod except the case of the water-to-fuel volume ratio 2.95.

(3) The Dy activity in the 7×7 lattice relative to the driver lattice of the U system is higher than that of the Pu system, however, the power distribution is in an opposite relation. This relation is evidently observed between the 1.76Pu and 1.76U cores or the 2.95Pu and 2.95U cores. This fact can be explained as the PuO_2-UO_2 fuel has stronger absorption and fission of neutrons than the JR-II·UO_2 fuel.

5. 1. 3 Vertical reflector saving

The vertical reflector saving δ_z was deduced from the vertical power distribution in the 1.76Pu, 2.38Pu, and 2.95U cores used for the horizontal power distribution measurements. The positions of the measured fuel rod were at the center of the 7×7 region and at a mid point of the driver region as shown in **Fig. 62**.

The measured power distribution Y was fitted to the function

$$Y(x)=A\cdot\cos(B\cdot x+C), \tag{5.1}$$

where A, B and C are constants to be determined and x is vertical measured position. The data Y(x) were omitted stepwise from the end points of the fuel rod towards the center and the variation of fitted values of the constants were observed. The values in the range of minimum variation of the fitted values were adopted as the most probable A, B and C, and their values are listed in **TABLE 13**. An example of the fitted function is shown in **Fig. 62**.

The reflector saving δ_z was deduced by using the constant B by

$$\delta_z=\frac{\pi}{B}-H, \tag{5.2}$$

where H is the effective fuel height, that is effective core height. The vertical reflector saving of each core is listed in **TABLE 14**, and their mean value was 12.0±0.1 cm. The difference of δ_z between the 7×7 and the driver regions could not be recognized as significant. The dependence on the water-to-fuel volume ratio in the 7×7 region could not be also recognized. In order to check the dependence on the water level, the measurement of δ_z in the 1.76Pu core was made at the low water level of 50.79 cm and compared with the value at the higher water level of 69.19 cm. There was no significant difference between them and they were within the limit of the experimental errors.

5.2 Analysis on power distributions

5.2.1 Correction factors for power distributions in multi-regional cores

The ratio of calculated thermal power created in a lattice cell in the driver region to that in the 7×7 region is defined by

$$\frac{\text{Thermal power of a lattice in the driver region}}{\text{Thermal power of a lattice in the 7×7 region}} = \frac{\sum_{i=1}^{3} (\kappa \cdot \phi\Sigma_f)_{DR,\,i} \cdot V_{DR}}{\sum_{i=1}^{3} (\kappa \cdot \phi\Sigma_f)_{7\times7,\,i} \cdot V_{7\times7}}, \tag{5.3}$$

where

κ: thermal power per fission, W·sec/fission,
$\phi\Sigma_f$: number of fissions per volume of a lattice cell, fission/cm^3·sec,
V: volume of a lattice cell per length of a fuel rod, cm^3,
i: energy group number,
DR: driver region,
7×7: 7×7 region.

The calculation was made by using the two-dimensional diffusion code PDQ·5 as described in Chapter 3.

In the comparison between the experimental and theoretical power distributions, the measured counts of the fission product γ-rays from a fuel rod should be converted to the thermal power of the corresponding lattice cell. The γ-ray count of the fuel rods must be corrected for the number of fissions per fuel length, fission product γ-ray activity per fission, time decaying of fission product γ-ray activity and γ-ray attenuation by fuel pellet. On the PuO_2-UO_2 fuel, the fission rates of plutonium and uranium in the mixed oxide fuel must be taken into consideration. Thus, the measured powers of the 26PA·UO_2 fuel rod in the driver region and of the PuO_2-UO_2 fuel rod in the 7×7 region are expressed as

$$A_{\gamma,26PA} \propto (\phi\Sigma_f \cdot S \cdot l)_{26PA} \cdot w_U \cdot \frac{\mu(t)_U}{\mu(t)_{26PA}} \cdot f_{26PA}, \tag{5.4}$$

$$A_{\gamma,PuR} \propto (\phi\Sigma_f \cdot S \cdot l)_{PuR} \cdot \left\{ R_{Pu} \cdot w_{Pu} \cdot \frac{\mu(t)_{Pu}}{\mu(t)_{PuR}} + R_U \cdot w_U \frac{\mu(t)_U}{\mu(t)_{PuR}} \right\} \cdot f_{PuR}, \tag{5.5}$$

where

A_γ: measured count rate of fission product γ-ray from a fuel rod,
$\phi\Sigma_f \cdot S \cdot l$: number of fissions per fuel length l observed from the γ-ray detector,
S: cross-sectional area of a fuel pellet,
w: fission product γ-ray activity per fission,
$\mu(t)$: decay factor of fission product γ-ray activity at cooling time t,
f: γ-ray attenuation factor,
R: fission ratio between plutonium or uranium and mixture of plutonium and uranium [see Eqs. (5.11) and (5.12)],
ϕ: $\phi = \int \phi(\tau) \cdot d\tau$, τ is duration time of irradiation.

Suffixes are

26PA: 26PA·UO_2 fuel rod,
PuR: PuO_2-UO_2 fuel rod,
JPII: JP-II·UO_2 fuel rod,
U: uranium,
Pu: plutonium.

The measured power ratio of the PuO_2-UO_2 fuel rod in the 7×7 region to the 26PA·UO_2 fuel rod in the driver region is derived from Eqs. (5. 4) and (5. 5) as

$$\frac{\kappa_U\cdot(\phi\Sigma_f\cdot V')_{26PA}}{\kappa_M\cdot(\phi\Sigma_f\cdot V')_{PuR}}=\frac{A_{\gamma,26PA}}{A_{\gamma,PuR}}\cdot\left\{R_{Pu}\cdot\frac{w_{Pu}\cdot\mu(t)_{Pu}}{w_U\cdot\mu(t)_{PuR}}+R_U\cdot\frac{\mu(t)_U}{\mu(t)_{PuR}}\right\}\cdot\frac{f_{PuR}}{f_{26PA}}\cdot\frac{\kappa_U}{\kappa_M}=\frac{A_{\gamma,26PA}}{A_{\gamma,PuR}}\cdot C_{\gamma,Pu}, \tag{5.6}$$

where

M: mixture of plutonium and uranium

V′: volume of fuel pellets observed from the γ-ray detector, S·l.

In Eq. (5. 6), the relations $l_{26PA}=l_{PuR}$ and $\mu(t)_U=\mu(t)_{26PA}$ are assumed. The measured value expressed by Eq. (5. 6) can be directly compared with the calculated one of Eq. (5. 3), since the fissions in the volume V′ is equivalent to the fissions in the volume V in Eq. (5. 3).

In the same manner as the case of the PuO_2-UO_2 fuel rod, the measured power ratio of the JP-II·UO_2 fuel rod in the 7×7 region to the 26PA·UO_2 fuel rod in the driver region is expressed as

$$\frac{\kappa_U\cdot(\phi\Sigma_f\cdot V')_{26PA}}{\kappa_U\cdot(\phi\Sigma_f\cdot V')_{JPII}}=\frac{A_{\gamma,26PA}}{A_{\gamma,JPII}}\cdot\frac{f_{JPII}}{f_{26PA}}=\frac{A_{\gamma,26PA}}{A_{\gamma,JPII}}\cdot C_{\gamma,U}. \tag{5.7}$$

In this equation, it is not necessary to take into consideration about the fission product γ-ray activity per fission.

To obtain the power distribution in the multi-regional core, the ratio of the measured values A_γ must be corrected with the correction factor C_γ as shown in Eqs. (5. 6) and (5. 7). This correction factor was conveniently separated into three parts as shown below and evaluated respectively.

$$C_1=\frac{w_{Pu}}{w_U}\cdot\frac{\mu(t)_{Pu}}{\mu(t)_{PuR}}\cdot R_{Pu}+\frac{\mu(t)_U}{\mu(t)_{PuR}}\cdot R_U,$$

$$=\left\{\frac{w_{Pu}}{w_U}\cdot\frac{\mu(t)_{Pu}}{\mu(t)_U}\cdot R_{Pu}+R_U\right\}\cdot\frac{\mu(t)_U}{\mu(t)_{PuR}}, \tag{5.8}$$

$$C_2=\frac{f_{PuR}}{f_{26PA}}\ \text{or}\ \frac{f_{JPII}}{f_{26PA}}, \tag{5.9}$$

$$C_3=\frac{\kappa_U}{\kappa_M}. \tag{5.10}$$

The numerical values of these factors are shown in TABLE 15.

(1) C_1: Intensity ratio of fission product γ-ray activities per unit thermal power

This correction factor is necessary for the plutonium system. The ratio of $w_{Pu}\cdot\mu(t)_{Pu}/w_U\cdot\mu(t)_U$ in Eq. (5. 8) was measured by using a double fission chamber[18]. The ratio varied with the cooling time. The gamma scanning was made for the cooling time ranging from 54 min to 140 min. Therefore, the time dependent correction was applied to the each measured count of γ-ray.

The time decay correction factor of uranium $\mu(t)_U$ was assumed to be the same as that of pultonium $\mu(t)_{PuR}$, because, the ratio of the correction factors between the uranium and the plutonium fuel rods as shown in Section **5. 1. 1** was nearly 1.0 in the time duration of the measurement.

The fission rates of plutonium and uranium in the PuO_2-UO_2 fuel rod (R_{Pu} and R_U) were difficult to be deduced experimentally, and were obtained by using the calculated macroscopic fission cross-section Σ_f, and the calculated neutron flux ϕ as

$$R_{Pu}=\frac{\sum_{i=1}^{3}(\phi\Sigma_f)_{Pu,i}}{\sum_{i=1}^{3}(\phi\Sigma_f)_{M,i}}, \tag{5.11}$$

$$R_U=\frac{\sum_{i=1}^{3}(\phi\Sigma_f)_{U,i}}{\sum_{i=1}^{3}(\phi\Sigma_f)_{M,i}}. \tag{5.12}$$

(2) C_2: Ratio of γ-ray shielding factors

When diameters or densities of each fuel pellet are different, the loss of γ-rays by attenuation must be corrected. The shielding factors f were obtained by calculation of γ-ray attenuation for disk sources with the observing point at side. The numerical results of the ratio C_2 were 1.15 for the PuO_2-UO_2 fuel and 1.05 for the JP-II·UO_2 fuel.

The accuracy of the calculational method was examined by the supplemental experiment. For the experimental purpose it was necessary to use the fuel pellets which had various diameters and uniformely distributed γ-ray sources in a sufficient amount. Eleven natural-UO_2 pellets which consisted of six kinds of diameter, were fabricated. Gamma-rays of 0.767 and 1.001 MeV emitted from ^{234}Pa were counted by the NaI(T*l*) scintillation detector. Protactinium-234 is a daughter isotope of ^{238}U and is uniformely distributed throughout the fuel pellet. The measured and the calculated γ-ray count rates are shown in **Fig. 63**. The calculated values were normalized to the measured ones by least square fitting. The theoretical dependence of the γ-ray attenuation on the pellet diameter agreed well with the experimental one.

(3) C_3: Ratio of thermal powers per fission

The ratio of thermal powers per fission is taken into consideration in case of the measurement on the multi-regional core composed of mixed oxide and uranium dioxide fuels. The numerical values on respective fissile materials are 193 MeV/fission for uranium and 199 MeV/fission for plutonium[19]. The ratio C_3 was, however, cancelled out in the present theory-experiment correlation, since the same ratio was included in both the experimental and the calculational powers.

5.2.2 Correlations of calculations and experiments

The comparison between the measured and calculated power distributions were made using Eqs. (5.3), (5.6), and (5.7). The calculated power distributions at every mesh point and in each fuel cell are shown in **Figs. 53a** through **61b** with measured ones. The average power in the 7×7 region was normalized to unity as well as the measured power. The calculated and measured powers, and the differences between them are shown in Appendix A3. To investigate the accuracy of the calculation over the core, the standard deviation of the differences was observed in the 7×7 and the driver regions, respectively. The numerical values of the standard deviation are shown in **TABLE 16**.

From the comparison, following remarks are noticed.

(1) In the 7×7 regions, the standard deviations σ_{77} of the differences between the calculation and the experiment are 1~4% relative to the experiment. There is no significant difference between the Pu and the U systems, and in both systems the standard deviation becomes greater in case of the core with water gap.

(2) The standard deviations σ_T in the driver regions are 5~10% in the Pu system and 2~7% in the U system.

(3) In the neighborhood of the boundary of the lattice adjacent to the reflector or the water gap, the gradent of the measured power distribution is larger than the calculated distribution. While, there is no significant difference in the neighborhood of the lattice boundary between the 7×7 and driver regions without water gap.

The difference between the calculation and experiment on the Pu system is greater than the U system as described above. One of the reasons of this tendency is considered to be caused by the factors C_1 and C_2. In the Pu system, the corrections with C_1 and C_2 were necessary, and these factors had the error of ±2% for C_1 and ±7% for C_2. Total error due to both factors was ±7.3%. In the U system, otherwise, only C_2 was necessary and had an error of ±7%. By considering these errors, the calculated values of both systems were in the range of the errors of

the experiments.

The calculated power fractions in the 7×7 and the driver regions were examined in the Pu and the U systems. The results of the diffusion calculation are shown in TABLE 17. In the Pu system, the fractional powers of the 7×7 region were 15~23% respect to the total core, and in the U system they were 15~21%. In the case of the comparison between 1.76Pu and 1.76U cores which had same numbers of the fuel rods in the driver region, the gross power of the PuO_2-UO_2 fuel rods in the 7×7 region was 3.5% higher than that of the JP-II·UO_2 fuel rods in the same region.

5.3 Summary on power distributions

The following relation were obtained by the experimental and theoretical analysis on the PuO_2-UO_2 and the JP-II·UO_2 fuels in the 7×7 region within the range of the water-to-fuel volume ratio used in this experiment.

$$A_P > A_U \tag{5.13}$$

$$B_P < B_U \tag{5.14}$$

$$\frac{A_P - B_P}{A_P} < \frac{A_U - B_U}{A_U} \tag{5.15}$$

where

$$A_P = \frac{\text{mean power of the } PuO_2\text{-}UO_2 \text{ fuels in the } 7\times7 \text{ region}}{\text{mean power over the core}}$$

$$A_U = \frac{\text{mean power of the JP-II}\cdot UO_2 \text{ fuels in the } 7\times7 \text{ region}}{\text{mean power over the core}}$$

$$B_P = \frac{\text{mean thermal neutron density in the } PuO_2\text{-}UO_2 \text{ lattice of the } 7\times7 \text{ region}}{\text{mean thermal neutron density over the core}}$$

$$B_U = \frac{\text{mean thermal neutron density in the JP-II}\cdot UO_2 \text{ lattice of the } 7\times7 \text{ region}}{\text{mean thermal neutron density over the core}}$$

These relations have following meanings.

(1) In case of the same water-to-fuel volume ratio, the PuO_2-UO_2 fuel produces much larger power than the JP-II·UO_2 fuel.

(2) Mean thermal neutron density in the PuO_2-UO_2 lattice is less than that in the JP-II·UO_2 lattice.

(3) The difference of the distribution patterns in the U system between the power and the thermal neutron density is more distinguishable than in the Pu system.

In addition to the above relations, following remarks are noticed.

(4) In respect to the power peaking factor in the 7×7 region, the Pu system of the 2.00Pu and 2.38Pu cores has greater factor than that of the U system of the 2.00U and 2.38U cores. These all cores have the water gap.

(5) The calculated powers in the driver region of the Pu system were 5~9% higher than the experimental ones as shown in the fifth column of TABLE 16. Otherhands, the calculated powers of the U system were in the range of −1~4% of the experimental ones. One of the causes of this discrepancy is considered due to the several correction factors, namely the fission product γ-ray activity per unit power and the γ-ray shielding factor.

To improve the accuracy of the experiment, following studies are necessary;

(a) Experiments of the factor of the γ-ray activities per unit power of plutonium and uranium in improved accuracy, or the development of direct measuring method of the number of fissions or thermal power in the fuel rod.

(b) Experiment of the γ-ray shielding factor of the fuel pellet in improved accuracy.

TABLE 13 Fitted function of vertical power distribution in 2.38Pu core.

Region	7×7	Driver
Fuel	PuO_2–UO_2	26PA·UO_2
Fitting parameters		
A	1.000±0.002	1.000±0.003
B, radian/cm	0.0387±0.0001	0.0387±0.0002
C, radian	−1.315±0.005	−1.320±0.006

Function $Y(x)=A\cdot\cos(B\cdot x+C)$
$Y(x)$: relative power
x : vertical position, cm

TABLE 14 Measured reflector savings.

Core name	Water level, cm	Reflector saving δ_z, cm	
		7×7 region	Driver region
2.95U	66.86	12.2±1.0	not measured
2.38Pu	69.27	11.9±0.1	11.8±0.1
1.76Pu	69.19	12.0±0.5	12.3±0.4
1.76Pu	50.79	12.0±0.6	11.6±0.6
Average		12.0±0.1*	

* standard error of mean value.

TABLE 15 Correction factors used in obtaining power distribution in multi-regional cores.

System		Pu				U
Core name		1.76Pu	2.00Pu	2.38Pu	2.95Pu	1.76U, 2.00U 2.38U, 2.95U
Power fraction in the PuO_2–UO_2 fuel	R_{Pu}	0.8522	0.8605	0.8564	0.8556	——
	R_U	0.1478	0.1395	0.1436	0.1444	
C_1		depends on cooling time				——
C_2		1.15				1.05
C_3		0.965				——

TABLE 16 Differences between measured and calculated power distributions.

Region / Core name	7×7	Driver	
	σ_{77}*1), %	σ_T*2), %	A_v*3), %
1. 76Pu	1. 2	9. 8	8. 4
2. 00Pu	4. 0	8. 6	7. 2
2. 38Pu	2. 5	10. 2	8. 9
2. 95Pu	0. 6	6. 4	5. 0
1. 76U	1. 0	5. 2	4. 0
2. 00U	3. 7	4. 7	1. 5
2. 38U	2. 5	6. 9	5. 4
2. 95U	0. 7	3. 1	−0. 8
1. 83TU	—	2. 8	—

Note :

*1) $\sigma_{77}=\sqrt{\dfrac{\sum_{i=1}^{49}\left\{\left(\dfrac{\text{cal.}-\text{meas.}}{\text{meas.}}\right)_i\times 100\right\}^2}{49-1}}$

*2) $\sigma_T=\sqrt{\dfrac{\sum_{i=1}^{n}\left\{\left(\dfrac{\text{cal.}-\text{meas.}}{\text{meas.}}\right)_i\times 100\right\}^2}{n-1}}$

*3) $A_v=\dfrac{\sqrt{\sum_{i=1}^{n}\left(\dfrac{\text{cal.}-\text{meas.}}{\text{meas.}}\right)_i\times 100}}{n}$

where n is the number of measured fuel rods.

TABLE 17 Calculated region-wise and energy-wise fractions of power in multi-regional cores.

Core name	Region	Region-wise power fraction	Energy-wise power fraction		
			Fast	Epi-thermal	Thermal
1. 76Pu	7×7	0. 150	0. 049	0. 079	0. 872
	Driver	0. 850	0. 053	0. 060	0. 887
2. 00Pu	7×7	0. 203	0. 035	0. 057	0. 908
	Driver	0. 797	0. 047	0. 053	0. 900
2. 38Pu	7×7	0. 229	0. 033	0. 053	0. 914
	Driver	0. 771	0. 047	0. 053	0. 900
2. 95Pu	7×7	0. 224	0. 035	0. 056	0. 908
	Driver	0. 776	0. 051	0. 057	0. 892
1. 76U	7×7	0. 145	0. 060	0. 069	0. 871
	Driver	0. 855	0. 052	0. 059	0. 889
2. 00U	7×7	0. 185	0. 042	0. 048	0. 910
	Driver	0. 815	0. 047	0. 053	0. 899
2. 38U	7×7	0. 210	0. 040	0. 045	0. 915
	Driver	0. 791	0. 047	0. 053	0. 900
2. 95U	7×7	0. 194	0. 042	0. 049	0. 907
	Driver	0. 806	0. 051	0. 057	0. 892

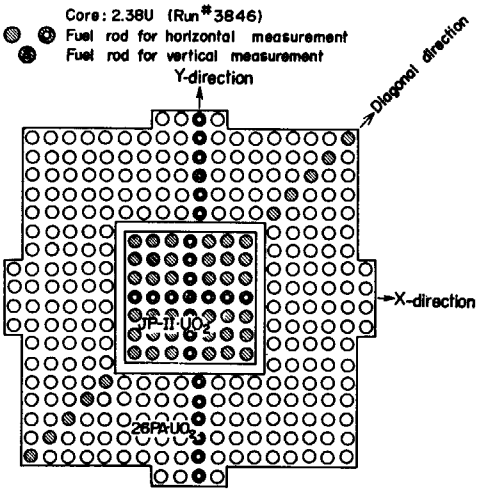

Fig. 50 Fuel arrangement for power distribution measurement.

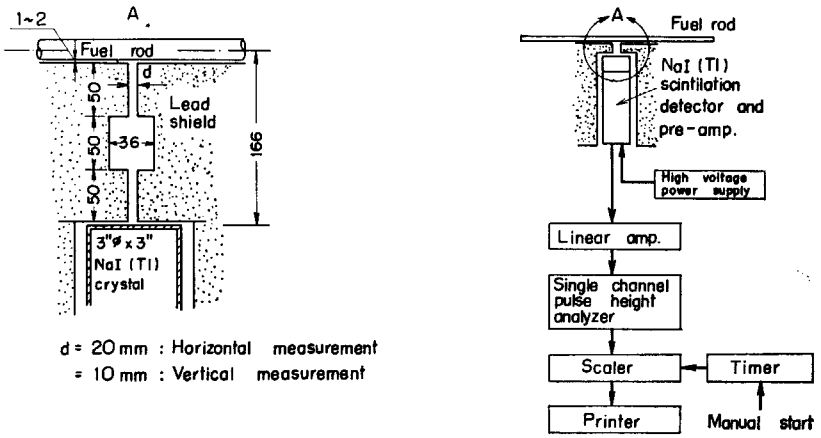

Fig. 51 Block diagram of γ-ray counting system for power distribution measurement.

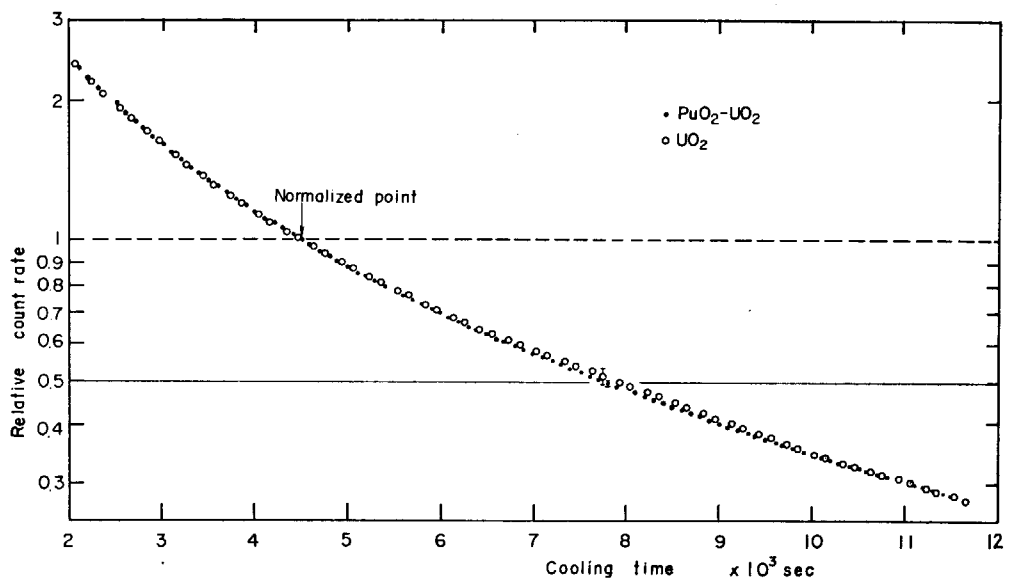

Fig. 52 Decay curves of fission product γ-ray intensity of mixed oxide and uranium oxide fuel pellets.

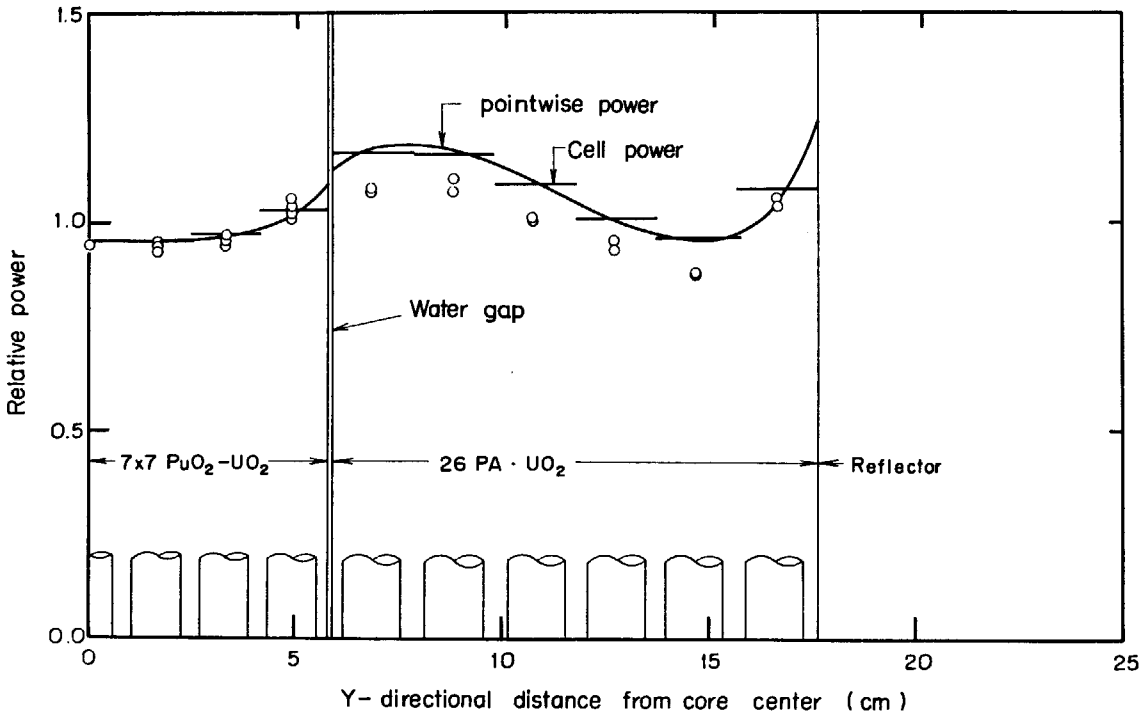

(a) Y-direction

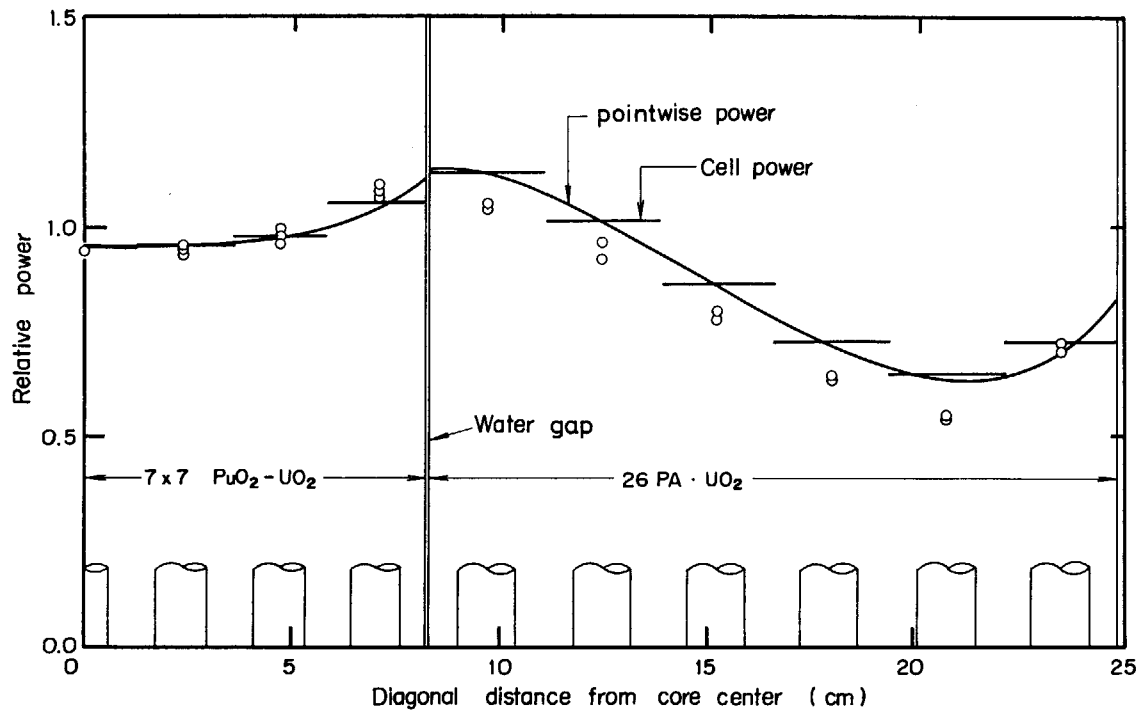

(b) diagonal direction.

○: Measured, ——: Calculated.

Fig. 53 Power distribution in 1.76Pu (RUN 3799) core.

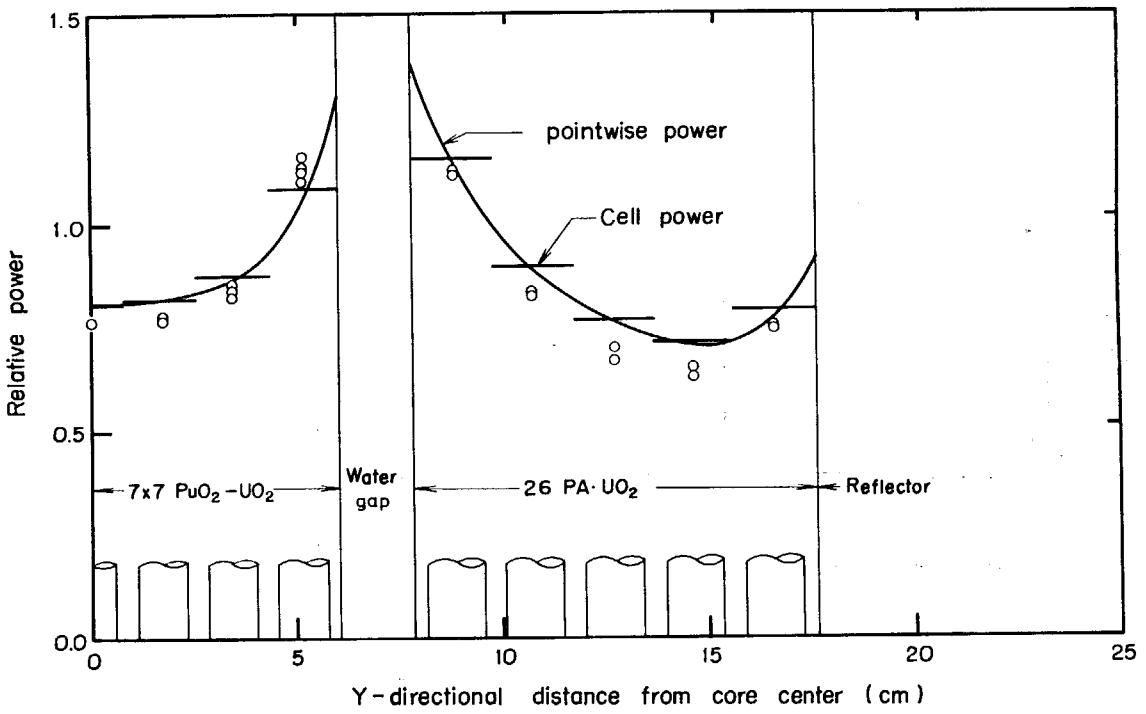

(a) Y-direction,

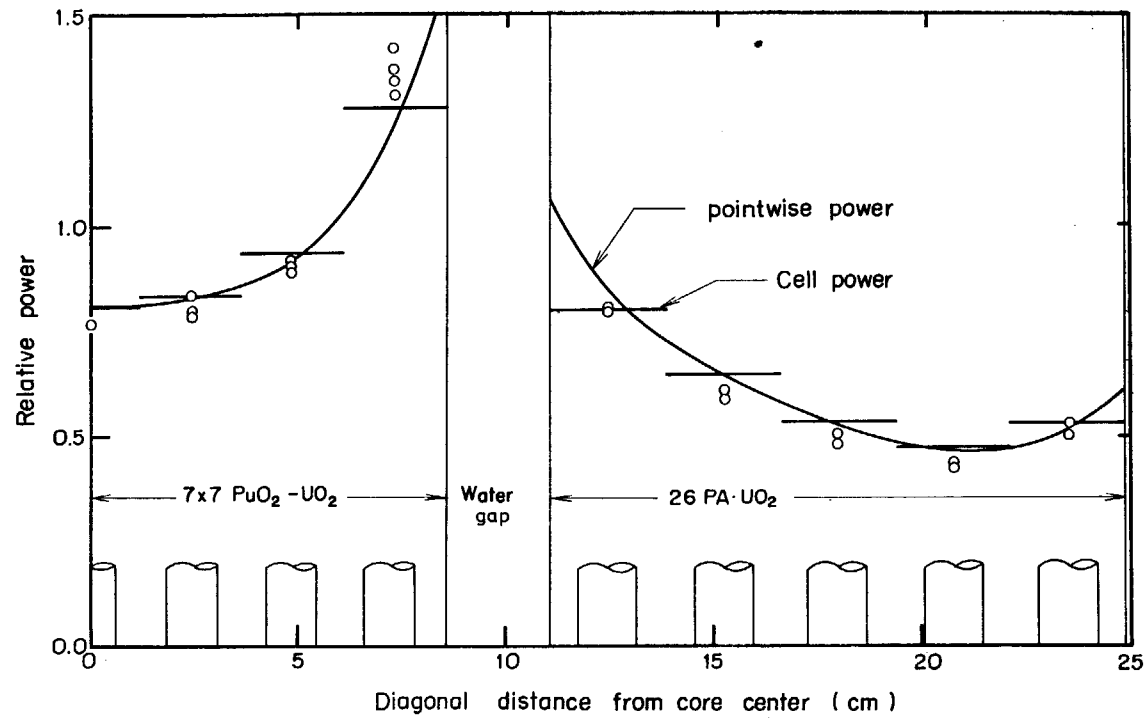

(b) diagonal direction,

○: Measured, ——: Calculated.

Fig. 54 Power distribution in 2.00Pu (RUN 3838) core.

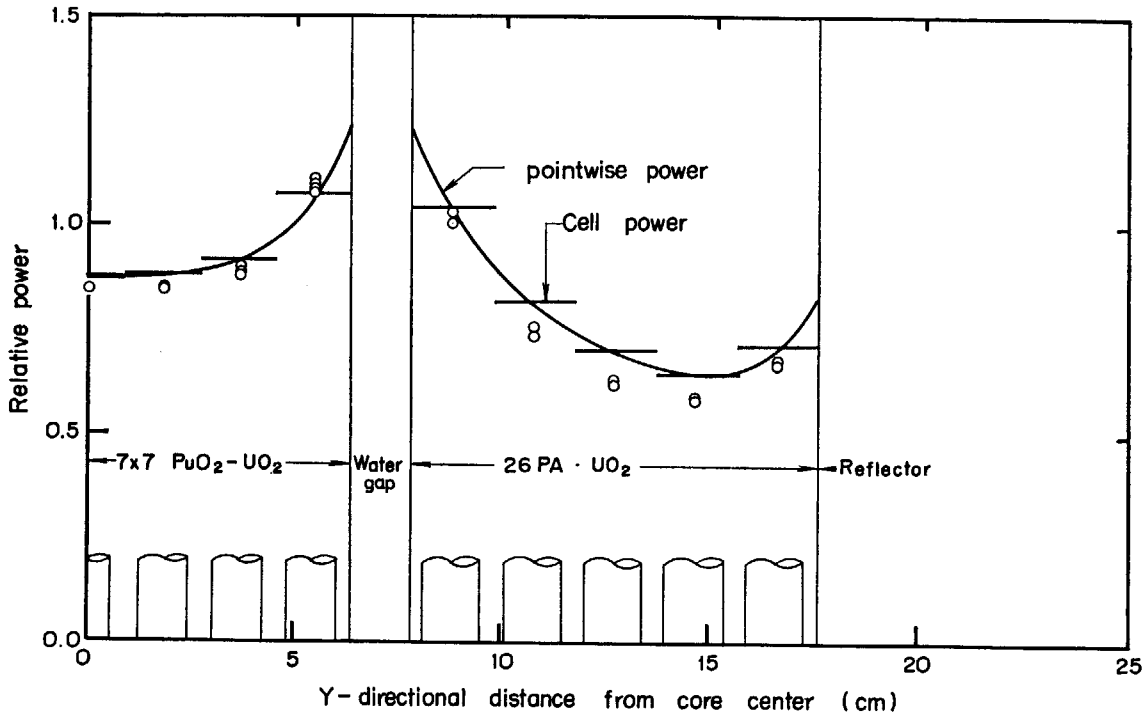

(a) Y-direction,

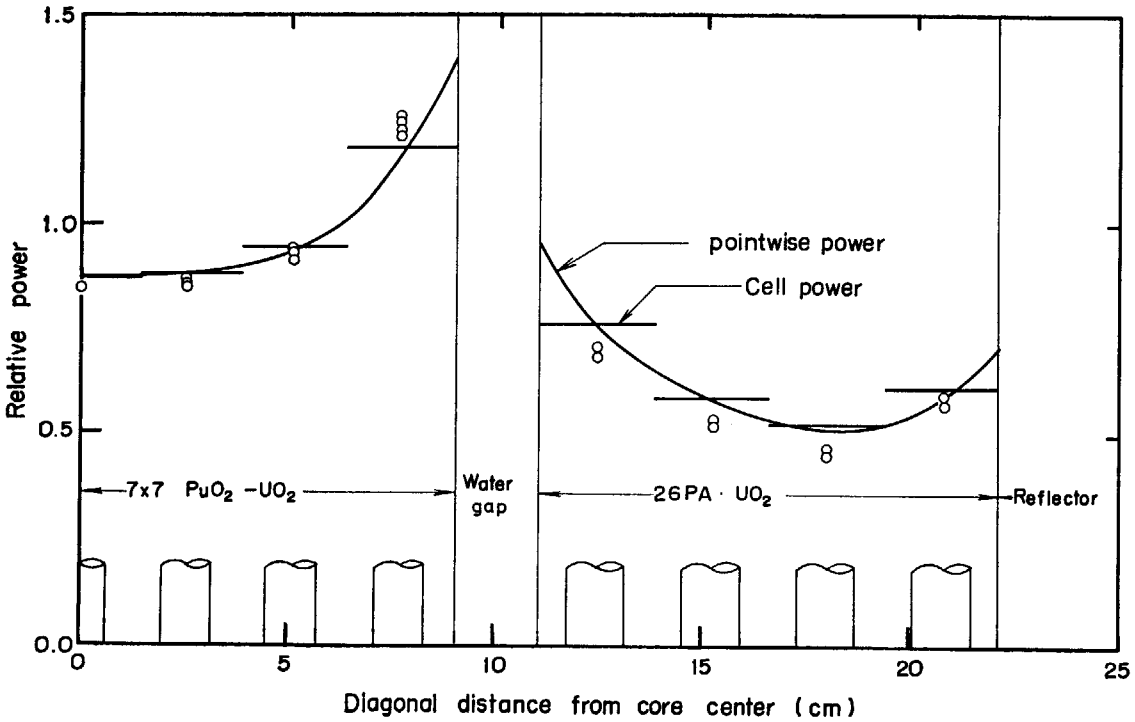

(b) diagonal direction.

○: Measured, ——: Calculated.

Fig. 55 Power distribution in 2.38Pu (RUN 3848) core.

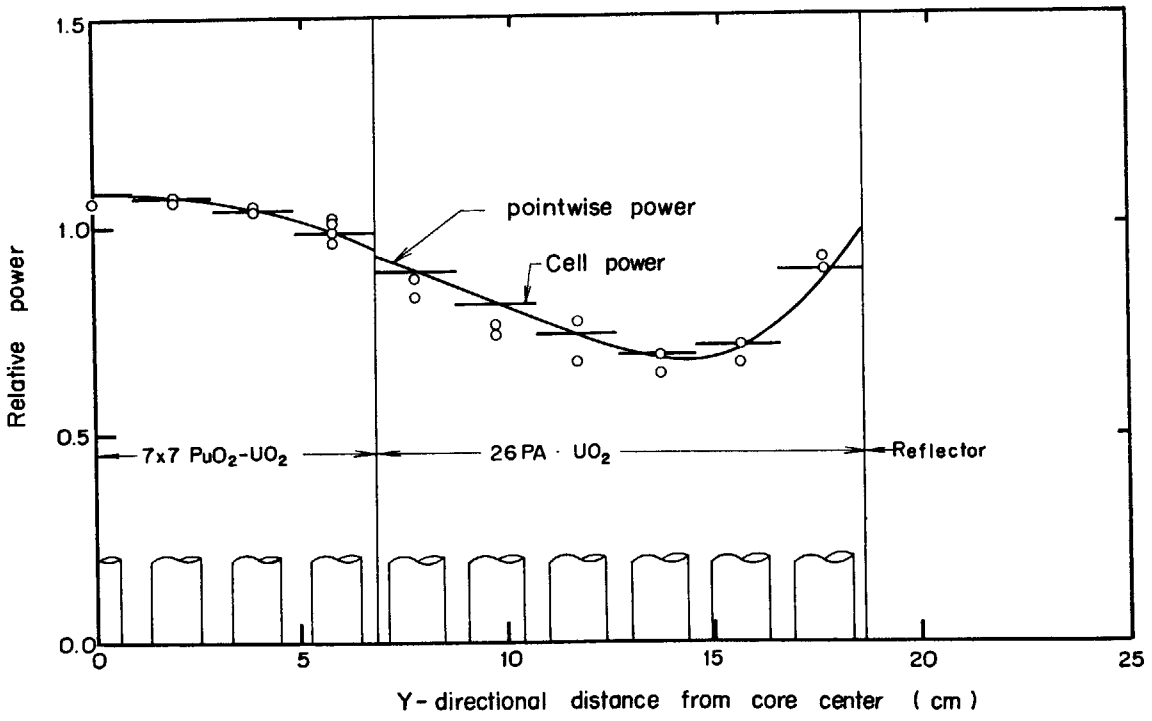

(a) Y-direction,

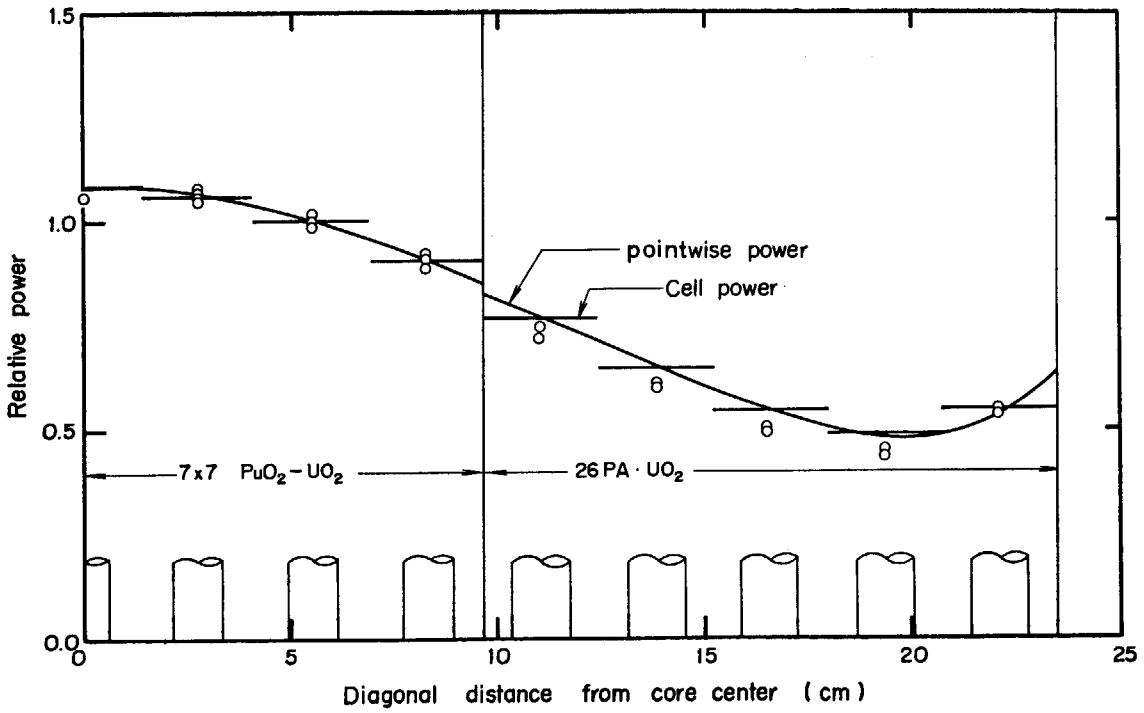

(b) diagonal direction.

○ : Measured, —— : Calculated.

Fig. 56 Power distribution in 2.95Pu (3830) core.

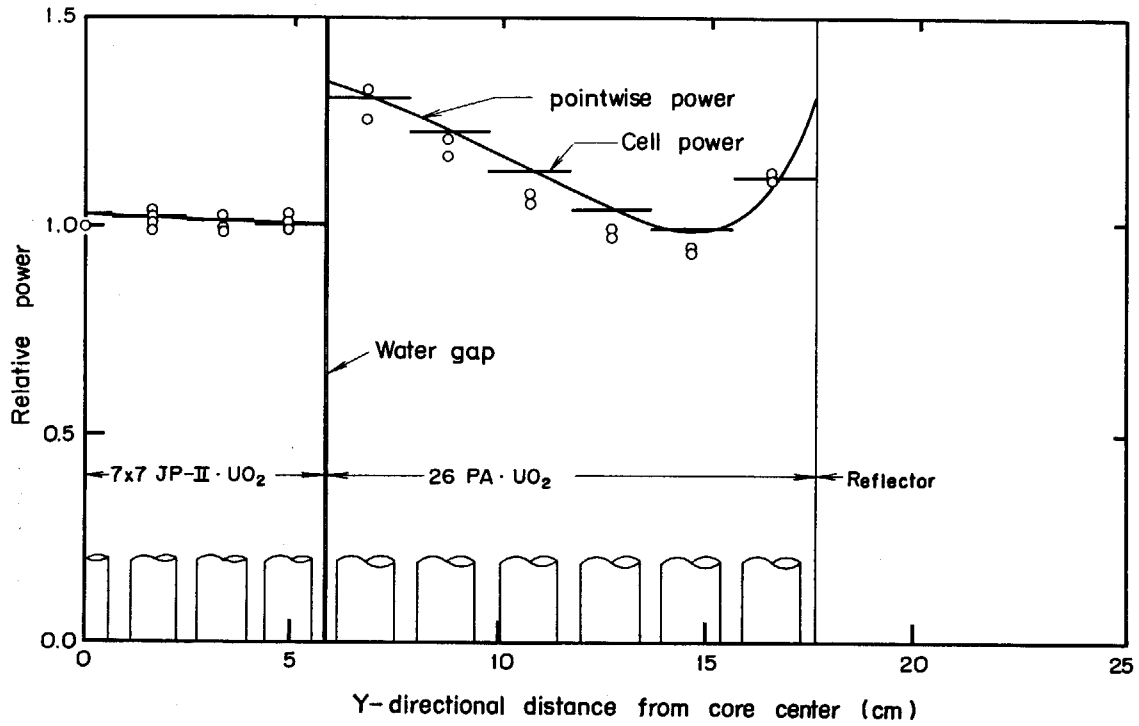

(a) Y-direction,

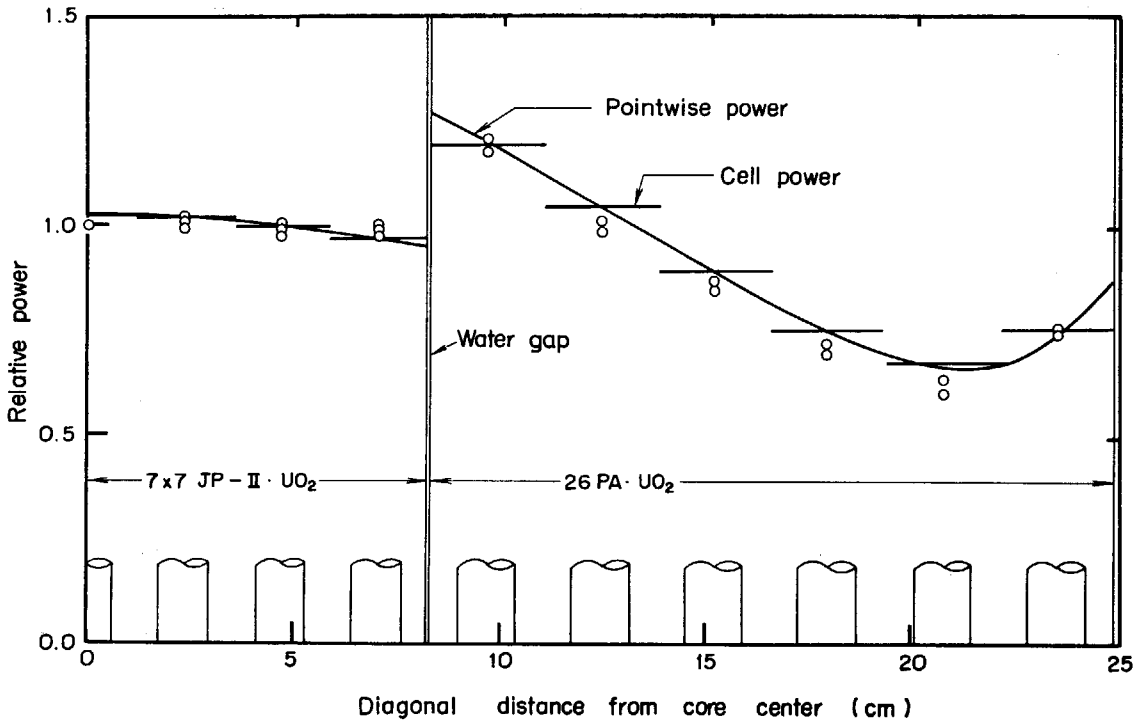

(b) diagonal direction.

○: Measured, ——: Calculated.

Fig. 57 Power distribution in 1.76U (RUN 3847) core.

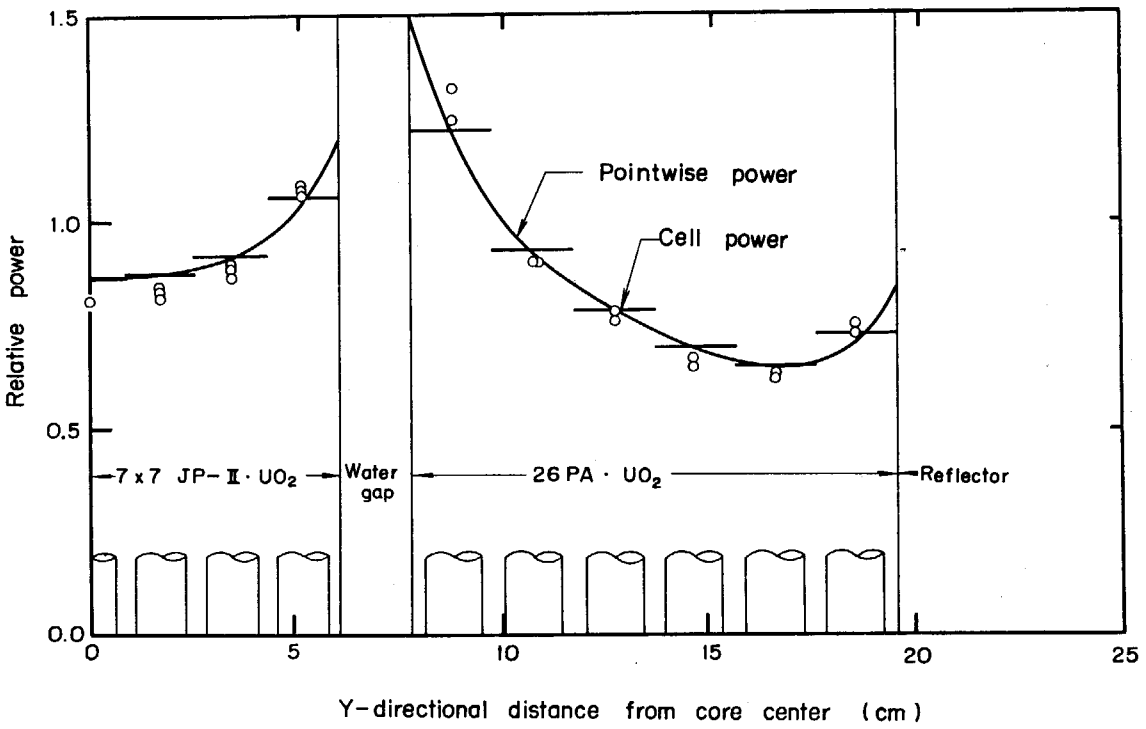

(a) Y-direction,

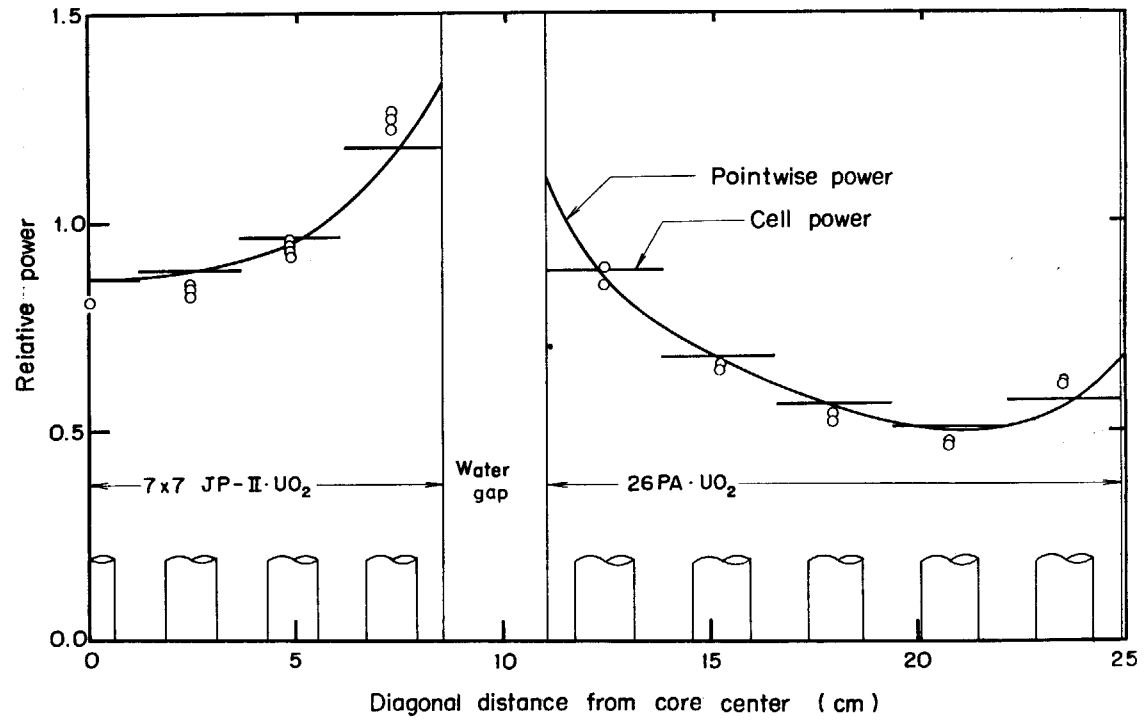

(b) diagonal direction.

○: Measured, ——: Calculated.

Fig. 58 Power distribution in 2.00U (RUN 3871) core.

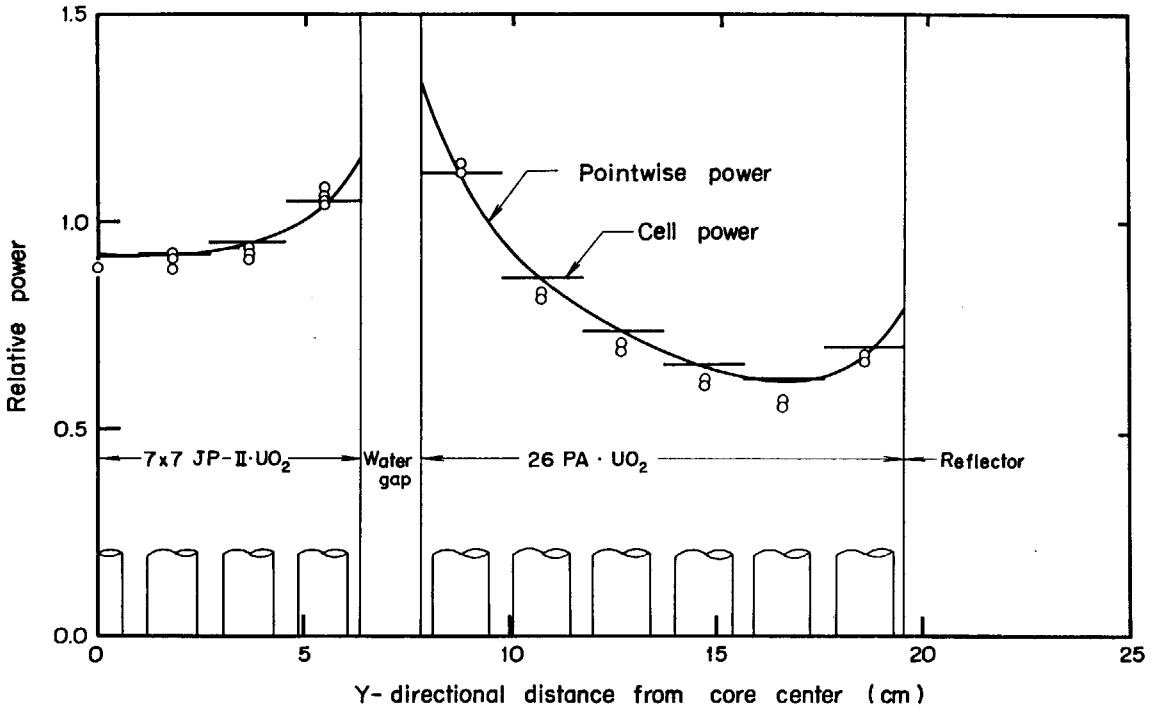

(a) Y-direction,

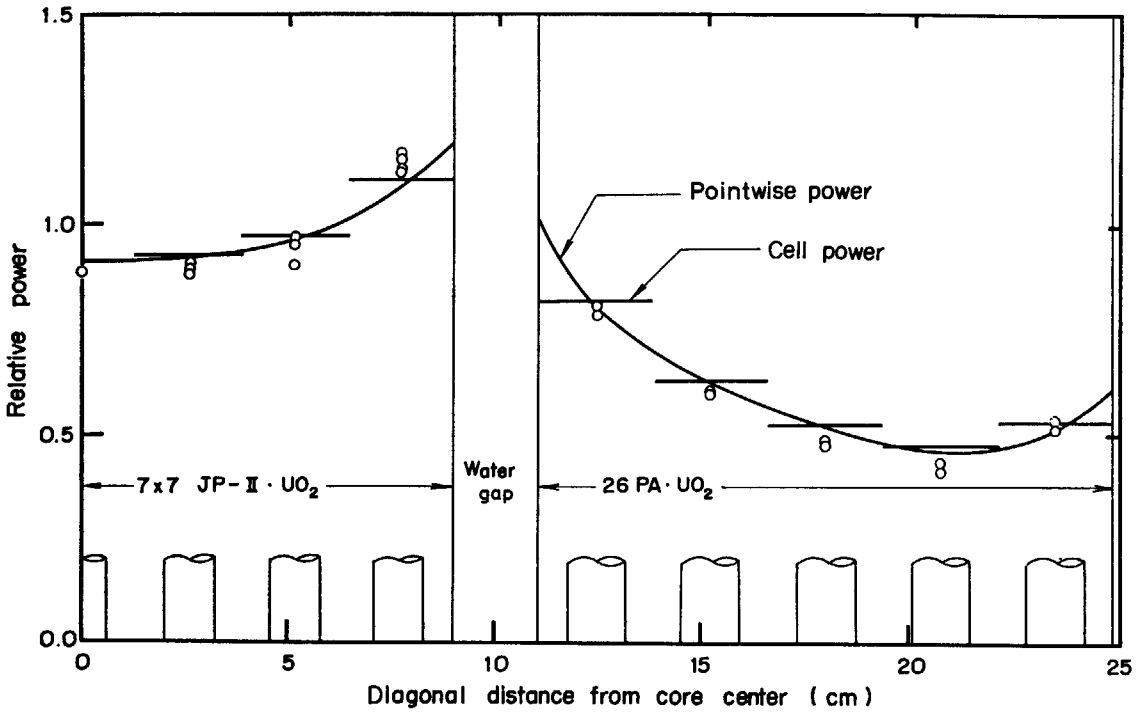

(b) diagonal direction.

○: Measured, ——: Calculated.

Fig. 59 Power distribution in 2.38U (RUN 3846) core.

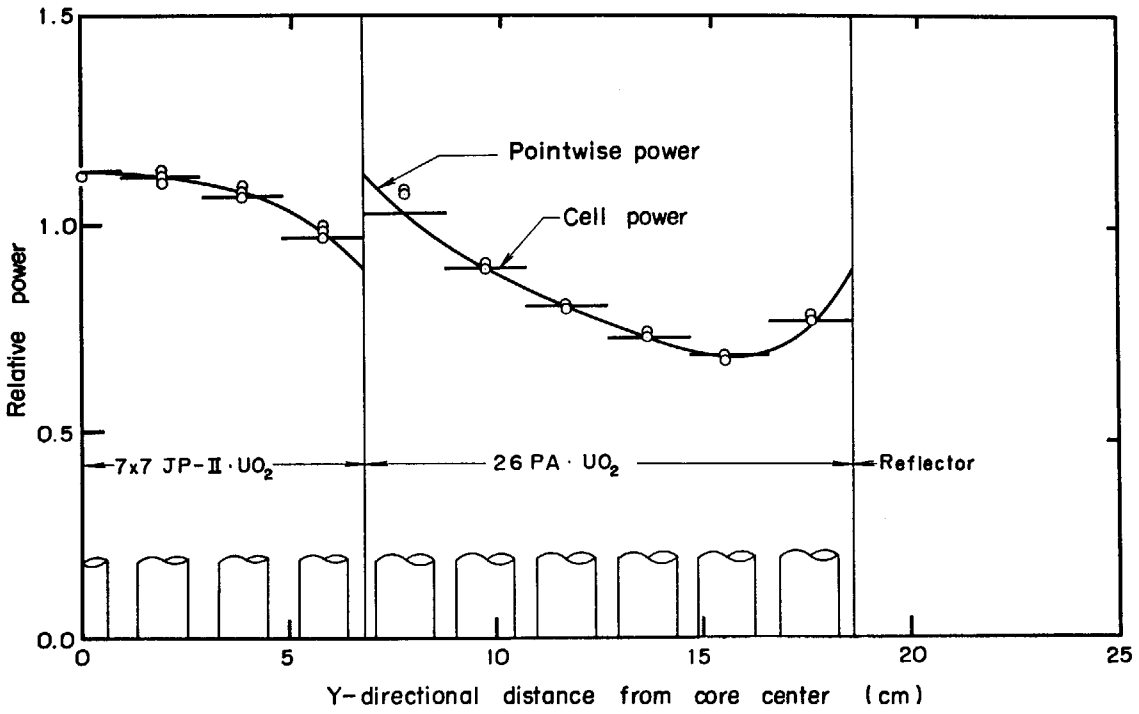

(a) Y-direction,

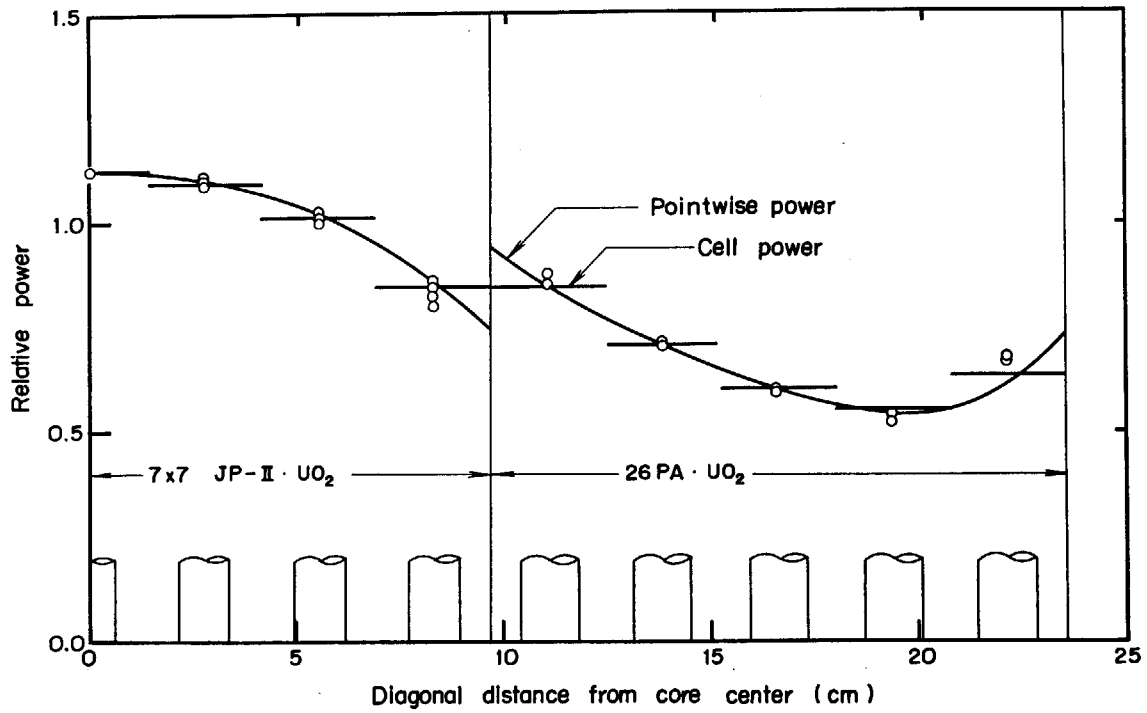

(b) diagonal direction.

○: Measured, ——: Calculated.

Fig. 60 Power distribution in 2.95U (RUN 3834) core.

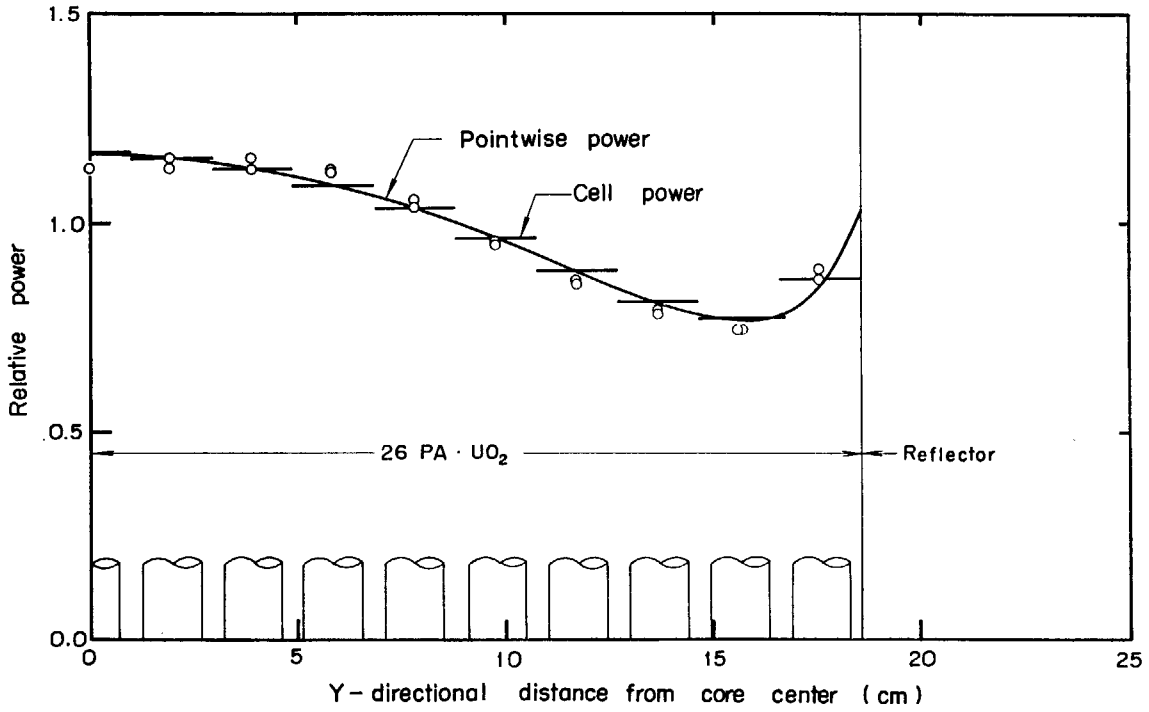

(a) Y-direction,

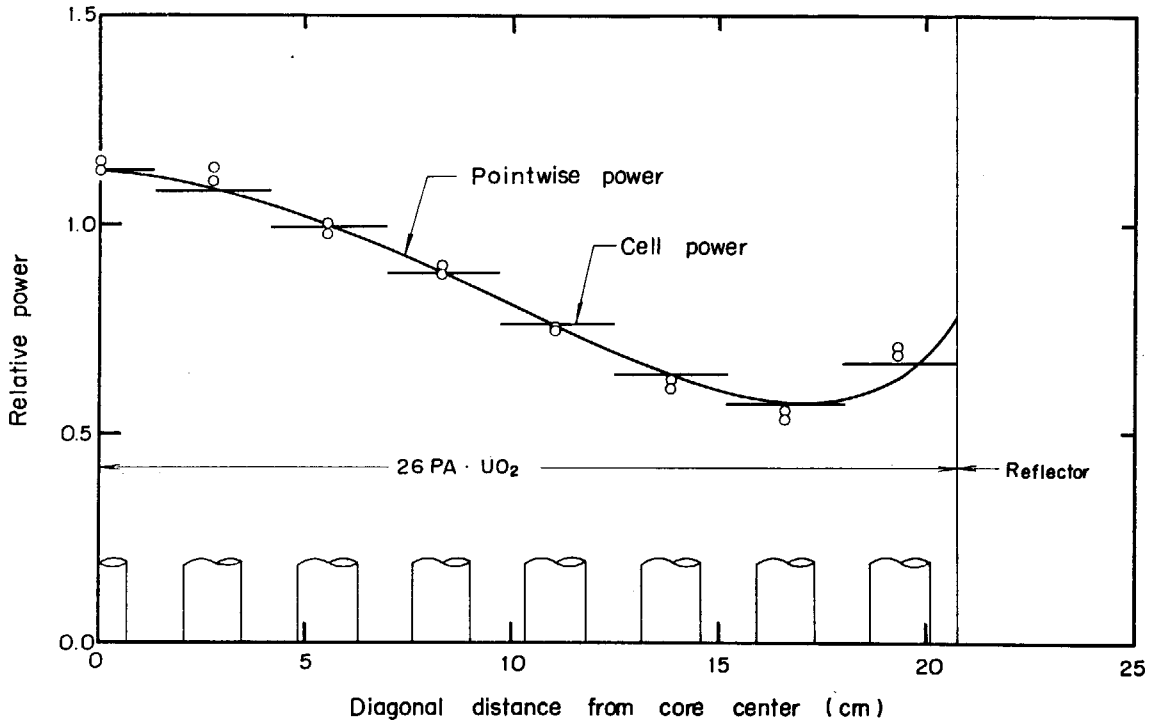

(b) diagonal direction.

○ : Measured, —— : Calculated.

Fig. 61 Power distribution in 1.83TU (RUN 3872) core.

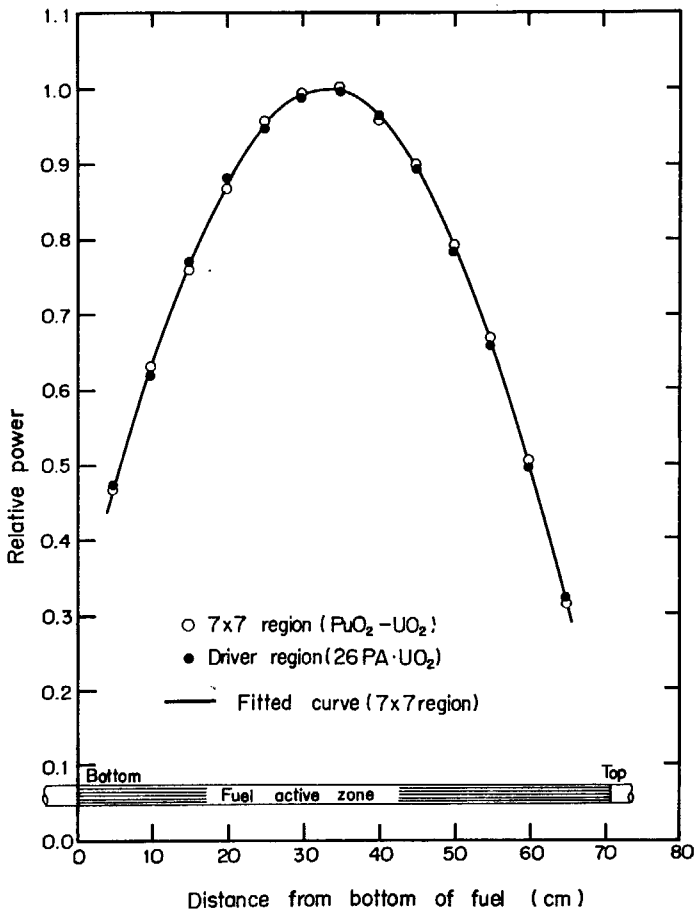

Fig. 62 Vertical power distributions and fitted value.

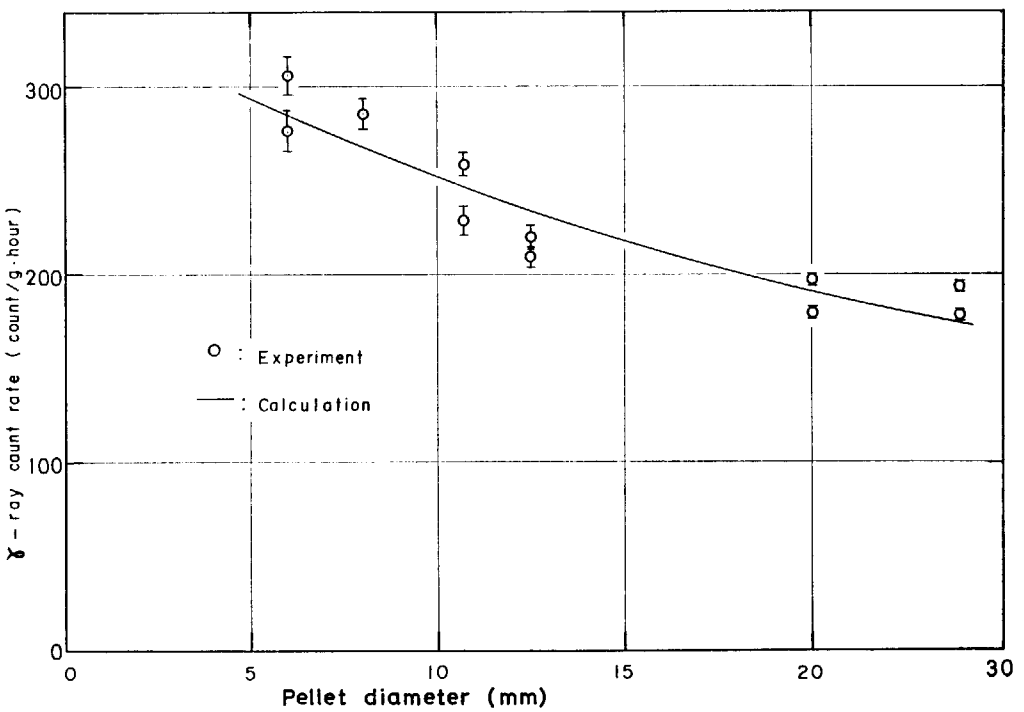

Fig. 63 Self-shielding of γ-ray by fuel pellet.

6. Conclusions

The purposes of this series of the experiments were,

(1) to compare the criticality as well as the neutron flux and power distributions in the plutonium fueled core with those in the uranium fueled core,

(2) to investigate the accuracy of a calculational method for plutonium recycle cores.

For these purposes, the multi-regional cores were assembled and the several parameters of mixed oxide and uranium dioxide fueled lattices were measured and analyzed. In the central zone of the core, two kinds of the fuel rods, the PuO_2-UO_2 and the JP-II·UO_2 fuels, which had the same diameter and the approximately same atomic number density of the fissile materials, were loaded.

From the analyses of the experiments, following remarks were obtained.

(1) The reactivity effect of the PuO_2-UO_2 fuel is larger than the JP-II·UO_2 fuel and its difference between both fuels becomes larger as the water-to-fuel volume ratio increases.

(2) By observing the neutron density distributions, it can be said that the PuO_2-UO_2 fuel has the larger neutron absorption than the JP-II·UO_2 fuel.

(3) The cadmium ratio in the PuO_2-UO_2 fueled lattice is lower than in the JP-II·UO_2 fueled lattice under the condition of the same water-to-fuel volume ratio between both lattices. The neutron spectrum in the central part of the 7×7 region, is not affected by the spectrum of the driver or the water gap region and has its own spectrum.

(4) From the comparison of the power distributions, the PuO_2-UO_2 fuel produces much power than the JP-II·UO_2 fuel under the same neutron flux level.

(5) The power peaking factor of the PuO_2-UO_2 fuel in the 7×7 region is greater than that of the UO_2 fuel.

(6) In the point of view of the matching between the 7×7 and driver regions, the 2.95Pu core is most optimum in the studied four cores. Where, the matching means that when UO_2 fuel rods in a uniform lattice are substituted by PuO_2-UO_2 fuel rods, power and neutron flux distributions, and neutron spectrum in the core is not affected so much.

The reasons why the 2.95Pu core is optimum on the matching are,

(a) the power distribution through the core is smoothly continuous and close to the distribution of cosine function,

(b) the neutron flux distribution is also smooth through the core,

(c) the cadmium ratio of Au is almost same in both regions. The reactivity effect of the PuO_2-UO_2 fuel is, however, greater than the UO_2 fuel.

In substituting of mixed oxide fuel assemblies into a light-water moderated power reactor, it has been pointed out theoretically that relatively large water-to-fuel volume ratio is necessary from the point of view of the power matching under the same dimension of the assembly[1),2),3)]. As far as the mixed oxide fuel having the same atomic number density of fissile material, the same result was obtained experimentally in this study.

Calculations were performed by using the LASER and PDQ·5 codes and following remarks were obtained.

(1) The effective multiplication factors k_{eff} are in the range of from 0.997 to 1.003 for the

critical cores.

(2) The calculated k_{eff} of the Pu system is greater than that of the U system.

(3) On the neutron density distribution in the 7×7 region under the normalization in the driver region, the difference between the calculated and measured values in the Pu system is greater than in the U system.

(4) The difference between the calculated and measured neutron densities in the multi-regional lattice is greater than in the uniform lattice.

(5) The calculated neutron density distribution has a tendency to become lower in the reflector and higher in the lattice than the measured values.

(6) On the power distribution under the normalization in the 7×7 region, the differences of the calculated values from the measured in the driver region are 5~9% for the Pu system and -1~5% for the U system.

From described results above, the conventional calculational technique are adaptable for the core loaded with the mixed oxide fuels which have power fraction of 20% of total power.

Acknowledgements

In performing this joint research by the Japan Atomic Energy Research Institute (JAERI) and the Power Reactor and Nuclear Fuel Development Corporation (PNC), the authors would like to acknowledge the continuing guidance and encouragement of Dr. S. Suguri (JAERI), Dr. Y. Nakamura, Dr. S. Suzuki, and Mr. Y. Miyawaki (PNC). They are also grateful to Messrs. K. Shiga, T. Takemura, H. Nakano, and other members of the fuel fabrication and inspection groups in PNC for fabrication of the PuO_2-UO_2 fuel rods, and Mr. Y. Nakano (Mitsubishi Atomic Power Industry) for preparing the UO_2 pellets used in the measurements of γ-ray attenuation factor and suggesting the shielding calculation.

References

1) Crowther R. L., Evance E. A., Levy S. and Macnabb W. V.: CONF-660308, 229 (1966)
2) Uematsu K., Yumoto R. and Yasukawa S.: Proceedings of a Symposium on the Use of Plutonium as a Reactor Fuel, IAEA, SM-88/34, (1967)
3) Yasukawa S., Uematsu K. and Yumoto R.: JAERI 1123 (1967)
4) Schmid L. C., Leonard B. R. Jr., Liikala R. C. and Smith R. I.: BNWL-801 (1968)
5) IAEA Panel on Plutonium Recycling in Thermal Power Reactor, Vienna, Austria, September 1968 and June 1971
6) Uotinen V. O., Leonard B. R. Jr. and Liikala R. C.: *Nucl. Technol.*, **18**, 115 (1973)
7) Suguri S. and Matsuura S.: *J. At. Energy Soc. Japan*, **11**(3), 150 (1969)
8) Matsuura S.: *Genshiryoku Kogyo*, **17**(12), 34 (1971)
9) Suguri S. and Miida J.: *J. At. Energy Soc. Japan*, **11**(3), 172 (1969)
10) Glasston S. and Edlund M. C.: "The Element of Nuclear Reactor Theory", D. Van Nostrand, 378 (1963)
11) Kobayashi I. and Hayata K.: JAERI-memo 2861 (1967)
12) Poncelet C. G.: WCAP-6073 (1966)
13) Honeck H. C.: BNL-5826

14) KATSURAGI M., MORIGUCHI K. and KUGE Y.: JAERI 1104 (1966)
15) CADWELL W. R., BUERGER P. F. and PFEIFER C. J.: WAPD-TM-477 (1965)
16) TAKEDA R. and INOUE K.: JAERI 1052 (1964)
17) MATSUURA S., KOBAYASHI I., TSURUTA H., ASAI N., HASHIMOTO M., OHNO A., YUMOTO R., KIKUCHI S. and KAJIYAMA T.: JAERI-memo 3438, PNCT-3127 (1969)
18) TSURUTA H.: *J. Nucl. Sci. Technol.*, **10**(9), 560 (1973)
19) JAMES M. F.: *J. nucl. Energy*, **23**, 517 (1969)

Nomenclatures

PuO_2–UO_2 : Plutonium and uranium mixed oxide fuel used in this experimental series. The enrichment of PuO_2 is 3.4 wt% and the active size is 1.07 cm in diameter and 70.6 cm in length.

JP-II·UO_2 : Uranium dioxide fuel of which enrichment is 2.6 wt% and the active size is 1.07 cm in diameter and 144.15 cm in length. This fuel rod was loaded in the central 7×7 region.

26PA·UO_2 : Uranium dioxide fuel of which enrichment is 2.6 wt% and the active size is 1.25 cm in diameter and 144.15 cm in length. This fuel rod was loaded in the driver region.

1.76Pu, 2.00Pu, 2.38Pu, 2.95Pu : Names of the multi-regional cores consisted of the central PuO_2–UO_2 fuel and the surrounding 26PA·UO_2 fuel lattices. Water-to-fuel volume ratios of the central 7×7 region are 1.76, 2.00, 2.38, and 2.95, respectively.

1.76U, 2.00U, 2.38U, 2.95U : Names of the multi-regional cores consisted of the central UO_2 fuel and the surrounding 26PA·UO_2 fuel lattices. Water-to-fuel volume ratios of the central 7×7 region are 1.76, 2.00, 2.38, and 2.95, respectively.

1.83TU : Name of the single regional core consisted of 26PA·UO_2 fuel lattice.

Pu system : General name for the 1.76Pu, 2.00Pu, 2.38Pu, and 2.95Pu cores.

U system : General name for the 1.76U, 2.00U, 2.38U, and 2.95U cores.

Appendix A1. Distributions of Dy activity

The numerical values of the measured distributions of Dy activity are listed in TABLES A1. 1 through A1. 6.

Nomenclatures in the tables are;

RUN : run number of the measurement,
NO. : position number of Dy-Al pellet in the core,
DISTANCE : detector position from the center of the core,
RELAT. DISTRI. : relative activity normalized to unity in the 7×7 region.

TABLE A1. 1 Dy activities in 1.76Pu (RUN 3799) and 2.00Pu (RUN 3837) cores.
TABLE A1. 2 Dy activities in 2.38Pu (RUN 3746) core.
TABLE A1. 3 Dy activities in 2.95Pu (RUN 3830) and 1.76U (RUN 3816) cores.

TABLE A1. 1

1.76PU RUN 3799

NO.	DISTANCE(CM)	RELAT. DISTRI.
1	0.0	0.887
2	0.41	0.971
3	0.83	1.028
4	1.25	0.952
5	1.66	0.908
6	2.07	0.975
7	2.49	1.037
8	2.90	0.936
9	3.32	0.928
10	3.74	1.021
11	4.15	1.094
12	4.57	1.066
13	4.98	1.002
14	5.39	1.059
15	5.81	1.158
16	6.36	1.365
17	6.85	1.295
18	7.34	1.325
19	7.82	1.461
20	8.31	1.354
21	8.80	1.283
22	9.29	1.380
23	9.78	1.468
24	10.27	1.302
25	10.76	1.189
26	11.25	1.133
27	11.74	1.277
28	12.22	1.174
29	12.71	1.021
30	13.20	1.106
31	13.69	1.208
32	14.18	1.052
33	14.67	1.029
34	15.16	1.134
35	15.65	1.222
36	16.14	1.194
37	16.63	1.222
38	17.11	1.477
39	17.60	1.851
40	18.09	2.304
41	18.58	2.520
42	19.07	2.735
43	19.56	2.855
44	20.54	2.806
45	21.52	2.723
46	22.49	2.477
47	23.47	2.189
48	24.45	1.903
49	25.43	1.608

2.00PU RUN 3837

NO.	DISTANCE(CM)	RELAT. DISTRI.
1	0.0	0.764
2	0.43	0.826
3	0.86	0.896
4	1.29	0.830
5	1.72	0.797
6	2.16	0.841
7	2.59	0.908
8	3.02	0.902
9	3.45	0.871
10	3.88	1.005
11	4.31	1.130
12	4.74	1.144
13	5.17	1.183
14	5.61	1.416
15	6.04	1.738
16	6.85	2.355
17	7.34	2.333
18	7.82	1.969
19	8.31	1.563
20	8.80	1.298
21	9.29	1.298
22	9.78	1.258
23	10.27	1.136
24	10.76	0.961
25	11.25	1.000
26	11.74	0.993
27	12.22	0.845
28	12.71	0.803
29	13.20	0.834
30	13.69	0.892
31	14.18	0.815
32	14.67	0.716
33	15.16	0.809
34	15.65	0.857
35	16.14	0.876
36	16.63	0.909
37	17.11	1.164
38	17.60	1.506
39	18.09	1.747
40	18.58	1.989
41	19.07	2.121
42	19.56	2.101
43	20.05	2.183
44	21.03	2.151
45	22.01	1.948
46	22.98	1.690
47	23.96	1.492
48	24.94	1.280
49	25.92	1.066

TABLE A1. 2

2.38PU RUN 3746

NO.	DISTANCE(CM)	RELAT. DISTRI.
1	0.0	0.813
2	0.45	0.919
3	0.91	0.949
4	1.37	0.912
5	1.82	0.815
6	2.27	0.899
7	2.73	0.980
8	3.19	0.943
9	3.64	0.873
10	4.10	0.984
11	4.55	1.079
12	5.00	1.080
13	5.46	1.081
14	5.91	1.277
15	6.11	1.442
16	6.36	1.737
17	6.37	1.620
18	6.60	1.773
19	6.85	1.992
20	7.09	1.848
21	7.34	1.953
22	7.58	1.774
23	7.82	1.657
24	8.07	1.441
25	8.31	1.337
26	8.56	1.207
27	8.80	1.179
28	9.05	1.126
29	9.29	1.171
30	9.54	1.174
31	9.78	1.113
32	10.03	0.976
33	10.27	0.944
34	10.51	0.862
35	10.76	0.834
36	11.00	0.856
37	11.25	0.897
38	11.49	0.881
39	11.74	0.838
40	11.98	0.864
41	12.22	0.745
42	12.47	0.729
43	12.71	0.664
44	12.96	0.707
45	13.20	0.711
46	13.45	0.738
47	13.69	0.749
48	13.94	0.673
49	14.18	0.688
50	14.43	0.611
51	14.67	0.644
52	14.91	0.638
53	15.16	0.724
54	15.40	0.730
55	15.65	0.778
56	15.89	0.762
57	16.14	0.771
58	16.38	0.753
59	16.63	0.814
60	16.87	0.854
61	17.11	1.038
62	17.36	1.081
63	17.60	1.301
64	17.85	1.376
65	18.09	1.516
66	18.34	1.558
67	18.58	1.639
68	18.83	1.658
69	19.07	1.785
70	19.32	1.758
71	19.56	1.882
72	20.29	1.784
73	20.54	1.848
74	21.27	1.763
75	21.52	1.702
76	22.25	1.551
77	22.49	1.530
78	23.23	1.358
79	23.47	1.381
80	24.21	1.133
81	24.45	1.184
82	25.18	1.015
83	25.43	0.956

TABLE A1. 3

2.95PU RUN 3830

NO.	DISTANCE(CM)	RELAT. DISTRI.
1	0.0	0.953
2	0.49	1.044
3	0.98	1.107
4	1.47	1.028
5	1.96	0.983
6	2.44	1.041
7	2.93	1.074
8	3.42	1.021
9	3.91	0.913
10	4.40	1.026
11	4.89	1.037
12	5.38	0.968
13	5.87	0.918
14	6.36	0.916
15	6.85	0.895
16	7.34	0.925
17	7.82	0.804
18	8.31	0.799
19	8.80	0.839
20	9.29	0.836
21	9.78	0.718
22	10.27	0.752
23	10.76	0.789
24	11.25	0.710
25	11.74	0.664
26	12.22	0.703
27	12.71	0.672
28	13.20	0.644
29	13.69	0.578
30	14.18	0.661
31	14.67	0.693
32	15.16	0.680
33	15.65	0.657
34	16.14	0.766
35	16.63	0.850
36	17.11	0.966
37	17.60	1.027
38	18.09	1.173
39	18.58	1.317
40	19.56	1.566
41	20.54	1.565
42	21.52	1.468
43	22.49	1.268
44	23.47	1.147
45	24.45	0.982

1.76U RUN 3816

NO.	DISTANCE(CM)	RELAT. DISTRI.
1	0.0	0.921
2	0.41	1.038
3	0.83	1.074
4	1.25	1.001
5	1.66	0.951
6	2.07	1.010
7	2.49	1.061
8	2.90	0.999
9	3.32	0.931
10	3.74	1.012
11	4.15	1.048
12	4.57	1.021
13	4.98	0.931
14	5.39	0.978
15	5.81	0.970
16	6.36	1.055
17	6.85	1.000
18	7.34	1.062
19	7.82	1.081
20	8.31	0.924
21	8.80	0.879
22	9.29	0.939
23	9.78	0.993
24	10.27	0.877
25	10.76	0.837
26	11.25	0.870
27	11.74	0.841
28	12.22	0.781
29	12.71	0.713
30	13.20	0.778
31	13.69	0.799
32	14.18	0.724
33	14.67	0.678
34	15.16	0.730
35	15.65	0.811
36	16.14	0.835
37	16.63	0.889
38	17.11	1.093
39	17.60	1.364
40	18.09	1.627
41	18.58	1.813
42	19.07	1.863
43	19.56	1.945
44	20.54	2.018
45	21.52	1.842
46	22.49	1.651
47	23.47	1.477
48	24.45	1.248
49	25.43	1.078

TABLE A1.4 Dy activities in 2.00U (RUN 3883) core.
TABLE A1.5 Dy activities in 2.38U (RUN 3845) core.
TABLE A1.6 Dy activities in 2.95U (RUN 3835) and 1.83TU (RUN 3872) cores.

TABLE A1.4

2.00U RUN 3883

NO.	DISTANCE(CM)	RELAT. DISTRI.
1	0.0	0.898
2	0.43	0.906
3	0.86	0.946
4	1.29	0.873
5	1.72	0.846
6	2.16	0.911
7	2.59	0.940
8	3.02	0.971
9	3.45	0.891
10	3.88	0.985
11	4.31	1.095
12	4.74	1.093
13	5.17	1.062
14	5.61	1.263
15	6.04	1.540
16	6.36	1.722
17	6.85	1.872
18	7.34	1.725
19	7.82	1.530
20	8.31	1.188
21	8.80	0.979
22	9.29	0.983
23	9.78	0.934
24	10.27	0.864
25	10.63	0.788
26	10.76	0.686
27	11.25	0.696
28	11.74	0.699
29	12.22	0.618
30	12.71	0.581
31	13.20	0.581
32	13.69	0.627
33	14.18	0.571
34	14.67	0.515
35	15.16	0.518
36	15.65	0.563
37	16.14	0.520
38	16.63	0.464
39	17.11	0.509
40	17.60	0.568
41	18.09	0.545
42	18.58	0.574
43	19.07	0.683
44	19.56	0.858
45	20.05	1.085
46	20.54	1.175
47	21.03	1.233
48	21.52	1.299
49	22.01	1.258
50	22.49	1.259
51	22.98	1.297
52	23.47	1.240
53	23.96	1.167
54	24.45	1.101
55	24.94	1.015
56	25.43	0.978
57	25.92	0.895
58	26.41	0.840
59	27.38	0.702
60	28.36	0.573

TABLE A1.5

2.38U RUN 3845

NO.	DISTANCE(CM)	RELAT. DISTRI.
1	0.0	0.880
2	0.45	0.934
3	0.91	0.981
4	1.37	0.938
5	1.82	0.893
6	2.27	0.925
7	2.73	0.961
8	3.19	0.974
9	3.64	0.917
10	4.10	0.981
11	4.55	1.069
12	5.00	1.065
13	5.46	1.042
14	5.91	1.182
15	6.37	1.399
16	6.60	1.439
17	6.85	1.510
18	7.09	1.494
19	7.34	1.475
20	7.58	1.351
21	7.82	1.269
22	8.07	1.082
23	8.31	1.004
24	8.56	0.866
25	8.80	0.791
26	9.05	0.791
27	9.29	0.788
28	9.54	0.842
29	9.78	0.778
30	10.03	0.756
31	10.27	0.710
32	10.51	0.642
33	10.76	0.635
34	11.00	0.585
35	11.25	0.622
36	11.49	0.630
37	11.74	0.634
38	11.98	0.564
39	12.22	0.541
40	12.47	0.501
41	12.71	0.521
42	12.96	0.494
43	13.20	0.505
44	13.45	0.542
45	13.69	0.525
46	13.94	0.510
47	14.18	0.469
48	14.43	0.440
49	14.67	0.413
50	14.91	0.428
51	15.16	0.449
52	15.40	0.465
53	15.65	0.474
54	15.89	0.440
55	16.14	0.428
56	16.38	0.394
57	16.63	0.419
58	16.87	0.418
59	17.11	0.477
60	17.36	0.479
61	17.60	0.549
62	17.85	0.491
63	18.09	0.511
64	18.34	0.453
65	18.58	0.556
66	18.83	0.543
67	19.07	0.666
68	19.32	0.704
69	19.56	0.804
70	19.80	0.906
71	20.05	0.964
72	20.29	1.039
73	20.54	1.079
74	21.27	1.144
75	21.52	1.123
76	22.25	1.118
77	22.49	1.118
78	23.23	1.062
79	23.47	1.025
80	24.21	0.943
81	24.45	0.939
82	25.18	0.821
83	25.43	0.788

TABLE A1.6

2.95U RUN 3835

NO.	DISTANCE(CM)	RELAT. DISTRI.
1	0.75	1.031
2	0.73	1.112
3	1.22	1.109
4	1.71	1.005
5	2.20	0.987
6	2.69	1.050
7	3.18	1.066
8	3.67	0.951
9	4.16	0.980
10	4.65	1.035
11	5.13	0.991
12	5.62	0.931
13	6.11	0.888
14	6.60	0.863
15	7.09	0.759
16	7.58	0.697
17	8.07	0.646
18	8.56	0.663
19	9.05	0.640
20	9.54	0.556
21	10.03	0.539
22	10.51	0.579
23	10.51	0.575
24	11.00	0.583
25	11.49	0.519
26	11.98	0.504
27	12.47	0.512
28	12.96	0.491
29	13.45	0.442
30	13.94	0.422
31	14.43	0.464
32	14.91	0.473
33	15.40	0.430
34	15.80	0.435
35	16.38	0.480
36	16.87	0.482
37	17.36	0.468
38	17.85	0.502
39	18.34	0.676
40	18.83	0.819
41	19.32	0.998
42	19.80	1.024
43	20.29	1.120
44	20.78	1.108
45	21.27	1.187
46	21.76	1.142
47	22.25	1.101
48	22.74	0.996
49	23.23	0.988
50	23.72	0.875
51	24.21	0.880
52	24.70	0.790
53	25.67	0.678

1.83TU RUN 3872

NO.	DISTANCE(CM)	RELAT. DISTRI.
1	0.0	1.006
2	0.98	1.107
3	1.96	1.003
4	2.93	1.198
5	3.91	1.045
6	4.89	1.173
7	5.87	0.981
8	6.85	1.029
9	7.82	0.876
10	8.80	0.984
11	9.78	0.866
12	10.76	0.937
13	11.74	0.765
14	12.71	0.922
15	13.69	0.907
16	14.67	1.407
17	15.65	1.948
18	16.63	2.157
19	17.60	2.187
20	18.58	2.065
21	19.56	1.846
22	20.54	1.606
23	21.52	1.412
24	22.49	1.214
25	23.47	1.003
26	24.45	0.845
27	25.43	0.709
28	26.41	0.579
29	27.38	0.471
30	28.36	0.389
31	29.34	0.327
32	30.32	0.250
33	31.30	0.207
34	33.25	0.175
35	35.21	0.106
36	37.16	0.077
37	39.12	0.052
38	41.08	0.037

Appendix A2. Distributions of Au activity and cadmium ratio-1.0

The numerical values of Au activity and cadmium ratio minus one are listed in TABLES A2. 1 through A2. 9.

Nomenclatures in the tables are;

DISTANCE : detector pellet position from the center of the core,

BARE : count rate of γ-ray from bare Au pellet,

CD COVER : count rate of γ-ray from cadmium covered Au pellet,

R_{cd}-1.0 : cadmium ratio-1.0 of Au detector by BARE/CD COVER-1.0

TABLE A2. 1 Au activities and cadmium ratio-1.0 in 1.76Pu (RUN 3813) core.

DISTANCE cm	1.76Pu RUN 3813 BARE count/mg	CD COVER count/mg	R_{cd}-1.0
0. 0	1346. 0		
0. 41	1447. 2		
0. 83	1520. 9	619. 8	1. 45
1. 25	1431. 4		
1. 66	1371. 7	617. 6	1. 22
2. 07	1508. 9		
2. 49	1514. 5	613. 9	1. 46
2. 90	1455. 4		
3. 32	1428. 1	615. 0	1. 32
3. 74	1535. 2		
4. 15	1601. 4	601. 0	1. 66
4. 57	1550. 0		
4. 98	1518. 2	577. 6	1. 62
5. 39	1577. 7		
5. 81	1695. 7	589. 1	1. 87
6. 36	1714. 0		
6. 85	1688. 5	572. 6	1. 94
7. 34	1710. 8		
7. 82	1808. 8	578. 8	2. 12
8. 31	1760. 8		
8. 80	1648. 3	535. 8	2. 07
9. 29	1657. 6		
9. 78	1732. 1	504. 7	2. 43
10. 27	1696. 7		
10. 76	1537. 1	471. 3	2. 26
11. 25	1503. 5		
11. 74	1565. 7	460. 8	2. 39
12. 22	1493. 5		
12. 71	1367. 6	425. 5	2. 21
13. 20	1333. 3		
13. 69	1424. 5	398. 4	2. 57
14. 18	1371. 9		
14. 67	1234. 9	352. 3	2. 50
15. 16	1249. 5		
15. 65	1321. 0	325. 4	3. 05
16. 14	1407. 4		
16. 63	1400. 2	299. 5	3. 67
17. 11	1451. 0		
17. 60	1734. 8	267. 6	5. 48
18. 09	2075. 5		
18. 58	2356. 4	235. 9	8. 98
19. 56	2646. 6	202. 0	12. 10
20. 54	2625. 0	167. 5	14. 67
21. 52	2485. 1		
22. 49	2258. 2		
23. 47	1977. 4		
22. 45	1701. 3		
25. 43	1459. 5		
26. 41	1213. 3		
27. 38	1015. 3		

TABLE A2. 2 Au activities and cadmium ratio-1.0 in 2.00Pu (RUN 3838) core.

DISTANCE cm	2.00Pu RUN 3838 BARE count/mg	CD COVER count/mg	R_{cd}-1.0
0. 0	167. 4		
0. 43	181. 6		
0. 86	183. 8	72. 3	1. 54
1. 29	173. 7		
1. 72	180. 2	65. 8	1. 73
2. 16	179. 2		
2. 59	189. 6	66. 0	1. 87
3. 02	191. 4		
3. 45	195. 1	65. 2	1. 99
3. 88	196. 8		
4. 31	228. 9	66. 5	2. 44
4. 74	222. 2		
5. 17	226. 3	64. 1	2. 53
5. 61	255. 7		
6. 04	321. 2	70. 8	3. 53
6. 36	369. 5		
6. 85	401. 4	66. 6	5. 02
7. 34	403. 7		
7. 82	373. 5	63. 2	4. 90
8. 31	309. 6		
8. 80	252. 6	60. 5	3. 17
9. 29	241. 0		
9. 78	233. 5	55. 7	3. 19
10. 27	212. 0		
10. 76	191. 9	54. 2	2. 53
11. 25	190. 1		
11. 74	182. 7	48. 6	2. 75
12. 22	171. 1		
12. 71	158. 3	47. 8	2. 31
13. 20	152. 6		
13. 69	159. 6	40. 4	2. 95
14. 18	158. 5		
14. 67	138. 4	37. 8	2. 66
15. 16	141. 2		
15. 65	146. 3	35. 7	3. 09
16. 14	154. 6		
16. 63	146. 4	33. 4	3. 38
17. 11	161. 6		
17. 60	200. 0	29. 9	5. 69
18. 09	245. 4		
18. 58	287. 1	25. 4	10. 30
19. 07	289. 3		
19. 56	292. 1	21. 5	12. 55
20. 54	318. 5	18. 0	16. 71
21. 52	293. 6	13. 8	20. 33
22. 49	269. 7	11. 5	22. 47
23. 47	226. 0	9. 0	24. 19
24. 45	199. 4	7. 6	25. 17
25. 43	173. 8	5. 4	31. 05
26. 41	141. 2		
27. 38	120. 3		
28. 36	92. 1		

TABLE A2. 3 Au activities and cadmium ratio-1.0 in 2.38Pu (RUN 3877) core.

DISTANCE cm	2.38Pu RUN 3877 BARE count/mg	CD COVER count/mg	R_{cd}-1.0
0.0	329.8		
0.45	337.4		
0.91	366.6	122.4	1.99
1.37	360.7		
1.82	342.8	122.6	1.79
2.27	361.0		
2.73	388.1	116.3	2.33
3.19	368.4		
3.64	361.8	115.2	2.13
4.10	374.0		
4.55	402.9	118.6	2.39
5.00	409.7		
5.46	407.1	113.3	2.59
5.91	440.8		
6.37	547.6	116.9	3.68
6.36	491.0		
6.85	574.1	120.3	3.77
7.34	579.5		
7.82	537.7	109.7	3.90
8.31	444.0		
8.80	387.1	97.2	2.98
9.29	387.4		
9.78	377.5	98.8	2.81
10.27	346.8		
10.76	309.8	86.7	2.57
11.25	295.5		
11.74	306.5	84.3	2.63
12.22	286.5		
12.71	258.8	75.4	2.43
13.20	255.6		
13.69	259.6	74.1	2.50
14.18	252.7		
14.67	226.2	66.5	2.40
15.16	236.6		
15.65	253.1	62.3	3.06
16.14	257.1		
16.63	251.9	56.4	3.46
17.11	272.1		
17.69	321.7	48.4	5.64
18.00	398.7		
18.58	448.6	43.8	9.24
19.07	466.3		
19.56	492.2	38.4	11.82
20.54	477.8	29.2	15.38

TABLE A2. 4 Au activities and cadmium ratio-1.0 in 2.95Pu (RUN 3831) core.

DISTANCE cm	2.95Pu RUN 3831 BARE count/mg	CD COVER count/mg	R_{cd}-1.0
0.0	360.3		
0.49	375.3		
0.98	385.5	111.0	2.47
1.47	376.8		
1.96	355.0	111.7	2.17
2.44	367.2		
2.93	381.4	113.0	2.37
3.42	359.2		
3.91	344.6	104.1	2.30
4.40	359.6		
4.89	365.1	105.3	2.47
5.38	350.3		
5.87	333.1	98.2	2.39
6.36	339.1		
6.85	340.5	97.5	2.49
7.34	321.8		
7.82	296.0	89.2	2.32
8.31	304.4		
8.80	320.1	86.8	2.68
9.29	300.9		
9.78	277.1	82.4	2.36
10.27	281.6		
10.76	288.8	76.5	2.77
11.25	262.4		
11.74	249.1	72.2	2.44
12.22	245.6		
12.71	245.7	68.3	2.59
13.20	238.3		
13.69	217.8	63.5	2.43
14.18	220.2		
14.67	232.1	55.2	3.20
15.16	238.4		
15.65	228.8	51.4	3.44
16.14	234.8		
16.63	264.0	46.6	4.66
17.11	281.9		
17.60	308.0	41.2	6.47
18.09	353.3		
18.58	383.3	34.1	10.24
19.56	416.5	29.3	13.20
20.54	411.6	25.2	15.30
21.52	385.7	20.4	17.94
22.49	355.3	16.6	20.37
23.47	302.4	13.3	21.82
24.45	268.2	9.9	26.04

TABLE A2. 5 Au activities and cadmium ratio-1.0 in 1.76U (RUN 3822) core.

1.76U RUN 3822

DISTANCE cm	BARE count/mg	CD COVER count/mg	R_{cd}-1.0
0. 0	177. 9		
0. 41	185. 8		
0. 83	190. 9	58. 3	2. 27
1. 25	187. 1		
1. 66	175. 4	55. 7	2. 14
2. 07	180. 9		
2. 49	191. 5	59. 8	2. 20
2. 90	183. 4		
3. 32	174. 9	54. 9	2. 18
3. 74	188. 7		
4. 15	187. 7	54. 1	2. 47
4. 57	181. 2		
4. 98	177. 1	54. 3	2. 26
5. 39	180. 6		
5. 81	187. 8	53. 8	2. 49
6. 36	192. 7		
6. 85	180. 2	52. 2	2. 45
7. 34	183. 0		
7. 82	191. 3	51. 8	2. 69
8. 31	178. 5		
8. 80	160. 7	48. 8	2. 29
9. 29	158. 3		
9. 78	172. 0	50. 5	2. 40
10. 27	163. 8		
10. 76	152. 2	45, 1	2. 37
11. 25	145. 7		
11. 74	156. 3	43. 7	2. 57
12. 22	144. 6		
12. 71	133. 7	38. 4	2. 48
13. 20	127. 0		
13. 69	137. 9	38. 5	2. 58
14. 18	134. 4		
14. 67	119. 3	33. 2	2. 59
15. 16	121. 0		
15. 65	129. 4	32. 3	3. 00
16. 14	134. 8		
16. 63	138. 8	27. 5	4. 05
17. 11	145. 6		
17. 60	173. 8	26. 1	5. 66
18. 09	212. 2		
18. 58	235. 8	24. 3	8. 69
19. 07	245. 4		
19. 56	256. 4	19. 0	12. 47
20. 54	263. 5	15. 9	15. 61
21. 52	244. 0	11. 5	20. 16
22. 49	221. 2		
23. 47	194. 8		
24. 45	184. 0		
25. 43	141. 3		
26. 41	120. 1		
27. 38	100. 2		

TABLE A2. 6 Au activities and cadmium ratio-1.0 in 2.00U (RUN 3884) core.

2.00U RUN 3884

DISTANCE cm	BARE count/mg	CD COVER count/mg	R_{cd}-1.0
0. 0	193. 9		
0. 43	203. 5		
0. 86	214. 2	58. 0	2. 69
1. 29	214. 1		
1. 72	203. 5	56. 2	2. 62
2. 16	210. 0		
2. 59	215. 3	56. 8	2. 79
3. 02	211. 1		
3. 45	213. 9	56. 0	2. 81
3. 88	221. 7		
4. 31	246. 2	57. 9	3. 25
4. 74	243. 7		
5. 17	240. 9	57. 3	3. 20
5. 61	279. 1		
6. 04	323. 5	56. 4	4. 73
6. 36	340. 1		
6. 85	355. 3	58. 8	5. 04
7. 34	347. 9		
7. 82	308. 6	54. 9	4. 62
8. 31	247. 6		
8. 80	211. 8	52. 3	3. 04
9. 29	211. 4		
9. 78	207. 0	47. 5	3. 36
10. 27	185. 9		
10. 76	163. 0	45. 5	2. 58
11. 25	161. 7		
11. 74	163. 9	44. 1	2. 71
12. 22	155. 3		
12. 71	138. 3	41. 8	2. 30
13. 20	140. 6		
13. 69	143. 9	41. 6	2. 45
14. 18	129. 7		
14. 67	120. 8	35. 0	2. 45
15. 16	119. 5		
15. 65	126. 5	34. 0	2. 72
16. 14	120. 5		
16. 63	108. 9	30. 0	2. 63
17. 11	111. 5		
17. 60	119. 1	28. 1	3. 23
18. 09	120. 9		
18. 58	122. 4	24. 1	4. 08
19. 07	132. 5		
19. 56	157. 1	23. 0	5. 84
20. 54	195. 5		
21. 52	211. 1	20. 5	9. 29
22. 49	224. 0		
23. 47	228. 0	16. 5	12. 86
24. 47	232. 3		
25. 43	230. 6	13. 6	16. 01
26. 41	220. 9		
27. 38	215. 3	10. 3	19. 9
27. 87	205. 3		

TABLE A2.7 Au activities and cadmium ratio-1.0 in 2.38U (RUN 3846) core.

	2.38U RUN 3846		
DISTANCE cm	BARE count/mg	CD COVER count/mg	R_{cd}-1.0
0.0	468.2		
0.45	503.4		
0.91	500.0	128.8	2.88
1.37	500.4		
1.82	463.5	123.8	2.74
2.27	489.2		
2.73	516.8	134.1	2.85
3.19	502.5		
3.64	490.2	128.4	2.81
4.10	512.7		
4.55	557.1	131.0	3.25
5.00	538.6		
5.46	532.3	125.6	3.23
5.91	600.0		
6.37	681.0	127.6	4.33
6.85	713.9	120.2	4.93
7.34	713.3		
7.82	647.0	118.7	4.45
8.31	528.4		
8.80	438.5	114.8	2.81
9.29	434.6		
9.78	421.2	98.2	3.28
10.27	404.2		
10.76	344.3	95.9	2.59
11.25	335.0		
11.74	340.1	99.5	2.41
12.22	314.7		
12.71	283.0	90.3	2.13
13.20	298.8		
13.69	301.9	91.2	2.31
14.18	286.7		
14.67	245.1	79.1	2.10
15.16	253.2		
15.65	260.2	74.9	2.47
16.14	250.1		
16.63	228.8	70.5	2.24
17.11	245.0		
17.60	257.6	66.4	2.87
18.09	249.8		
18.58	251.9	51.5	3.89
19.07	277.2		
19.56	349.1	50.6	5.90
20.05	418.4		
20.54	440.9	39.7	10.11
21.52	501.0	35.0	13.29
22.49	474.5	30.3	14.63
23.47	434.9	24.5	16.76
24.45	402.4	22.1	17.22
25.43	340.9	15.9	20.44

TABLE A2.8 Au activities and cadmium ratio-1.0 in 2.95U (RUN 3834) core.

	2.95U RUN 3834		
DISTANCE cm	BARE count/mg	CD COVER count/mg	R_{cd}-1.0
0.0	505.9		
0.49	522.4		
0.98	547.0	111.8	3.89
1.47	549.1		
1.96	508.6	113.5	3.48
2.44	546.9		
2.93	542.6	110.2	3.92
3.42	516.6		
3.91	499.3	107.4	3.64
4.40	497.4		
4.89	508.0	106.4	3.77
5.38	492.2		
5.87	450.9	107.8	3.18
6.36	435.6		
6.85	439.2	99.4	3.41
7.34	403.6		
7.82	352.9	95.0	2.71
8.31	350.1		
8.80	368.6	88.4	3.17
9.29	343.4		
9.78	309.6	85.8	2.61
10.27	311.0		
10.76	316.7	84.0	2.76
11.25	307.0		
11.74	281.3	79.9	2.52
12.22	276.6		
12.71	281.4	74.4	2.78
13.20	261.2		
13.69	245.5	70.3	2.48
14.18	245.8		
14.67	258.7	60.1	3.30
15.16	237.9		
15.65	215.4	54.0	2.98
16.14	230.5		
16.63	229.5	50.0	3.59
17.11	229.2		
17.60	232.3	45.6	4.09
18.09	258.4		
18.58	321.3		
19.56	437.6	35.1	11.48
20.54	467.7	29.8	14.70
21.52	467.5	20.7	21.57
22.49	433.0	15.1	27.73
23.47	391.7	12.3	30.97
24.45	342.3	7.2	46.41

TABLE A2.9 Au activities and cadmium ratio-1.0 in 1.83TU (RUN 3872) core.

	1.83TU RUN 3872		
DISTANCE cm	BARE count/mg	CD COVER count/mg	R_{cd}-1.0
0.0	1287.0		
1.96	1279.1	399.5	2.20
3.91	1336.9	399.2	2.34
5.87	1287.9	376.8	2.41
7.82	1107.6	350.6	2.15
9.78	1082.8	308.7	2.50
11.74	956.0	257.5	2.71
13.69	1021.7	211.1	3.83
14.67	1415.3	197.4	6.16
15.65	1935.6	173.2	10.17
16.63	2110.0		
17.60	2100.5		
19.56	1727.8		
21.52	1318.7		
23.47	929.6		
25.43	643.0		
27.38	430.6		
29.34	284.7		

Appendix A3. Power distributions

The values of the measured and calculated power distributions are shown in **Figs. A3. 1** through **A3. 9**. In the figures, a quater of the core is illustrated and each block represents a unit fuel rod cell. In a block, the first line shows the calculated value, the second is the measured one and the third is the difference between both values in percentages. The measured power is the average of the values at the equivalent positions in the core.

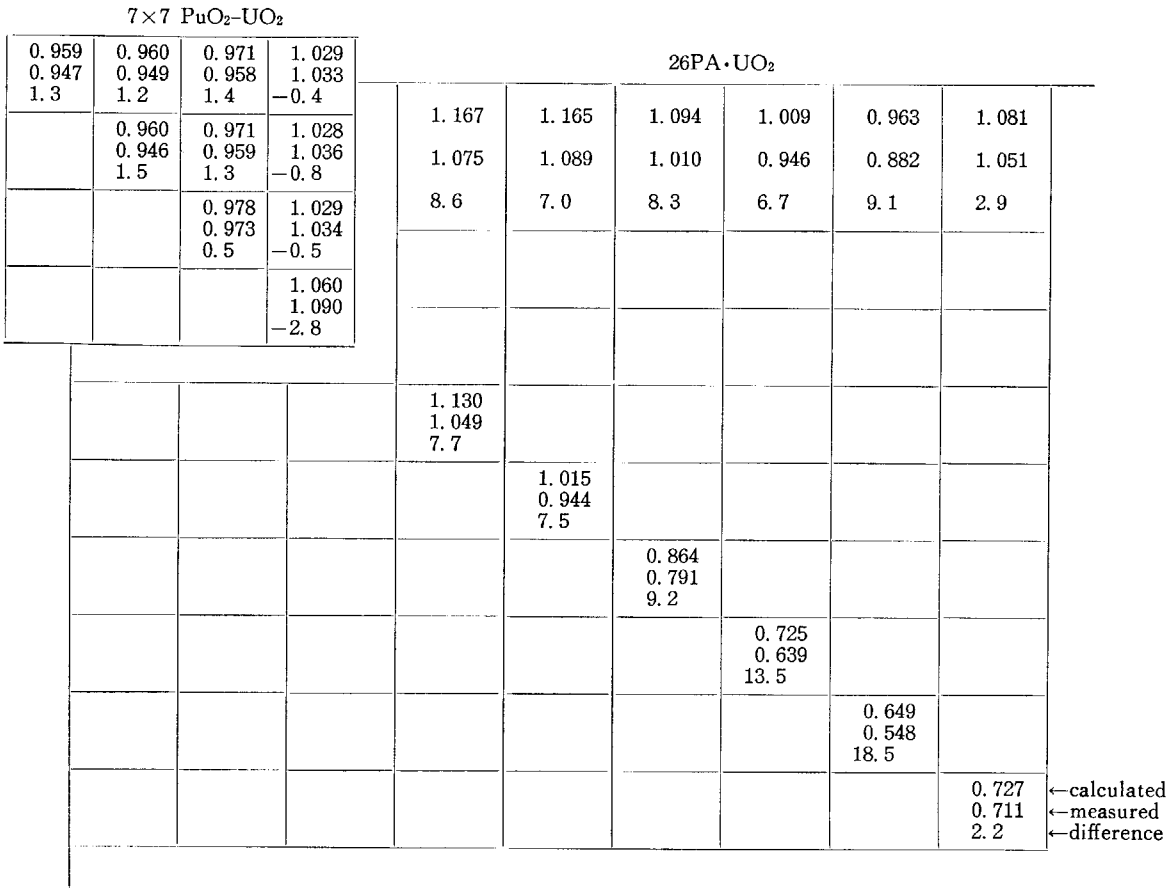

$$\text{Difference} = \left(\frac{\text{cal.} - \text{meas.}}{\text{meas.}}\right) \times 100, \quad \%.$$

Fig. A 3. 1 Power distributions in 1.76Pu (RUN 3799) core.

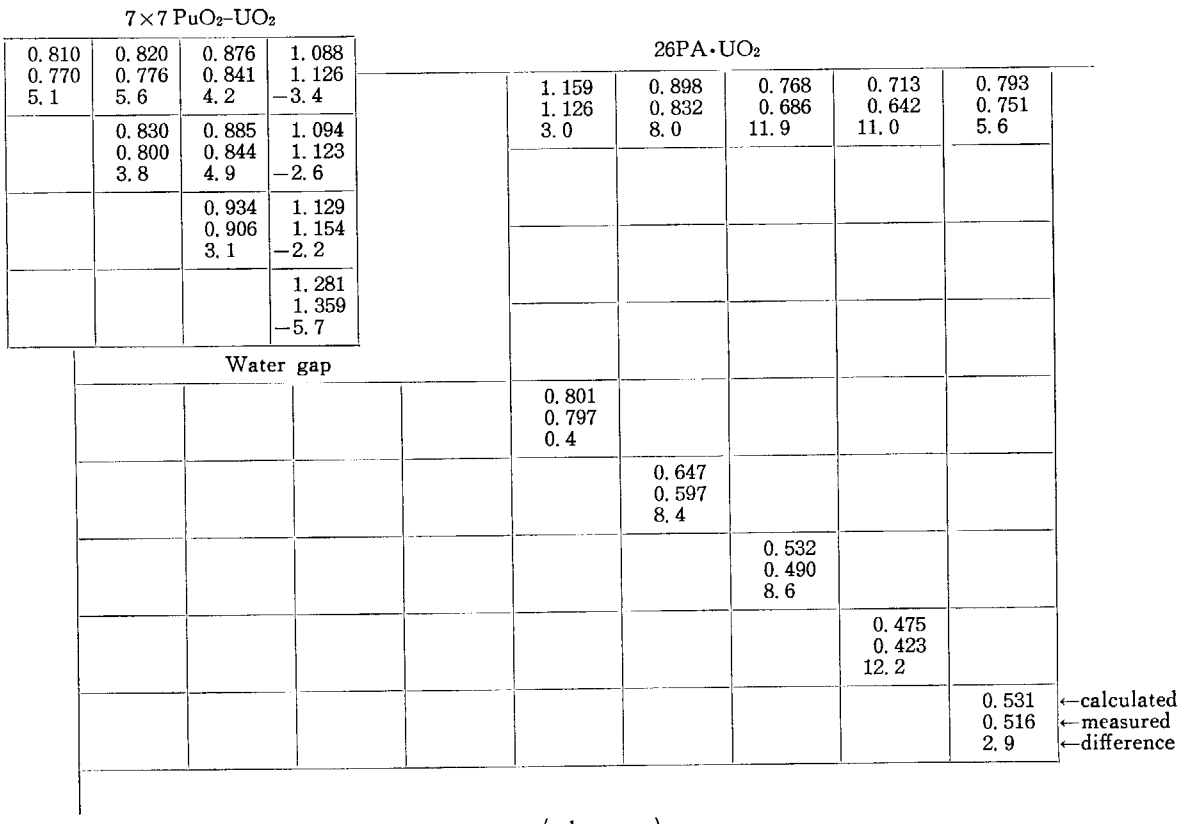

$$\text{Difference} = \left(\frac{\text{cal.} - \text{meas.}}{\text{meas.}}\right) \times 100, \quad \%.$$

Fig. A 3.2 Power distributions in 2.00Pu (RUN 3838) core.

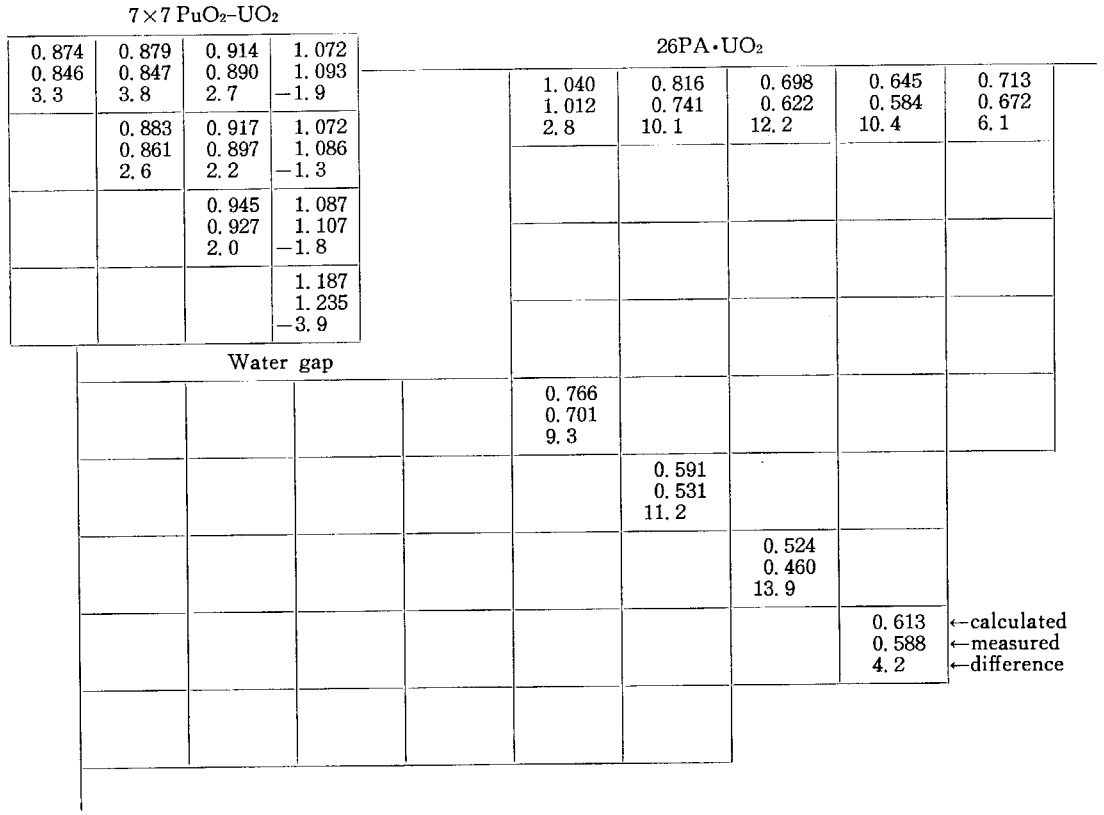

$$\text{Difference} = \left(\frac{\text{cal.} - \text{meas.}}{\text{meas.}}\right) \times 100, \quad \%.$$

Fig. A 3.3 Power distributions in 2.38Pu (RUN 3848) core.

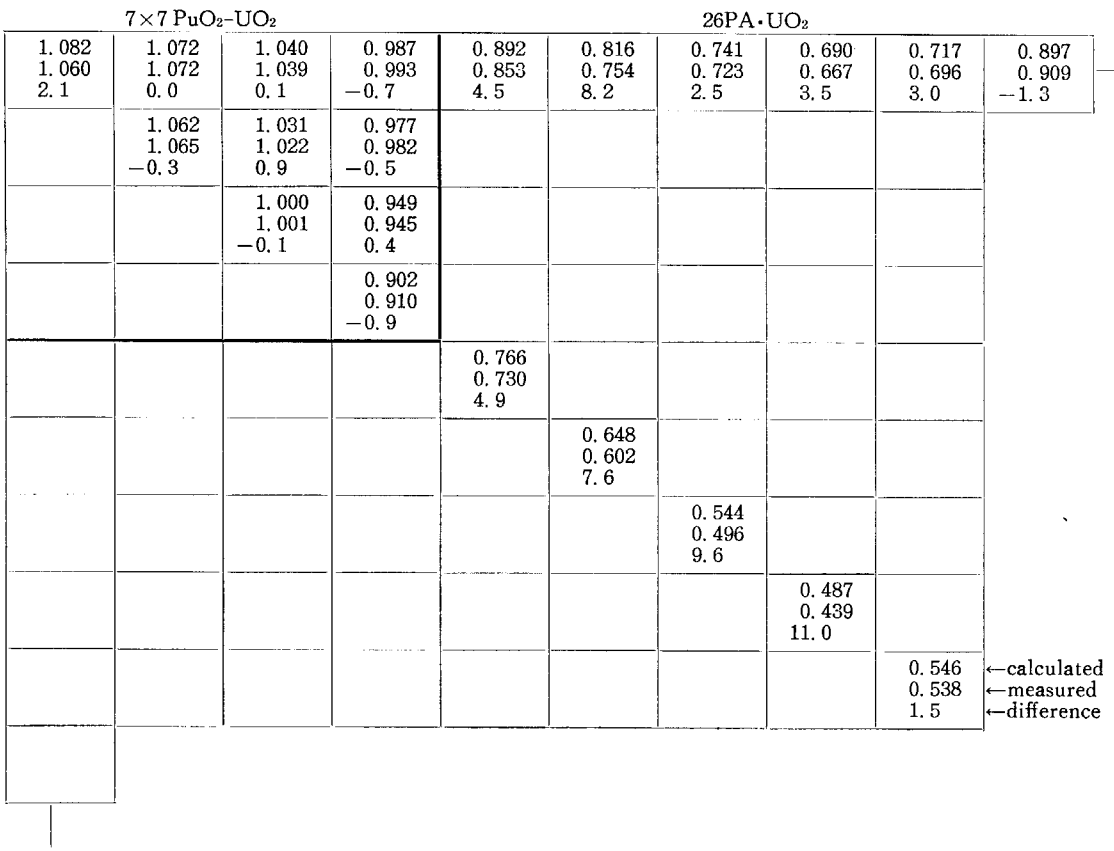

$$\text{Difference} = \left(\frac{\text{cal.} - \text{meas.}}{\text{meas.}}\right) \times 100, \quad \%.$$

Fig. A 3.4 Power distributions in 2.95Pu (RUN 3830) core.

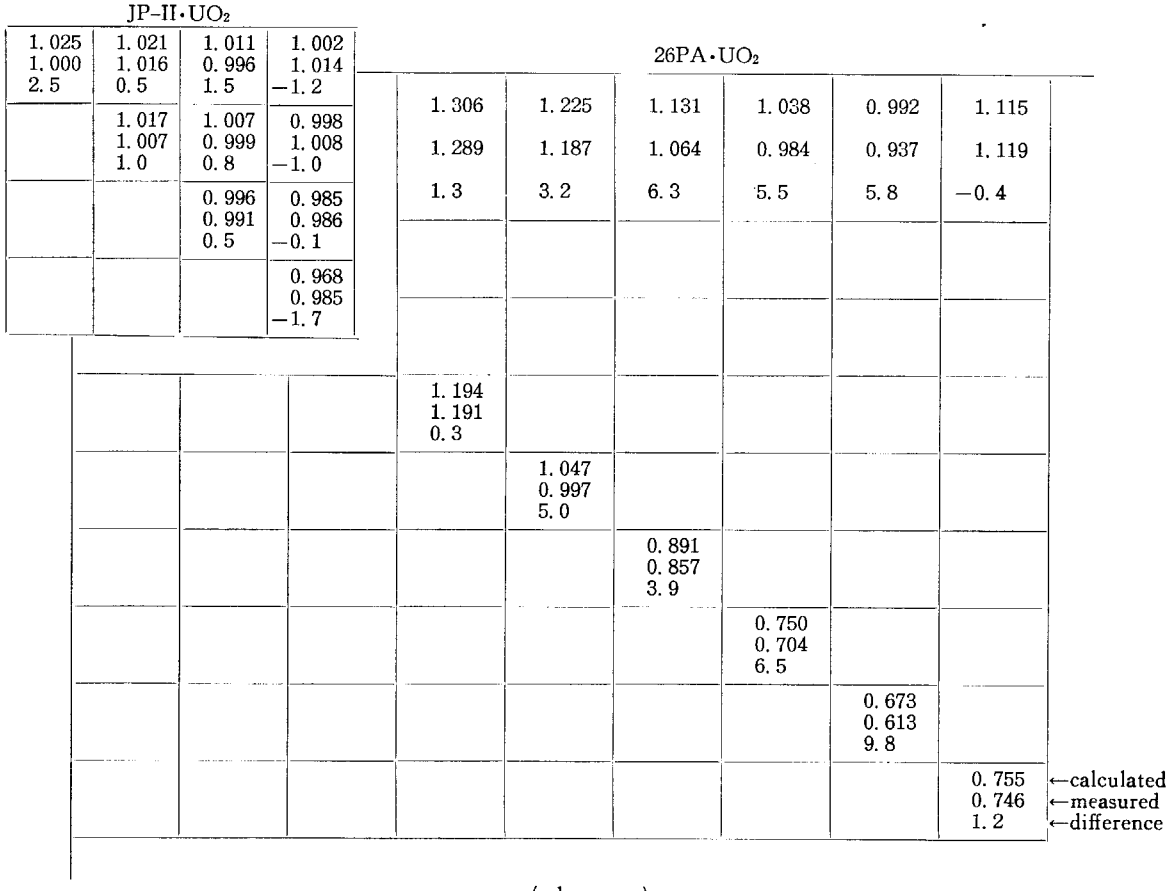

$$\text{Difference} = \left(\frac{\text{cal.} - \text{meas.}}{\text{meas.}}\right) \times 100, \quad \%.$$

Fig. A 3.5 Power distributions in 1.76U (RUN 3847) core.

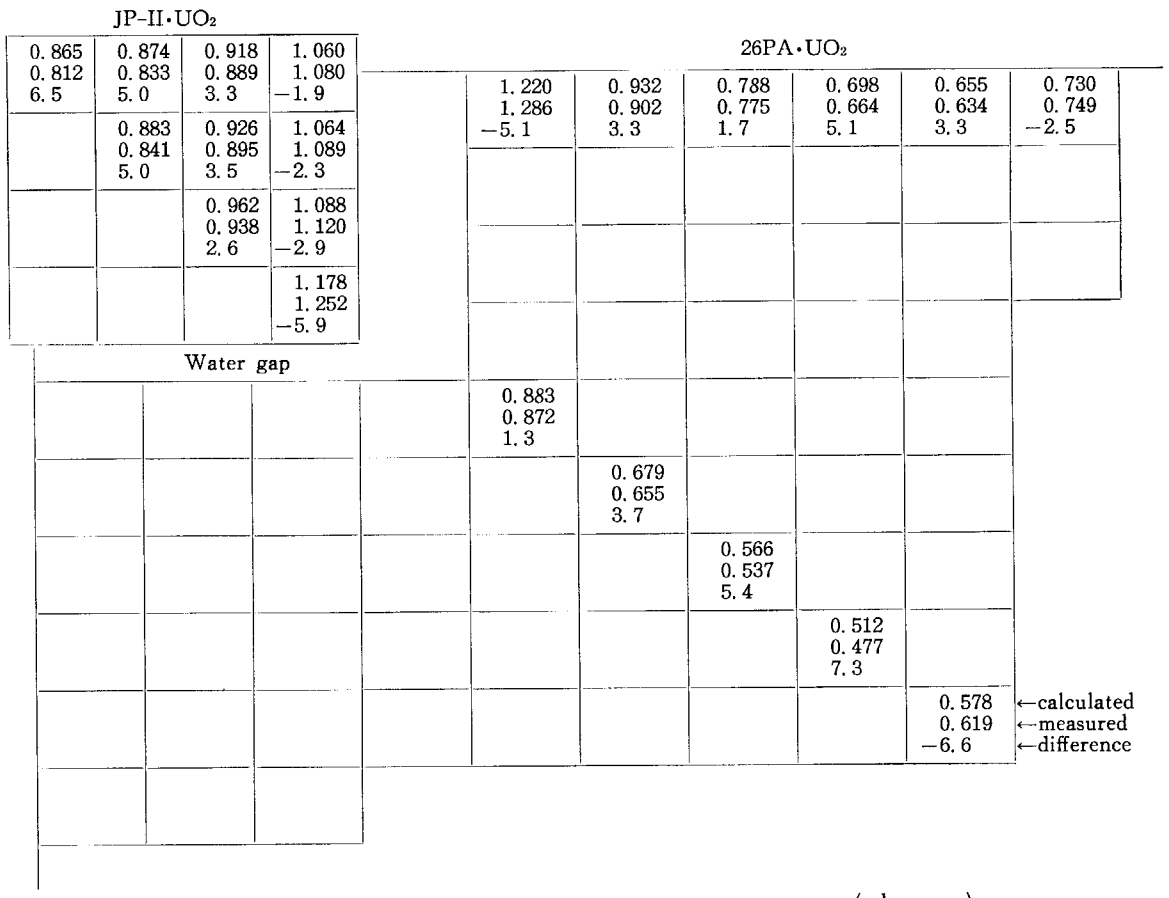

Fig. A 3.6 Power distributions in 2.00U (RUN 3871) core. Difference $=\left(\frac{\text{cal.}-\text{meas.}}{\text{meas.}}\right)\times 100$, %.

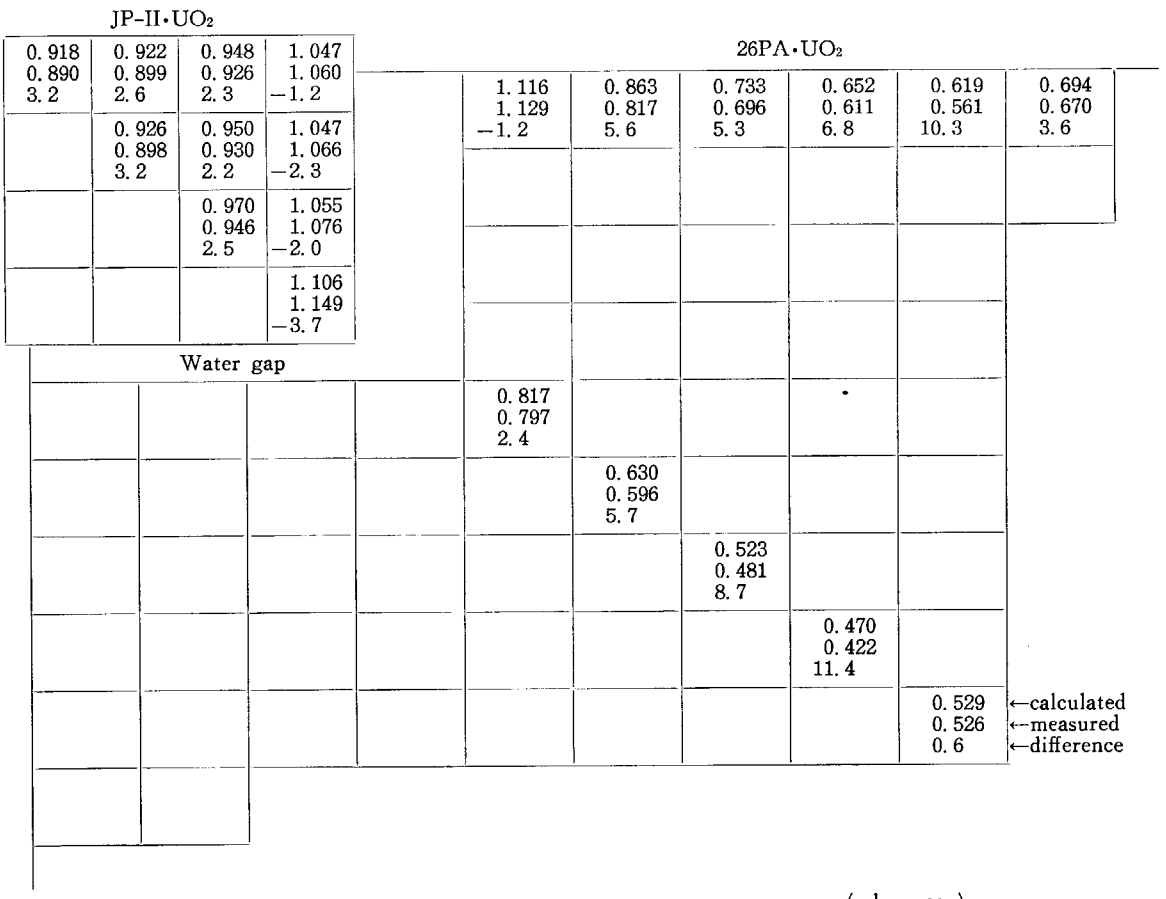

Fig. A 3.7 Power distributions in 2.38U (RUN 3846) core. Difference $=\left(\frac{\text{cal.}-\text{meas.}}{\text{meas.}}\right)\times 100$, %.

JP-II·UO_2				26PA·UO_2					
1.121 1.112 0.8	1.110 1.114 −0.4	1.065 1.074 −0.8	0.966 0.974 −0.8	1.022 1.071 −4.6	0.891 0.896 −0.5	0.797 0.796 0.2	0.720 0.728 −1.1	0.679 0.667 1.8	0.760 0.767 −0.9
	1.097 1.094 0.3	1.054 1.058 −0.4	0.956 0.954 0.2						
		1.014 1.018 −0.4	0.923 0.918 0.6						
			0.849 0.834 1.8						
				0.845 0.865 −2.4					
					0.710 0.710 0.0				
						0.603 0.596 1.1			
							0.551 0.530 4.0		
								0.633 0.679 −6.7	←calculated ←measured ←difference

$$\text{Difference}=\left(\frac{\text{cal.}-\text{meas.}}{\text{meas.}}\right)\times 100,\ \%.$$

Fig. A 3.8 Power distributions in 2.95U (RUN 3834) core.

26PA·UO_2								
1.161 1.133 2.5	1.149 1.170 −1.8	1.116 1.149 −2.9	1.062 1.089 −2.5	0.993 1.013 −2.0	0.922 0.928 −0.6	0.890 0.877 1.4	1.009 1.033 −2.3	
1.153 1.146 0.6								
1.128 1.140 −1.1								
1.088 1.123 −3.1	1.077 1.118 −3.7							
1.032 1.046 −1.3		0.993 0.992 0.1						
0.964 0.952 1.2			0.882 0.894 −1.4					
0.886 0.860 3.0				0.758 0.752 0.7				
0.811 0.790 2.6					0.643 0.615 4.5			
0.772 0.745 3.6						0.581 0.544 6.9		
0.866 0.880 −1.6							0.666 0.695 −4.2	←calculated ←measured ←difference

$$\text{Difference}=\left(\frac{\text{cal.}-\text{meas.}}{\text{meas.}}\right)\times 100,\ \%.$$

Fig. A 3.9 Power distributions in 1.83TU (RUN 3872) core.